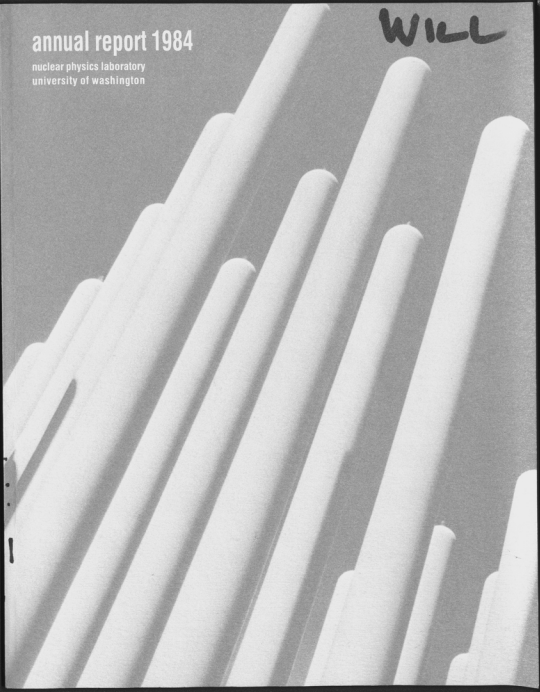


annual report 1984

nuclear physics laboratory
university of washington

WILL



ANNUAL REPORT

Nuclear Physics Laboratory
University of Washington
April, 1984

Supported in part by the United States Department of Energy
under contract DE-AC06-81ER40048

We have initiated a new program to look for low-energy gamma-ray transitions in the ^{152}Sm nucleus. This program is a continuation of the work done in the ^{152}Sm nucleus by the late Dr. J. J. Griffin. The program is designed to provide a better understanding of the collective excitations of the nucleus and to provide a better understanding of the structure of the nucleus.

TECHNICAL REPORT

Research Triangle Institute
University of North Carolina

This report was prepared as an account of work sponsored in part by the United States Government. Neither the United States nor the United States Department of Energy, nor any of their employees, makes any warranty, express or implied, or assumes any legal liability or responsibility for the accuracy, completeness or usefulness of any information, apparatus, product or process disclosed, or represents that its use would not infringe privately-owned rights.

Approved for release by the United States Department of Energy
under contract DE-AC02-76-OR00000

INTRODUCTION

This Report summarizes all work during the year ending in April, 1984 done in the Nuclear Physics Laboratory or by our staff at other research institutions. Most staff projects are supported by the Laboratory's Department of Energy contract, two major projects are supported in part by the Murdock Charitable Trust, and outside users receive support from a variety of sources.

The big news this year is certainly the start of the booster LINAC project. Money began to flow late in 1983. In April, 1984, after a little suspense, our low- β prototype resonator was successfully tested at Stony Brook signalling the start of full-scale production for the low- β portion of the LINAC. Construction noise, concrete dust and new staff members are increasingly in evidence as production deadlines begin to loom on the horizon.

The saga of the new polarized ion source has entered another chapter with receipt of existing hardware from Auckland in October. This followed efforts over the summer, first to negotiate a new contract with ANAC (in receivership), and when that failed, to legally secure our property and ship it to Seattle. Remaining construction and assembly are now well underway.

In the field of nuclear astrophysics we note that recent measurements made here seem to eliminate both s- and r-process flow through ^{180}Hf as possible sources for nucleosynthesis of ^{180}Ta . So there remains a puzzle: Where does the observed ^{180}Ta come from?

We have made careful measurements of certain isospin-forbidden Fermi β decays in order to test new shell-model codes which employ much larger bases for calculation. When the accuracy of the calculation is not dominated by use of a restricted basis, such decays provide very sensitive tests of the charge-dependent interaction.

We have greatly expanded our program to understand giant dipole resonances built on excited nuclear states (e.s.-GDR). We have confirmed in detail in (p, γ) reactions the simple one-step semidirect GDR excitation mechanism which populates the same residual states made in proton stripping. Our statistical GDR decay studies of C + C and C + O provide new information on compound nuclear isospin mixing in light nuclei. Some of our statistical studies in the mass-60 region have revealed a new puzzle—namely, that the average e.s.-GDR decay strength required is only a fraction of the classical dipole sum rule. And, we are very excited to observe splitting of the e.s.-GDR in alpha plus samarium, providing indication of the persistence of nuclear deformation at elevated temperature.

We have initiated a new program to look for isovector quadrupole and higher multipolarity giant resonances with the (γ ,n) reaction. This complements our previous (n, γ) work and offers a particularly clean way to observe the collective excitations free of masking direct-reaction effects.

Using the mass asymmetry of sequential fission fragments we have determined the division of excitation energy in partially damped collisions between heavy ions. In contrast to earlier results with other methods we find that the excitation energy is divided almost equally between the two fragments rather than according to the mass ratio. This means that the collision time is shorter than the thermalization time.

In the area of heavy ion collisions at intermediate energies we have identified a new mode of dissociation for the heavy-ion projectile - the decay of the relatively light excited nucleus into multiple heavy fragments, with a probability higher than previously expected.

Development work continues on hardware for the ^{14}N nuclear parity mixing experiment. This experiment is sensitive to $\Delta I=0$ mixing between $I=1$, O^+ and O^- levels in ^{14}N near $E_x = 8.7$ MeV. The longitudinal analyzing power A_L for elastic proton scattering is measured over the narrow O^- level. To date the beam line hardware and electronic systems are complete. Systematic asymmetries with unpolarized beam are less than a statistical upper limit of 8×10^{-6} . We are continuing to study systematics and refine our beam stabilization system while awaiting installation of the new polarized ion source.

A new solenoid for the hydrogen atom parity experiment has required very accurate physical measurements and careful assembly this year to insure our required $1/10^5$ field homogeneity. The new magnet plus better vacuum and gold-plated rf cavities should, we expect, bring our systematic errors down by a factor of 100.

It is generally accepted that inelastic pion scattering from nuclei proceeds mainly via single scattering from constituent nucleons. In order to study the departures from free pion-nucleon scattering caused by the nuclear medium we have compared spectra for the four lightest target nuclei and find that, even in the simplest composite systems, there are some fairly complicated medium effects.

A new NMR-controlled isotope switching system has allowed us to measure the ^{14}C distribution across a single Sitka spruce tree ring and show a definite correlation with the ^{14}C atmospheric abundance history of that year, 1963, when nuclear weapons testing was at its peak.

One of our biggest outside user programs was terminated in February. The Fast Neutron Radiotherapy Program has moved to its own quarters in the University Medical Center and is preparing to begin patient therapy with its own new cyclotron. A very interesting and novel outside user program carried out this year has been a study of cosmic-ray induced integrated circuit bit errors simulated by charge deposition by fast heavy ions passing through integrated circuits.

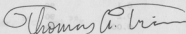
Our data acquisition and analysis systems continue to proliferate in speed and flexibility, both because of creative in-house hardware and software development and also because of extensive software exchange with other

laboratories, thanks to increasing world-wide hardware compatibility.

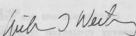
We close this introduction with a reminder that the articles in this report describe work in progress and are not to be regarded as publications or quoted without permission of the investigators. In each article the names of the investigators have been listed alphabetically, but where appropriate the names of those primarily responsible for the report have been underlined.

As always, we welcome applications from outsiders for the use of our facilities. As a convenient reference for potential users, the table on the following page lists the vital statistics of our accelerators. For further information please write or telephone Dr. W.G. Weitkamp, Technical Director, Nuclear Physics Laboratory, University of Washington, Seattle, WA 98195; (206) 543-4080.

The editors are grateful to Barbara Fulton for keeping this project together in the face of many new demands, and to Maria Ramirez who, among many other things, made sure the figures figured.



Thomas A. Trainor
Scientific Editor



William G. Weitkamp
Technical Editor

THREE STAGE TANDEM VAN DE GRAAFF ACCELERATOR

A High Voltage Engineering Corp. Model FN purchased in 1966 with NSF funds; operation funded primarily by the U.S. Department of Energy. See W.G. Weitkamp and F.H. Schmidt, "The University of Washington Three Stage Van de Graaff Accelerator," Nucl. Instrum. Meth. 122, 65 (1974).

Available Energy Analyzed Beams:

Ion	Max. Current	Max. Practical	Max. Current	Max. Practical
	2 Stage (μ A)	Energy 2 Stage (MeV)	3 Stage (μ A)	Energy 3 Stage (MeV)
p,d	20	18	5	24
polarized p,d	0.1	18		
He	1.5	27		
Li	0.2	36		
C	1.8	63		
N	0.2	62	0.2	67
O	1	72	0.5	78
Si	0.1	90		
Cl	0.2	90	0.02	114
Ni	0.005	99		
Br	0.05	108		
Ag	0.001	108		

60-INCH CYCLOTRON

A fixed energy cyclotron constructed in 1950-52 with State of Washington funds; operated with income from outside users. See F.H. Schmidt, G.W. Farwell, J.E. Henderson, T.J. Morgan, and J.F. Streib, "The University of Washington Sixty-Inch Cyclotron," Rev. Sci. Instrum. 25, 499 (1954).

Available Target Box Beams:

Ion	Maximum	Energy (MeV)
	Current (μ A)	
p	100	11
d	150	22
⁴ He	30	42

TABLE OF CONTENTS

	PAGE
1. ASTROPHYSICS AND COSMOLOGY	
1.1 Alpha-Particle Cross Sections Relevant to Gamma-Ray Astronomy	1
1.2 Gamma Ray Lines from SS432	1
1.3 Searches for $\beta^+\beta^+$, β^+/EC , and EC/EC Decays	2
1.4 Search for ^{92}Nb in Nature	3
1.5 Equilibration of $^{176}\text{Lu}^{\text{G,M}}$ Under Stellar Conditions	3
1.6 Nucleosynthesis of $^{180}\text{Ta}^{\text{M}}$	3
2. NUCLEAR STRUCTURE	
2.1 The β^+ Decays of ^{34}Ar , ^{34}Cl and ^{38}K	5
3. GIANT RESONANCES	
3.1 Schematic Model Calculations of Nucleon Decay Strengths from Giant Dipole Resonances Built on Excited States	7
3.2 Compound Nuclear Isospin Purity and the Statistical Decay of the GDR in Light Nuclei	8
3.3 Statistical GDR Decays over a Wide Range of Energy from the $^{63}\text{Cu}^*$ Compound Nucleus	9
3.4 Statistical GDR Decays in $^{16}\text{O} + \text{Ni}$ for Various Ni Isotopes	10
3.5 Study of Excited-State GDR's in the 1f-2p Shell Nuclei	11
3.6 Deformation Effects in the Statistical Decay of the Giant Dipole Resonance	13
3.7 Excited-State Giant Resonances Observed in the $^{38}\text{K}(p,\gamma)^{40}\text{Ca}$ and $^{40}\text{Ca}(p,\gamma)^{41}\text{Sc}$ Reactions	14
3.8 Forward-to-Backward Asymmetries in the (γ,n) Reactions around the E2 Isovector Giant Resonance	16
3.9 Determination of a Time Scale for the Emission of High Energy Photons in Heavy Ion Fusion Reactions	17

4. HEAVY ION REACTIONS

4.1	Study of Spin-Spin Correlations in Deep Inelastic Collisions	21
4.2	Nuclear Rainbow Scattering with Carbon Isotopes	22
4.3	Penetrability of the Centrifugal Barrier and the Spin Distribution of the Compound Nucleus	23
4.4	Search for High Spin States in ^{32}S	25
4.5	A New Scheme for Calibration Sub-Coulomb Heavy Ion Proton Transfer Reactions	27
4.6	Measurement of Total Reaction Cross Sections at 15 to 35 MeV/A	27
4.7	Calculation of Critical Energies as a Function of Nuclear Size	29
4.8	Projectile Breakup into Coincident Heavy Fragments	30
4.9	Reactions of ^{24}Mg with ^{16}O	31
4.10	How is the Excitation Energy Divided in Partially Damped Collisions?	32
4.11	The Effect of Particle Evaporation in the $^{136}\text{Xe} + ^{56}\text{Fe}$ Reaction and a Reinvestigation of the $^{86}\text{Kr} + ^{82}\text{Mo}$ Reaction	34

5. FUNDAMENTAL SYMMETRIES IN NUCLEI: $0^+ - 0^-$ ISOSCALAR PARITY MIXING IN ^{14}N

5.1	Theory of the Parity Mixing Measurement	36
5.2	High Count-Rate Low-Energy Proton Detectors	39
5.3	^{14}N Beam Position Stabilization System	40
5.4	^{14}N Data Collection Electronics	42
5.5	Data Acquisition and Analysis Programs	43
5.6	Design and Construction of the ^{14}N Parity Experiment Beamline	44
5.7	Studies of System Performances Using an Unpolarized Beam	45

6.	FUNDAMENTAL SYMMETRIES IN ATOMS: PARITY MIXING IN HYDROGEN AND DEUTERIUM	
6.1	Introduction	47
6.2	Cleaning and Plating of RF Cavities	48
6.3	Alignment and Field Scans of the New Solenoid	48
6.4	Control System for a New Solenoid	50
7.	MEDIUM ENERGY PHYSICS	
7.1	Inclusive Scattering of Pions from very Light Nuclei at 100 MeV	52
8.	ACCELERATOR MASS SPECTROMETRY (AMS)	
8.1	AMS with Carbon and Beryllium: C-14 and Be-10 Radiochronology	54
8.2	AMS: Technical Improvements	55
8.3	Isotope Alternation System: Two-Level, NMR-Controlled Rapid Switching	56
9.	RESEARCH BY OUTSIDE USERS	
9.1	Lifetime and Magnetic Moments of States of ^{16}N by the Recoil-into-Vacuum Method	59
9.2	Simultaneous Measurement of Nuclear Magnetic Moments by the Transient Field Method	60
9.3	Short-Lived Radionuclides for Biomedical Research	62
9.4	Irradiation of Optical Materials	64
9.5	Light Ion Irradiation Creep	64
9.6	Simulation of Cosmic-Ray Upset in Integrated Circuits	65
9.7	Fast Neutron Beam Radiotherapy: Medical Radiation Physics	66
9.8	Fast Neutron Beam Radiotherapy: Clinical Program	66
9.9	Neutron Radiobiology in Support of Radiotherapy	67
9.10	Normal Tissue Neutron Radiobiology	69

9.11	Effect of Antibiotic Decontamination of the GI Tract on Survival Time after Neutron and Gamma Irradiation	70
9.12	Measurement of Total Body Calcium by Neutron Activation	70
10.	ACCELERATORS AND ION SOURCES	
10.1	Van de Graaff Accelerator Operations and Development	72
10.2	Cyclotron Operations and Development	72
10.3	Predicting Tandem Parameters	74
10.4	Crossed-Beams Polarized Ion Source	74
10.5	Sputter Source Elevation	76
11.	NUCLEAR INSTRUMENTATION	
11.1	Design and Construction of Electronic Equipment	77
11.2	Construction and Testing of a Breskin Counter	78
11.3	Use of the LED-PIN Diode Light Pulser for Gain Stabilization of the 10" x 10" NaI Spectrometer	78
11.4	Improvement and Testing of the Momentum Filter	79
11.5	A Polarimeter for the Momentum Filter	81
11.6	Target Preparation	82
12.	COMPUTER SYSTEMS	
12.1	Data Acquisition System Enhancements	83
12.2	Data Analysis System Enhancements	85
12.3	Hardware Enhancements to the Laboratory Data Collection System	87
12.4	A Continuous- λ Optical Model Program	88
13.	BOOSTER LINAC PROJECT	
13.1	Introduction	90
13.2	Design and Construction of Superconducting Resonators	91
13.3	Lead Plating of Low Beta Resonator	93

13.4 Tests of the Low Beta Resonator	94
13.5 The Pretandem Buncher	96
13.6 Beam Dynamics for the UW Booster Project	97
13.7 Phase Control of the Tandem-LINAC System	98
13.8 Resonator Test Facility	99
13.9 Resonator Control System	100
13.10 Booster Cryogenics	101
13.11 The Plating Laboratory	101
14. APPENDIX	
14.1 Nuclear Physics Laboratory Personnel	103
14.2 Ph.D. Degrees Granted, Academic Year 1983-1984	105
14.3 List of Publications	106

1.7 Quasi-Ray Lines from ^{24}Mg

B. Bolinsky and A.B. Norman

The identification of observed quasi-ray lines from the astronomical source $\text{Ae} 1$ was examined in the light of quasi-ray production cross sections measured at the University of Washington¹ and elsewhere. It had been initially suggested by Loh et al. that the observed lines were the blue- and red-shifted components of the 1.04-MeV line from the $^{24}\text{Mg}(p,\alpha)^{21}\text{Mg}$ reaction between ^{24}Mg nuclei in the jet of $\text{Ae} 1$, moving at a speed equivalent to 10 km per nucleus, and ambient protons. However, this explanation implied that the shifted components of the doublet at 1.04 MeV from the $^{24}\text{Mg}(p,\alpha)^{21}\text{Mg}$ and $^{24}\text{Mg}(p,p')^{24}\text{Mg}$ reactions should be seen with nearly the same intensity. The apparent absence of these lines argued against the original simple interpretation.

1. ASTROPHYSICS AND COSMOLOGY

1.1 Alpha-Particle Cross Sections Relevant to Gamma-Ray Astronomy

D. Bodansky, P. Dyer,* D.D. Leach, E.B. Norman, and A.G. Seamster

The analysis of gamma-ray production cross sections for alpha-particle induced reactions¹ on light nuclei (^{12}C , ^{14}N , and ^{16}O) is nearing completion. The cross section for production of the 4.44-MeV line in (α, α') reactions on ^{12}C is found to exceed 200 mb for incident energies from $E_{\alpha} = 10$ Mev to the maximum energy studied, $E_{\alpha} = 27$ Mev, and exceeds 400 mb at some points. These cross sections are somewhat greater than those for producing the 4.44-MeV line in (p, p') reactions on ^{12}C .² Similarly the cross sections for the production of the 1.63-MeV and 2.31-MeV lines in (α, α') reactions on ^{14}N slightly exceed those for the corresponding (p, p') lines.²

The analysis of the cross sections for alpha-particle induced reactions on heavier, abundant nuclei (^{20}Ne , ^{24}Mg , ^{27}Al , ^{28}Si , and ^{56}Fe) has been completed.

References:

- * Los Alamos National Laboratory, Los Alamos, NM 87545.
1. Nuclear Physics Laboratory Annual Report, University of Washington (1983) p. 4.
2. P. Dyer, D. Bodansky, A.G. Seamster, E.B. Norman, and D.R. Maxson, Phys. Rev. C 23, 1865 (1981).
3. A.G. Seamster, E.B. Norman, D.D. Leach, P. Dyer, and D. Bodansky, Phys. Rev. C 29, 394 (1984).

1.2 Gamma-Ray Lines from SS433.

D. Bodansky and E.B. Norman

The interpretation of observed gamma-ray lines from the astronomical source SS433¹ was examined in the light of gamma-ray production cross sections measured at the University of Washington² and elsewhere.³ It had been initially suggested by Lamb *et al.*¹ that the observed lines were the blue- and red-shifted components of the 1.369-MeV line from the $^{24}\text{Mg}(p, p')^{24}\text{Mg}$ reaction between ^{24}Mg nuclei in the jet of SS433, moving at a speed equivalent to 33 MeV per nucleon, and ambient protons. However, this explanation implied that the shifted components of the doublet at 1.64 MeV from the $^{24}\text{Mg}(p, p\alpha)^{20}\text{Ne}$ and $^{24}\text{Mg}(p, 2p)^{23}\text{Na}$ reactions should be seen with nearly the same intensity.⁴ The apparent absence of these lines argued against the original simple interpretation.

It has been subsequently proposed by Ramaty, Kozlovsky, and Lingenfelter⁵ that the 1.369-MeV line could be produced by a combination of the $^{24}\text{Mg}(p,p')^{24}\text{Mg}$ and $^{28}\text{Si}(p,pa)^{24}\text{Mg}$ reactions taking place in collisions between grains in the jet and ambient protons. The addition of the $^{28}\text{Si}(p,pa)^{24}\text{Mg}$ somewhat relieves the constraint imposed by the upper limit on the observed flux for the 1.64-MeV line but suggests the presence of the 1.779-MeV line from ^{28}Si at slightly reduced intensity. A test of the model of Ramaty et al.⁵ can in principle be provided by further examination of the gamma-ray spectra from S5433. The uncertainties in this test would be reduced were measured cross sections available for gamma-ray production at 33 Mev per nucleon, but at present it is still necessary to rely largely on extrapolations from data near 24 Mev.

References:

1. R.C. Lamb, J.C. Ling, W.A. Mahoney, G.R. Riegler, W.A. Wheaton, and A.S. Jacobson, *Nature* **305**, 37 (1983).
2. P. Dyer, D. Bodansky, A.G. Seamster, E.B. Norman, and D.R. Maxson, *Phys. Rev. C* **23**, 1865 (1981).
3. W. Zobel, F.C. Maienschein, J.H. Todd, and G.T. Chapman, *Nucl. Sci. Eng.* **32**, 392 (1968).
4. E.B. Norman and D. Bodansky, *Nature* **308**, 212 (1984).
5. R. Ramaty, B. Kozlovsky, and R.E. Lingenfelter, preprint (1984).

1.3 Searches for $\beta^+\beta^+$, β^+/EC and EC/EC Decays

M.A. Nelson and E.B. Norman

As described in last year's Annual Report,¹ we have begun a search for $\beta^+\beta^+$, β^+/EC , and EC/EC decays using a 4π NaI detector system. In an attempt to reduce the background counting rate due to cosmic rays, we installed a large plastic scintillator veto paddle above the detector. However, this was found to produce no observable decrease in the background rate. Thus it appears that the origin of our background must be radioactive impurities in the detector itself and in the shielding material. For the immediate future, in order to obtain greater sensitivity for detecting $\beta^+\beta^+$, β^+/EC , and EC/EC decays we simply plan to count for long periods of time.

Reference:

1. Nuclear Physics Laboratory Annual Report, University of Washington (1983) p. 36.

1.4 Search for ^{92}Nb in Nature

E.B. Norman

Apt et al.¹ have reported the observation of the $t_{1/2} = 3.5 \times 10^7$ year ^{92}Nb in a sample of natural niobium. Although the inferred abundance ratio of $^{92}\text{Nb}/^{93}\text{Nb}$ is only 2×10^{-13} , it is far larger than can be accounted for by any conventional nucleosynthetic process. Because of the difficulty in accounting for the presence of ^{92}Nb in terrestrial material, it was felt that a remeasurement of ^{92}Nb abundance should be performed. To do so, two ~1 kg samples of Nb were acquired. Using the 4 π NaI detector system at the UW Laboratory for Radiation Ecology, searches are currently being made for the 561- and 935-keV γ rays known to be emitted in the decay of ^{92}Nb . To date, no positive evidence of these two γ rays has been observed.

Reference:

1. K.E. Apt et al., *Geochim. Cosmochim. Acta* **38**, 1485 (1974).

1.5 Equilibration of $^{176}\text{Lu}^{g,m}$ Under Stellar Conditions

T. Bertram, S. Gil, S.E. Kellogg, E.B. Norman, and P. Wong

As discussed in previous Annual Reports,¹ we are studying processes that can occur in stellar environments by which $^{176}\text{Lu}^g$ and $^{176}\text{Lu}^m$ could come into thermal equilibrium. From our observation of the photoactivation of $^{176}\text{Lu}^g$ - $^{176}\text{Lu}^m$ using a large ^{60}Co γ -ray source, we have found that in environments in which the temperature is $\geq 4 \times 10^8$ °K photoexcitation alone guarantees thermal equilibrium. By including the effects of positron-annihilation-excitation we find that even at the canonical s-process temperature of 3.5×10^8 °K $^{176}\text{Lu}^{g,m}$ are in equilibrium. Thus ^{176}Lu is probably not a reliable cosmochronometer but instead may be useful as a stellar thermometer.

Reference:

1. Nuclear Physics Laboratory Annual Report, University of Washington (1983) p. 2; *ibid.* (1982) p. 3.

1.6 Nucleosynthesis of $^{180}\text{Ta}^m$

S.E. Kellogg and E.B. Norman

Our interest in the nucleosynthetic mechanism responsible for the production of the naturally occurring isomer, $^{180}\text{Ta}^m$ continues unabated. Beer and Ward¹ suggested that $^{180}\text{Ta}^m$ may in fact be produced in stars by the

standard s and/or r neutron capture processes through the fractional β decay, f_{β} , of 5.5 hr ^{180}Hf directly to ^{180}Ta . As described in last year's Annual Report,² we have been using a VETO technique to suppress the dominant and rich spectrum of conversion electrons which masks the 204 keV endpoint β continuum. We successfully suppressed contaminant β decays from ^{181}Hf by introducing a 50 μsec software delay in the MSD code to allow an 18 μsec level in ^{181}Ta to γ decay and be eligible for vetoing (see Sec. 12.1). Our new limit, $f_{\beta} < 0.6\%$, implies that the s process alone is insufficient by a factor of 5 in explaining the observed ^{180}Ta abundance.

We also searched for β decays to excited states above the long-lived isomer by replacing our e^{-} detector with a high-resolution GeLi detector and looking for single γ events in our VETO arrangement. Our observation of a 100.8 keV γ ray following a 2×10^{-4} β -decay branch of ^{180}Hf , though too small to be astrophysically important, nevertheless represents the first observed gamma transition that feeds the long-lived isomer in ^{180}Ta . Log-ft considerations lead us to conclude that the nuclear structure of the Hf isomer is principally that of a broken proton pair ($9/2$ [514] + $7/2$ [404]). Further, we verify Naumann's³ objection to Warde's⁴ placement of the low-lying 7^{-} level in ^{180}Ta .

Beer and Ward identified the possibility of an r-process contribution through the fractional β decay, f_{β} , of 5.7 min ^{180}Lu to ^{180}Hf . We repeated our radiochemical separation of ^{180}Lu from a cyclotron activated Hf sample described in last year's Annual Report. We increased our sensitivity by using ^{181}Hf as a radiochemical tracer and have established a firm upper limit of $f_{\beta} < 0.06\%$. If we exclude the possible existence of a high-spin short-lived isomer in ^{180}Lu , less than 10% of the observed abundance of ^{180}Ta can be produced through the r process.

While our work virtually closes the s- and r-process paths through ^{180}Hf , recently Yokoi and Takahashi⁵ suggested that a tiny s-process branch proceeding through ^{179}Ta may be the preferred route for the stellar production of ^{180}Ta . If ^{180}Ta is to be produced in a hot star, then possible destruction mechanisms must be considered. We established limits on the photodeactivation cross section of ^{180}Ta to 8.1 hr ^{180}Ta by exposing natural Ta foils to kilocurie strength hospital sources of ^{137}Cs and ^{60}Co γ rays. A paper based on this work and describing the effects of stellar temperatures and densities on the destruction rates of ^{180}Ta has been accepted for publication.

References:

1. H. Beer and R. Ward, *Nature* **291**, 308 (1981).
2. Nuclear Physics Laboratory Annual Report, University of Washington (1983) p. 1.
3. R. Dewberry and R. Naumann, *Phys. Rev. C* **28**, 2259 (1983).
4. E. Warde et al., *Phys. Rev. C* **27**, 98 (1983).
5. K. Yokoi and K. Takahashi, *Nature* **305**, 198 (1983).

2. NUCLEAR STRUCTURE

2.1 The β^+ Decays of ^{34}Ar , ^{34}Cl and ^{38}K

E.G. Adelberger, J.L. Osborne, H.E. Swanson, and V.J. Zeps

We have performed a series of preliminary experiments using the gas-transfer system to investigate the feasibility of measuring weak branches in the β^+ decays of ^{34}Ar , ^{34}Cl and ^{38}K . As in previous experiments,¹ the activities of interest were produced by bombarding a gas target and transporting the gas to a well-shielded counting station where the decay γ rays were counted by a large GeLi detector. A 2.5-cm lead 'hardener' was placed in front of the detector to reduce the counting rate of annihilation radiation relative to the more energetic beta-delayed γ rays. The 0.845s ^{34}Ar activity was produced by the $^{32}\text{S}(\text{He}, n)$ reaction on H_2S gas at a bombarding energy of 14.5 MeV. At the same time, the 1.526s positron decay of the daughter nucleus, ^{34}Cl was also investigated. The 3^- ground state of ^{38}K and its 0^+ isomer, the analogue of the ground state of ^{38}Ar , were produced by the reaction $^{35}\text{Cl}(\alpha, n)$ at a bombarding energy of 11 MeV, using Freon-11 (CFC1_3) as the target gas.

These decays are of interest for several reasons. Recent Ohs shell model calculations in a complete $(2s-1d)^n$ space predict the $M(0^+)$ values for most of these decay branches.² In general, the theory does extremely well in reproducing the observed ft values for all but the weakest transitions. The largest discrepancy between the calculated values and experimental data for any strong Gamow-Teller transition in the $2s-1d$ shell occurs in the decay of ^{34}Ar to the 3128 keV state in ^{34}Cl , for which the measured branch is nearly twice the calculated value. We therefore felt it would be interesting to check the experimental branching ratio. In the short preliminary runs we were able to identify all of the previously known branches from these positron decays. With a few days of data collection it should be possible to improve the statistical accuracy of these ratios branching and to extend the search to other allowed decay channels.

In the ^{34}Ar and ^{34}Cl decays and in the decay of the 0^+ isomer in ^{38}K , there is the possibility of observing isospin-forbidden $T=1 \rightarrow T=1$, $0^+ \rightarrow 0^+$ Fermi transitions. Superaligned $0^+ \rightarrow 0^+$ decays in light nuclei have been used to measure the vector coupling constant, but charge-dependent mixing alters these analogue states and necessitates small theoretical corrections. The $0^+ \rightarrow 0^+$, $T=1 \rightarrow T=1$ isospin-forbidden decays proceed only through charge-dependent mixing and thereby provide a stringent test of the calculations of charge-dependent corrections. To date, the only decay of this type that has been observed is in ^{42}Sc .³ However, it is difficult to do a good shell model calculation of the expected effects in $A = 42$. B.A. Brown⁴ has developed a shell model treatment of charge dependent mixing in the $2s-1d$ shell using the known mass splitting of isobaric multiplets to fix the parameters of the charge-dependent interaction. With these fitted charge-dependent matrix elements, Brown predicts that the $T=1 \rightarrow T=1$ forbidden Fermi transitions in ^{34}Cl or ^{34}Ar should have branchings ratio of $< 10^{-7}$. Unreasonable increases in running time or decreases in γ -ray background would be needed to detect such a

small branch.

Finally, in the decay of ^{38}K there is a first-forbidden $3^- \rightarrow 3^-$ transition to the 3810 keV state in ^{38}Ar . Using the prescription of Wilkinson and Macefield⁶ to calculate $f(E)$, and assuming a $\log(f)$ value similar to that measured for the $0^+ \rightarrow 0^+$ branch in ^{18}Ne ,⁸ we may roughly estimate a branching ratio of 10^{-4} for this transition. This should be detectable.

References:

1. Nuclear Physics Laboratory Annual Report, University of Washington (1981) p. 201.
2. B.A. Brown and B.H. Wildenthal, to be published in At. Data and Nucl. Data Tables.
3. P.D. Ingalls, J.C. Overley, and H.S. Wilson, Nucl. Phys. A 293, 117 (1977)
4. B.A. Brown, Bull. Am. Phys. Soc. 29, 678 (1984).
5. D.H. Wilkinson and B.E.F. Macefield, Nucl. Phys. A 232, 58 (1974).
6. E.G. Adelberger, C.D. Hoyle, H.E. Swanson, and R.D. Von Lintig, Phys. Rev. Lett. 46, 695 (1981).

3. GIANT RESONANCES

3.1 Schematic Model Calculations of Nucleon Decay Strengths from Giant Dipole Resonances Built on Excited States

J.A. Behr and K.A. Snover

A simple relation between experimental (p, γ) giant dipole resonance integrated strengths and spectroscopic factors from proton stripping reactions has been noted.¹ This relation has been explained within the context of an independent-particle direct emission model; it also follows from the simple schematic model of the GDR in the limit of equal decay penetrabilities for all decay channels.² We have now used the schematic model to calculate nucleon decay branching ratios to various excited states following photoexcitation of the GDR; the effects of Coulomb plus centrifugal barrier penetration have now been explicitly included.

The schematic model, in the extreme limit in which we employ it, treats the GDR as a sum of $1p-1h$ dipole excitations in a harmonic oscillator basis. We identify residual configurations produced by nucleon decay of these $1p-1h$ excitations directly with excited states in the daughter nucleus. Escape probabilities of the excited nucleons are treated using Coulomb penetrabilities in an R-matrix formalism. Branching ratios are calculated by integrating over the shape of the GDR.

Branching ratios calculated for ground-state ^{16}O and ^{28}Si (γ , nucleon) reactions have been compared with experiment. For ^{16}O , the relative branching ratios to $p_{3/2}$ and $p_{1/2}$ neutron and proton hole states are calculated correctly within experimental error. In this case, barrier penetration effects are essential; if they are not included, the model predicts far too much $p_{3/2}$ strength. For ^{28}Si , calculated decays to eight proton hole states produce fair agreement with experiment. However, the dominant branch, proton decay to the ground state of ^{27}Al , is calculated to be a factor of two too strong, independent of the details of the calculation. This over-predicted p_0 strength appears to be a clear indication of the need for a statistical component of the ground-state GDR in ^{28}Si with a relative strength (spreading width)/(total width) of about 50%.

The calculation is currently being extended to (nucleon, γ) reactions populating GDR's on excited states, where much more experimental data exist.

References:

1. D.H. Dowell, G. Feldman, K.A. Snover, A.M. Sandorfi, M.T. Collins, Phys. Rev. Lett. **50**, 1191 (1983).
2. Nuclear Physics Laboratory Annual Report, University of Washington (1983) p. 18. See also "Giant Resonances Built on Highly Excited States," K.A. Snover, Proceedings of the International Symposium on Highly Excited States and Nuclear Structure, Orsay, France, Sept. 1983, Editions de Physique, to be published.

3.2 Compound Nuclear Isospin Purity and the Statistical Decay of the GDR in Light Nuclei

D.H. Dowell, G. Feldman, M.N. Harakeh, C.A. Gossett, R. Loveman,
T. Murakami, J.L. Osborne, and K.A. Snover

In light self-conjugate nuclei the study of statistical excited-state GDR decays can provide a sensitive measure of compound nuclear isospin purity at moderate excitation energies. This follows from the well-known selection rule for $N=Z$ nuclei that $E1$ decays must change isospin; hence an $E1$ decay from a $T=0$ state must go to a $T=1$ final state, and vice versa. Thus, if isospin is good, one expects an inhibition for statistical GDR decays from a $T=0$ entrance channel, since the density of $T=1$ final states at moderate excitation energies is much less than the density of $T=0$ states. The sensitivity to the isospin purity in such an experiment scales as the final-state level density ratio $\rho(T=0)/\rho(T=1)$, which can easily be greater than a factor of 10, making this method much more sensitive than many other types of experiments which have been previously employed. The restriction to moderate energies follows from two considerations: If the energy is too high, then 1) the level density ratio $\rho(T=0)/\rho(T=1)$, and hence the sensitivity, drops, and 2) high energy γ -ray decays from daughter nuclei become important, further washing out the effect. This limits the sensitivity to E_x (initial) < 30 MeV + $E_{\text{GDR}} - 50$ MeV in light nuclei.

We have made two different types of measurements of these effects in the $A = 24 - 28$ mass region. The first is $^{12}\text{C} + ^{16}\text{O}$ at excitation energies similar to those studied in $^{25}\text{Mg} + ^4\text{He}$ (see last year's Annual Report¹). Here, one directly sees the effect of isospin purity in the strong inhibition of high energy γ -ray production in $^{12}\text{C} + ^{16}\text{O}$ ($T=0$ entrance channel) relative to $^{25}\text{Mg} + ^4\text{He}$ ($T=0 + T=1$). The spectrum shape and a preliminary analysis for 40 MeV $^{12}\text{C} + ^{16}\text{O}$ are shown in Fig. 3.2-1. For $E_\gamma > 13$ MeV the yield comes

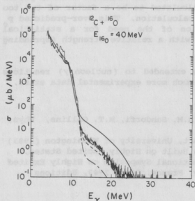


Fig. 3.2-1 Gamma rays from $^{12}\text{C} + ^{16}\text{O}$, $E(^{16}\text{O}) = 40$ MeV, $E(^{28}\text{Si}^*) = 34$ MeV. Cascade calculations: solid line - completely mixed isospin; long dash - 3% isospin mixing; short dash - pure isospin, all curves $E1 + E2$; long-short dash - $E2$ only.

mainly from the initial compound nucleus and is much less than the mixed isospin limit. However, the measured yield is somewhat larger than the pure isospin calculation, requiring about 3% isospin mixing in the initial compound nucleus. This is about five times less than other experiments have indicated for lower excitation energies.

The second type of measurement consists of comparing $^{12}\text{C} + ^{12}\text{C}$, $^{12}\text{C} + ^{13}\text{C}$ and $^{13}\text{C} + ^{13}\text{C}$ reaction yields. The latter two reactions lead to N=Z compound nuclei and hence have "normal" γ -ray yields, whereas high energy γ -ray yields from $^{12}\text{C} + ^{12}\text{C}$ are again observed to be strongly inhibited. Spectrum shape analyses for all of these reactions, including $^{12}\text{C} + ^{16}\text{O}$ and $^{24}\text{Mg} + ^3\text{He}$, lead to similar GDR energies and widths. Quantitative analysis of the C + C data is complicated by the presence of strong individual lines at low ($E_\gamma \sim 4-7$ MeV) gamma ray energy. Preliminary fits indicate somewhat less isospin inhibition for $^{12}\text{C} + ^{12}\text{C}$ than for $^{12}\text{C} + ^{16}\text{O}$, but this conclusion is sensitive to details of the statistical analysis. Final analysis for the various isotopes is in progress including all the effects of individual level densities, GDR parameters and isospin mixing in a proper, self-consistent manner.

References:

1. Nuclear Physics Laboratory Annual Report, University of Washington (1983) p. 16.

3.3 Statistical GDR Decays over a Wide Range of Energy from the $^{63}\text{Cu}^*$ Compound Nucleus

E.F. Garman, J. Gundlach, G. Feldman, M.N. Harakeh, J.A. Behr, J.L. Osborne, and K.A. Snover

As a follow-up investigation of statistical GDR emission from highly excited states in medium mass nuclei, we have made a study of $^{63}\text{Cu}^*$ over a wide range of excitation energy. We have formed this compound nucleus via $\alpha + ^{59}\text{Co}$ for a range of different initial excitation energies $E_x = 16.9$ to 28.2 MeV, and via $^{12}\text{C} + ^{51}\text{V}$ for $E_x = 34.7$ to 52.3 MeV.

The experiments were performed using pulsed ^4He and ^{12}C beams, which permitted the direct measurement of the inclusive γ -ray production cross section. Neutron-induced events from the target were eliminated by time-of-flight (time resolution was 3-4 nsec). And γ -rays were detected in the large NaI spectrometer. All spectra have an apparently statistical shape, with an exponentially falling intensity between 6 and 10 MeV and a broad bump in the region of the GDR ($E_\gamma \sim 10-20$ MeV).

The data have been fitted to obtain the GDR strength function using a modified version of the statistical code Cascade. The excitation energy,

width and strength of the GDR were extracted, the GDR being parameterized as a Lorentzian. Preliminary results indicate a confirmation of the small (-5-10%) downward shift in the resonance energy of the excited-state GDR decays, as compared to the ground-state GDR. Also apparent is the surprising feature that the excited state GDR strength is significantly less than one Energy Weighted Sum Rule (EWSR). In this mass region the ground state GDR is known experimentally to exhaust approximately one EWSR. The reduced strength for the excited state GDR decays depends quantitatively on knowledge of the accuracy of the Cascade description of the statistical process. This is confirmed in detail by the data of Parker *et al.*² This puzzling strength reduction is not understood.

Reference:

1. E.F. Garman, K.A. Snover, S.H. Chew, S.K.B. Hesmondhalgh, W.N. Catford, and P.M. Walker, Phys. Rev. C 28, 2554 (1983).
2. D. Parker, J. Asher, T.W. Conlon, and I. Naqib, Harwell Internal Report AERE-R-10408 and private communication.

3.4 Statistical GDR Decays in $^{16}\text{O} + \text{Ni}$ for Various Ni Isotopes

E.F. Garman, J. Gundlach, G. Feldman, M.N. Harakeh, J.A. Behr, J.L. Osborne, and K.A. Snover

In addition to studying $^{63}\text{Cu}^*$ decays over a wide excitation energy range, as described in the preceding section of this report, we are also examining the inclusive γ -ray production cross section for $^{16}\text{O} + ^X\text{Ni}$ - induced reactions over a wide range of nickel isotope number ($X = 58$ to 64). Results have been obtained to date for 60-MeV $^{16}\text{O} + ^{58,61,64}\text{Ni}$. Preliminary Cascade fits to the ^{61}Ni and ^{64}Ni data indicate similar GDR parameters: GDR resonance energies $E_G \approx 15.5$ MeV, widths $\Gamma \approx 5.5$ MeV and strengths $S_{E1} \approx 0.33$ in units of the classical dipole sum rule. The resonance energies are similar to, and the widths somewhat narrower than the $^{16}\text{O} + ^{58}\text{Ni}$ results previously reported.¹ This pulsed-beam singles experiment, in contrast to the previous coincidence experiment,¹ has a well-determined absolute cross section, and thus is sensitive to S_{E1} , the average GDR strength built on excited states. These results, as with the $^{63}\text{Cu}^*$ study (see Sec. 3.3), indicate a surprisingly small value for S_{E1} : a typical value for ground-state GDR strength in this region is $S_{E1} \approx 1$. The accuracy of essential aspects of the Cascade calculation pertinent to extracting this strength, such as reasonable values for the fusion cross section, is substantiated by comparison with $^{16}\text{O} + \text{Ni}$ reaction data in the literature.

Reference:

1. E.F. Garman, K.A. Snover, S.H. Chew, S.K.B. Hesmondhalgh, W.N. Catford, and P.M. Walker, Phys. Rev. C 28, 2554 (1983).

3.5 Study of Excited-State GDR's in the 1f-2p Shell Nuclei

J.A. Behr, D.H. Dowell, G. Feldman, E.F. Garman, C.A. Gossett,
J. Gundlach, M.N. Harakeh, R.A. Loveman, J.L. Osborne, and
K.A. Snover

An earlier study of the $^{27}\text{Al}(p,\gamma)^{28}\text{Si}^*$ reaction revealed a series of GDR's built upon excited states in ^{28}Si up to $E_X^f = 14.36$ MeV.^{1,2} We are continuing our investigation of the properties of excited-state GDR's by studying (p,γ) reactions in the $f_{7/2}$ nuclei ($A = 45-60$). Our emphasis is on understanding how the (p,γ) GDR capture strength is related to the single-proton stripping spectroscopic factors $C^2S_p^*$ for states in these nuclei up to $E_X^* = 8$ MeV. We will also study statistical γ -ray spectra from heavy-ion fusion reactions forming the same compound system to determine the extent to which the observed (p,γ) strength comes from statistical decay of a thermally equilibrated compound nucleus.

Several targets in the $f_{7/2}$ shell were chosen to yield a combined system with interesting $C^2S_p^*$ distributions below 10 MeV, including strong, resolvable states. Data have already been obtained for the $^{45}\text{Sc}(p,\gamma)^{46}\text{Ti}^*$ and $^{51}\text{V}(p,\gamma)^{52}\text{Cr}^*$ reactions from $E_p = 4-15$ MeV ($E_X = 14-25$ MeV) at $\theta_\gamma = 90^\circ$, in addition to five-point angular distributions for $E_p = 7, 11, 15$ MeV. The statistical reaction $^{46}\text{Ti}(\alpha,\gamma)^{50}\text{Cr}^*$ has also been studied at $E_\alpha = 24$ and 17.2 MeV ($E_X = 32$ and 25 MeV). We plan to extend the (p,γ) excitation functions up to $E_p = 24$ MeV ($E_X = 34$ MeV), and also possibly to study the $^{28}\text{Si}(^{18}\text{O},\gamma)^{46}\text{Ti}^*$ statistical reaction and the $^{52}\text{Cr}(p,\gamma)^{53}\text{Mn}^*$ reaction.

Our results indicate that the γ -ray strength distribution does in fact correspond qualitatively with the proton stripping strength. An example is shown in Fig. 3.5-1 for the case of $^{51}\text{V}(p,\gamma)^{52}\text{Cr}^*$ at $E_p = 8$ and 15 MeV ($E_X = 18.4$ and 25.2 MeV). For the higher bombarding energy three distinct regions can be identified and compared to the plot of spectroscopic strength³ -- a low-lying $\ell=3$ ($f_{7/2}$) region, an intermediate $\ell=1$ ($p_{3/2}$) section, and a high-lying ($E_X^f > 7$ MeV) mixed $\ell=1$ and $\ell=3$ ($p_{1/2}$ and $f_{5/2}$) region. At lower proton energies, statistical contributions are expected to be more apparent, as evidenced by the smoothly rising part below $E_\gamma = 14$ MeV in the $E_p = 8$ MeV

case. It is interesting to note that the observed strength in the region near $E_x^F = 3.5-4.5$ MeV is in excess of that expected from the spectroscopic information, again qualitatively consistent with strong statistical contributions at low E_p . Another feature present in this spectrum is the enhancement of the highest energy γ rays near $E_\gamma = 18$ MeV (close to the peak of the ground state GDR).

Analysis is proceeding on the (p, γ) data using a lineshape deconvolution technique. The states used in the fitting are taken to be those populated strongly in proton stripping. Excitation functions for the various states will be generated, and the integrated $\sigma(\gamma, p_0)$ strengths obtained from these excitation functions will serve to test microscopic schematic model calculations of semi-direct decay strengths (see Sec. 3.1 of this Report). The statistical γ -ray spectra from the heavy-ion fusion reactions are being analyzed with the compound nuclear evaporation code Cascade.

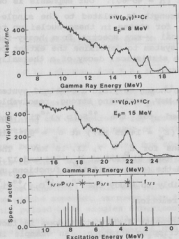


Fig. 3.5-1 Gamma-ray spectra from the $^{52}\text{V}(p, \gamma)^{52}\text{Cr}^*$ reaction at two different bombarding energies. Below is the spectroscopic strength distribution for $E_x < 10$ MeV in ^{52}Cr obtained from the $(^3\text{He}, d)$ proton stripping reaction.³ Values shown are $[(2J_F + 1)/(2J_i + 1)]C^2S_p^+$. All three plots are shifted so as to align excitation energy in the vertical direction.

References:

1. D.H. Dowell, G. Feldman, K.A. Snover, A.M. Sandoz and M.T. Collins, Phys. Rev. Lett. 50, 1191 (1983).
2. Nuclear Physics Laboratory Annual Report, University of Washington (1983) p. 17.
3. J.R. Beene, Nucl. Data Sheets 25, 235 (1978).

3.6 Deformation Effects in the Statistical Decay of the Giant Dipole Resonance

J.A. Behr, G. Feldman, C.A. Gossett, T. Murakami, J.L. Osborne, and K.A. Snover

Very little is known about the degree of persistence of nuclear deformation at finite temperature. The effect of static deformation leading to a splitting of the GDR in ground-state photo-induced reactions in deformed rare earth nuclei is well-established. We have begun a study of the radiative emission of γ rays in complex particle collisions in several systems in the deformed rare-earth region. A deformation of excited nuclear states is expected to split or to broaden the GDR strength function required to account for high energy ($E_\gamma > 10$ MeV) statistical gamma-ray emission.

A measure of the effects of deformation on excited-state GDR's is obtained by comparing the gamma-ray yields from reactions in which the compound nucleus has low-lying levels which are highly deformed with those in which the compound nucleus has low lying levels which have little or no deformation. In particular, we have studied $^{12}\text{C} + ^{148}\text{Sm}$ and $^{12}\text{C} + ^{154}\text{Sm}$ for a ^{12}C incident energy of 63 MeV, in addition to $\alpha + ^{148}\text{Sm}$ and $\alpha + ^{154}\text{Sm}$ for $E_\alpha = 24$ and 27 MeV. A comparison of the gamma-ray spectra measured at $\theta_\gamma = 90^\circ$ for the alpha induced reactions is shown in Fig. 3.6-1. The additional structure observed in the high energy gamma yield for the $\alpha + ^{154}\text{Sm}$ reaction when compared to $\alpha + ^{148}\text{Sm}$ provides evidence of the splitting of the GDR strength function due to nuclear deformation at elevated nuclear temperatures. Results for the spectral shapes from the $^{12}\text{C} + ^{148}\text{Sm}$ and $^{12}\text{C} + ^{154}\text{Sm}$ reactions are currently being analyzed. Statistical model calculations from the code Cascade will be compared with the data in order to extract the energy, width and strength parameters for the GDR strength functions. These parameters will then provide quantitative information about the average deformation of excited states in the compound nucleus. Currently, we are looking for the effects of deformation on the angular distribution of emitted γ rays.

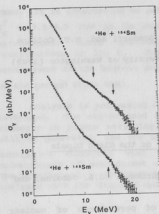


Fig. 3.6-1 Gamma-ray spectra from the $\alpha + {}^{148}\text{Sm}$ and $\alpha + {}^{154}\text{Sm}$ reactions for $E_\alpha = 27$ MeV. Neutron backgrounds were reduced using pulsed beam techniques and the data have been corrected for small (<1% by weight) carbon and oxygen contamination. The arrows indicate the energy locations of the ground state GDR's.

3.7 Excited-State Giant Resonances Observed in the ${}^{39}\text{K}(p,\gamma){}^{40}\text{Ca}$ and ${}^{40}\text{Ca}(p,\gamma){}^{41}\text{Sc}$ Reactions

D.H. Dowell, C.A. Gossett, L. Ricken,* A.M. Sandorfi,[†] and K.A. Snover

The study of excited-state giant dipole resonances using the (p,γ) reaction has become a new means of examining single-particle strength at high excitation. The nuclear configurations upon which GDR's are built in energetic (p,γ) reactions are those in which a single proton is coupled to the ground state of the target nucleus. The integrated GDR strengths, which are proportional to the proton transfer spectroscopic factors, provide quantitative information on single-particle strength at excitation energies well above those studied in conventional proton stripping reactions.

We have begun a study of excited-state giant resonances in the ${}^{39}\text{K}(p,\gamma){}^{40}\text{Ca}$ and ${}^{40}\text{Ca}(p,\gamma){}^{41}\text{Sc}$ reactions. The excited states upon which one expects GDR's to be built in these reactions are those of relatively simple nuclear configuration. In particular, the states populated in ${}^{40}\text{Ca}(p,\gamma){}^{41}\text{Sc}$ are those which look like a single proton coupled to doubly magic ${}^{40}\text{Ca}$, for example the $1f_{7/2}$, $2p_{3/2}$, $2p_{1/2}$, $1f_{5/2}$, and $1g_{7/2}$ single-proton states. States which resemble an f , p , or g proton coupled to the $d_{3/2}$ proton hole in ${}^{39}\text{K}$ are strongly populated in the ${}^{39}\text{K}(p,\gamma){}^{40}\text{Ca}$ reaction.

We have measured ${}^{39}\text{K}(p,\gamma){}^{40}\text{Ca}$ and ${}^{40}\text{Ca}(p,\gamma){}^{41}\text{Sc}$ cross sections at $\theta_\gamma = 90^\circ$ for $E_p = 10$ -36 MeV using the two-stage and three-stage tandem accelerators

at Brookhaven National Laboratory. Sample gamma-ray spectra for $^{39}\text{K}(p,\gamma)^{40}\text{Ca}$ at $E_p = 18$ MeV and for $^{40}\text{Ca}(p,\gamma)^{41}\text{Sc}$ at $E_p = 25$ MeV are shown in Fig. 3.7-1. Also illustrated are the proton stripping spectroscopic factors, $^1 C^2 S_p^+$. Strong correlation between the structure in the (p,γ) cross section and the distribution of stripping strength is observed. Evidence of a large concentration of single-particle strength at $E_x^f \approx 9.6$ MeV not previously observed in proton stripping is seen in the $^{39}\text{K}(p,\gamma)^{40}\text{Ca}$ data. We also find a broad concentration of strength near $E_x^f \approx 14.5$ MeV in ^{40}Ca . We observe structure in the final-state single-particle strength distribution in the $^{40}\text{Ca}(p,\gamma)^{41}\text{Sc}$ reaction up to $E_x^f \approx 10$ MeV, and evidence for excited-state GDR's built upon broad distributions of single-particle strength in ^{41}Sc up to $E_x^f \approx 23$ MeV.

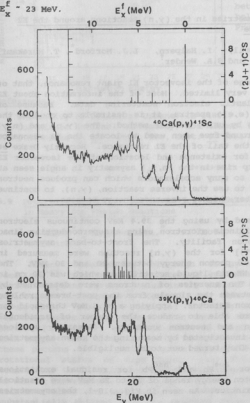


Fig. 3.7-1 Gamma-ray spectra at $\theta = 90^\circ$ from $^{39}\text{K}(p,\gamma)^{40}\text{Ca}$ for $E_p = 18$ MeV ($E_x^f = 25.9$ MeV) and $^{40}\text{Ca}(p,\gamma)^{41}\text{Sc}$ for $E_p = 25$ MeV ($E_x^f = 25.5$ MeV).^P Since the ground-state GDR's in ^{40}Ca and ^{41}Sc are located at excitation energies of approximately 20 MeV, one expects to be at the peak of the GDR for final states near $E_x^f \approx 5-6$ MeV at these proton energies. The distribution of proton-stripping spectroscopic strengths from Ref. 1 are displayed in the insert above each gamma-ray spectrum.

We are currently analyzing the $^{39}\text{K}(p,\gamma)^{40}\text{Ca}$ and $^{40}\text{Ca}(p,\gamma)^{41}\text{Sc}$ spectra in terms of a line-shape decomposition in order to extract (p,γ) strengths. We plan to use the GDR strengths obtained in this analysis to determine single-particle spectroscopic strengths in ^{40}Ca and ^{41}Sc up to $E_x \approx 20$ MeV.

References:

- * Ruhr-Universität Bochum, West Germany.
- † Brookhaven National Laboratory, Upton NY 11973.
- 1. P.M. Endt and C. Van der Leun, Nucl. Phys. A 310, 1 (1978)

3.8 Forward-to-Backward Asymmetries in the (γ,n) Reactions around the E2 Isovector Giant Resonance

P.T. Debevec, * D.H. Dowell, I. Halpern, L.J. Morford*, T. Murakami, D.W. Storm, D.R. Tieger, and S.A. Wender†

Compared with our knowledge of the isovector E1 giant resonance, that of the isovector E2 resonance is very limited. Most of the information about E2 has been obtained from inelastic electron scattering data. Because of uncertain backgrounds in the (e,e') spectra, it is desirable to confirm the suggested resonance parameters by using another method. The (γ,n) and (n,γ) reactions are virtually background-free when used to locate the E2 resonance through its interference with the tail of the E1 resonance. Recently Drake et al. found striking evidence for existence and location of the isovector E2 giant resonance, namely a sharp rise in the (n,γ_0) asymmetry in angle seen at ≈ 23 MeV.¹ Since there are not so many accelerators which can produce neutron beams above 20 MeV, we decided to use the inverse reaction, (γ,n) , to continue the same investigation to lighter, higher-resonance-energy targets.

Experiments were performed by using the 39.4 MeV continuous electron beam from the University of Illinois microtron using a superconducting linac (MUSL-2) and the tagged photon facility. The front-to-back asymmetries $[Y(55^\circ) - Y(125^\circ)]/[Y(55^\circ) + Y(125^\circ)]$ for the (γ,n) reaction were measured in three targets as a function of photon energy between 20 and 30 MeV. The neutrons were measured by an NE-213 liquid scintillator which was 30 cm in diameter and 5.1 cm thick. The energies of neutrons were determined by measuring the time interval between the signals from the post-bremsstrahlung electron counters and the neutron detector. Applying a ≈ 6.5 MeV threshold for the neutron detector, we were able to reduce the number of accidental coincidences between electron and neutron counters. Possible spurious asymmetries of the system were investigated by measuring the known asymmetries of the $^{16}\text{O}(\gamma,n_0)^{16}\text{O}$ reaction. They turned out to be negligible.

The asymmetry curves for ^{208}Pb and $^{208}\text{Pb}^{\text{nat}}$ for residual excitations between 0 and 4 MeV in the photon energy range of 20 to 26 MeV were identical within the experimental uncertainties. As seen in Fig. 3.8-1, the asymmetries

were about 0.2 for the lower photon energies and made a transition near $E_{\gamma} = 23$ MeV to ≈ 0.6 for the higher energies. For ^{nat}Cd the pattern was similar but the transition region was about 4 MeV higher, consistent with the expected $A^{-1/3}$ dependence of the locations of giant resonances. The detailed analysis of the energy dependence of the asymmetry, using the direct-semidirect model, is in progress.

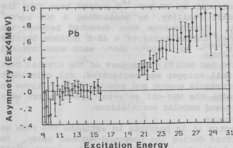


Fig. 3.8-1 Asymmetry curve for ^{nat}Pb for residual excitations between 0 and 4 MeV. The data below $E_{\gamma} = 16$ MeV are due to Professor P.T. Debevec.

References:

- * University of Illinois, Urbana, IL 61801.
- † Los Alamos National Laboratory, Los Alamos, NM 87545.
- 1. D.M. Drake et al., Phys. Rev. Lett. **47** 1581 (1981).

3.9 Determination of a Time Scale for the Emission of High Energy Photons in Heavy Ion Fusion Reactions

D. Habs,* W. Hennerici,* R. Kroth,* A. Lazzarini, V. Metag,† and J. Schirmer

Recent observations of high energy γ -rays emitted in (HI, Xn) reactions¹⁻⁶ have been interpreted as evidence for the existence of highly excited compound nuclear states in the nuclear continuum which are themselves collective excitations.⁷ Central to this interpretation are several assumptions. These are that i) the high energy photons originate from electromagnetic transitions between unbound states. The high energy of the photons (10-20 MeV) and their observed emission probability ($\approx 10^{-4}$ /fusion) both support this assumption. ii) the states of the compound system emitting these photons are collective giant dipole resonance excitations built upon rotational states of high spin. iii) The multipolarity of the gamma transitions is E1. Although these assumptions seem reasonable, there has been no direct experimental verification of their validity. The results of several recent studies indicate that the centroid of the γ -ray enhancement is substantially shifted from its expected value deduced from the GDR of $E_{\gamma} =$

79A^{-1/3}.⁸ It is not yet clear whether such a shift arises from a change in the interaction leading to the GDR with increasing excitation in the nucleus. High energy transitions in heavy ion reactions have, to date, defied any quantitative analysis. Yet recent (p, γ) studies⁹ have produced unambiguous evidence that the collective excitations of lower-lying particle-hole states in nuclei in the s-d shell do exist. It would be enlightening if similar results were found in heavy ion reactions.

The measurement was performed with an 80 MeV ¹⁶O pulsed beam from the MPI Heidelberg Tandem Van de Graaff Facility, by bombarding a 400 $\mu\text{g}/\text{cm}^2$ isotopically enriched ⁵⁸Ni target. Coincidences were detected between the MPI-GSI 4 π Crystal Ball Spectrometer and an array of 4 $\Delta\text{E-E}$ surface barrier telescopes positioned at angles $\theta_{\text{lab}} = 90^\circ, 120^\circ, 160^\circ$, each with typical solid angle $\Delta\Omega = 40$ msr. 159 of the 162 NaI(Tl) detectors of the Crystal Ball were employed. Once the Crystal Ball trigger was registered, all coincident NaI(Tl) detectors were accepted. Particle energy and angular distributions in coincidence with γ rays detected with the MPI-GSI 4 π γ -ray Spectrometer were measured, along with γ multiplicity and angular correlations.

From the particle energy spectra it is possible to estimate the time at which high energy photons are emitted during the compound-nuclear decay. In addition, the multiplicities of both charged particles and γ rays yield information from which details about the spin distribution in the compound nucleus responsible for the energetic photons could be deduced. From the various correlations we have learned the following:

i) The energy spectra of the coincident charged particles reflect the energy lost to the energetic photons. This is evidence for the time-order of the emission process, indicating that the photons are being emitted promptly from the compound system in the first or second step of the decay cascade (see Fig. 3.9-1).

ii) The proton-to-alpha multiplicity, which is a sensitive probe of initial compound nucleus spin, clearly indicates that the spins associated with the emission of energetic photons are about half the mean value of angular momentum brought into the reaction.

iii) The γ multiplicities corroborate our findings in point ii) above, and further indicate that emission of energetic γ rays produces a shift of 7 - 10 \hbar in the mean spin of the population of compound nuclei producing them compared to the overall mean for the fusion reaction (see Fig. 3.9-2). Further it is possible to determine the γ -multiplicity dependence of the emission probability for energetic photons. The results are presented in Fig. 3.9-3. The integrated emission probability for $E_\gamma > 14$ MeV is 8×10^{-4} /fusion.

iv) Particle (observed at 90°)- γ angular correlations are isotropic within error. The isotropy is an expected result arising from the fact that transitions are not expected to be stretched for this case.

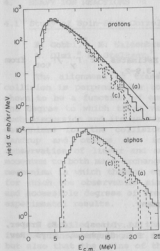


Fig. 3.9-1 Angle summed particle energy spectra in coincidence with γ rays. a) Gate on all γ . c) Gate on events for which $E_\gamma > 14$ MeV was observed. Solid curve is Cascade calculation for entire fusion cross section. Dashed curve corresponds to Cascade calculation under conditions similar to experimental gate c) above.

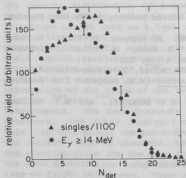


Fig. 3.9-2 γ -ray multiplicity distributions for this experiment. Singles distribution shown in triangles, coincidence with $E_\gamma > 14$ MeV shown as circles.

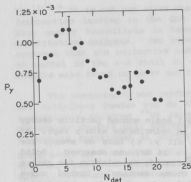


Fig. 3.9-3 Estimates of $\Gamma_\gamma / \Gamma_{tot}$ from data of Fig. 3.9-2.

References:

- * Max-Planck-Institut für Kernphysik, West Germany.
- † University of Giessen, West Germany.
- 1. J.O. Newton, B. Herakind, R.M. Diamond, E.L. Dines, J.E. Draper, K.H. Lindenberger, C. Schüick, S. Shih, and F.S. Stephens, *Phys. Rev. Lett.* **46**, 1383 (1981).
- 2. J.E. Draper, J.O. Newton, L.G. Sobotka, H. Lindenberger, G.J. Wozniak, L.G. Moretto, F.S. Stephens, R.M. Diamond, and R.J. McDonald, *Phys. Rev. Lett.* **49**, 434 (1982).
- 3. B. Haas, D.C. Radford, F.A. Beck, T. Byrski, C. Gehringer, J.C. Merdinger, A. Nourredine, Y. Schutz, and J.P. Vivien, *Phys. Lett.* **120B**, 79 (1983).
- 4. A.M. Sandorfi, J. Barrette, M.T. Collins, D.H. Hoffmann, A.J. Kreiner, D. Branford, S.G. Steadman, and J. Wiggins, *Phys. Lett.*, to be published; J. Barrette and A.M. Sandorfi, *Comments on Nucl. Part. Phys.*, to be published.
- 5. J.J. Gaardhøje, *Proceedings of the XX Winter Meeting on Nuclear Physics*, Bormio, Italy, (1982).
- 6. H. Hennerici, V. Metag, H.J. Hennrich, R. Repnow, W. Wahl, D. Habs, K. Helmer, U.V. Helmolt, H.W. Heyng, B. Kolb, D. Pelte, D. Schwalm, R.S. Simon, and R. Albrecht, *Nucl. Phys. A* **396**, 329c (1983).
- 7. D. Brink, D. Phil. Thesis, University of Oxford, 1955 (unpublished).
- 8. A. Bohr and B. Mottelson, *Nuclear Structure* (W.A. Benjamin Inc. Reading, MA, 1975), Vol. II.
- 9. D.H. Dowell, G. Feldman, K.A. Snover, A.M. Sandorfi, and M.T. Collins, *Phys. Rev. Lett.* **50**, 1191 (1983).

4. HEAVY ION REACTIONS

4.1 Study of Spin-Spin Correlations in Deep Inelastic Collisions

A. Gobbi,* K. Hildenbrand,* J. Kuzminski,* A. Lazzarini, W. Müller,*
A. Olmi,* H. Steltzer,* and J. Toke*

The alignment of transferred angular momentum in a deeply inelastic collision is perpendicular to the reaction plane and its magnitude has been shown to be a function of energy loss, scattering angle, and mass transfer. The degree to which these variables are interrelated is still a subject of much discussion and its answer may help to discriminate among several reaction mechanisms for the collision process. In the nucleon exchange model of Randrup and others the interrelationship is straightforward, and the conservation of linear and angular momentum relates the transferred angular momentum to both mass exchange and energy loss. On the other hand a reaction mechanism in which thermal equilibrium is achieved early in the collision and for which the observables simply reflect the thermalization of all intrinsic and accessible degrees of freedom has also had some success in describing the experimental results.

A detailed study of the nucleon exchange model indicates that not only is the transferred angular momentum aligned in a deeply inelastic collision, but also that the spins of the two fragments in such a collision remain very strongly co-aligned during the collision. In fact the co-alignment turns out in many cases to be greater than the alignment of the spin of either fragment relative to the reaction plane. These results can be traced to the conservation of angular momentum, which applies not only to the orbital component, but also to the randomly oriented component arising from the Fermi motion.

We have performed a measurement from which we can infer the spin-spin correlations in a deeply inelastic collision. We have exploited the fact that the angular distribution of fragments produced in the fission of a binary partner in a deeply inelastic collision is highly anisotropic, and that the anisotropy can be used as a tool to probe the alignment and magnitude of the spin of the fissioning system. Here we use a reaction in which both beam and projectile are fissile nuclei. In this manner the bulk of the deep inelastic yield results in final states in which both deeply inelastically scattered fragments have fissioned. The angular correlations of this four-body final state then contain information which may be related to the relative orientation of the spins of the two fragments before they fissioned. We have used the $^{208}\text{Pb} + ^{238}\text{U}$ reaction at $E_{\text{cm}} = 945$ MeV at the GSI Unilac to make our measurements. The four fragments were detected in an array of six avalanche detectors. One array consisted of two detectors on one side of the beam axis. In this manner the two correlated fragments arising from the fission of one nucleus could be observed, thus defining the mass transfer, energy loss and reaction plane for the deep inelastic collision. In addition, we sampled the mass distribution independently using three surface barrier detectors as time-of-flight telescopes. These were arranged on the periphery of the active area of one of the avalanche detectors. On the other side of the beam axis, a

matrix of four position-sensitive avalanche detectors was used to detect the pair of coincident fragments from the other nucleus. The angles of emission of the four fission fragments can be deduced, and these are the relevant quantities which are to be compared with theoretical calculations. By selecting both in-plane and out-of-plane angles on one side of the beam it is possible to observe the variations in the anisotropy of the other two fragments emitted by the other reaction partner. In this manner it is possible to determine the degree of correlation of the spins of the two deeply inelastic fragments.

Work is now in progress to analyze the experimental results.

Reference:

- * GSI, Darmstadt, West Germany

4.2 Nuclear Rainbow Scattering with Carbon Isotopes

H.G. Bohlen,* J.G. Cramer, B. Gebauer,* H. Michachaka,* W. von Oertzen,* and Chen Xue-shi*

The phenomenon of nuclear rainbow scattering or "far-side" scattering observed in elastic scattering with projectiles of $Z = 1 - 3$ has provided valuable insights into interaction potentials and light ion reaction mechanisms. Until recently there had been no evidence that projectiles with $Z > 3$ could exhibit such nuclear-rainbow/farside scattering effects. However, within the past two years groups at CERN¹ and at the Hahn-Meitner Institute² have observed the clear signature of this phenomenon in $^{12}\text{C} + ^{12}\text{C}$ scattering at laboratory bombarding energies above about 20 MeV/nucleon. It is therefore of considerable interest to determine if heavier systems can also show nuclear rainbow scattering effects.

Using the VICKSI accelerator system at the Hahn-Meitner Institute we have investigated this question for the systems $^{12}\text{C} + ^{16}\text{O}$, $^{13}\text{C} + ^{12}\text{C}$, and $^{13}\text{C} + ^{14}\text{C}$ with a ^{12}C beam at 22 and 25 MeV/nucleon and ^{13}C beam at 18 and 22 MeV/nucleon. Preliminary analysis indicates that the $^{13}\text{C} + ^{12-14}\text{C}$ systems show clear nuclear-rainbow/farside effects while the $^{12}\text{C} + ^{16}\text{O}$ system shows little evidence of this phenomenon.

References:

- * Hahn-Meitner-Institut für Kernforschung, Berlin, West Germany.
- 1. M. Buenerd, et al., Phys. Lett. 102B, 242 (1981).
- 2. H. G. Bohlen, M. R. Clover, G. Ingold, H. Lettau, and W. von Oertzen, Z. Phys. A 308, 121 (1982).

4.3 Penetrability of the Centrifugal Barrier and the Spin Distribution of the Compound Nucleus

D. Abriola,* P. DeYoung,* S. Gil, A. Lazzarini, D.-K. Lock, R. McGrath,*
A. Ray, and R. Vandenbosch

We have continued our studies of the penetrability of the centrifugal barrier and its effect on the spin distribution of the compound nucleus in heavy ion collisions.¹ This year we have performed a series of experiments to measure the total fusion cross section and the first moment of the gamma ray multiplicity M_γ utilizing an experimental technique previously described.^{1,2} We used the systems: α , ^{12}C , ^{16}O and ^{28}Si on ^{154}Sm .

The basic motivation of this study is to test experimentally the implication that if the observed broadening of the spin distribution of the compound nucleus at near-barrier energies² is due primarily to the penetrability of the centrifugal barrier, then one would expect that this broadening should increase as the reduced mass of the entrance channel increases. The underlying physics of this effect can easily be seen by recalling that the effective potential V_{eff} for the entrance channel can be written as the sum of nuclear, Coulomb, and centrifugal potentials. At the effective interaction distance R_0 , where V_{eff} reaches its maximum, we have the condition

$$\frac{\partial V_{\text{eff}}}{\partial l} = \frac{(2l+1)\hbar}{2\mu R_0^2}, \text{ where } R_0 = r_0 \left[A_1^{1/3} + A_2^{1/3} \right]$$

As the mass of the projectile changes, μ and R_0 vary. For the cases of α , ^{12}C , ^{16}O and ^{28}Si on ^{154}Sm , the values of μR_0^2 are in the ratio of 1 : 3.5 : 5 : 9 respectively. If the curvature of V_{eff} for the different systems does not change drastically at the effective interaction distance R_0 the penetrability T_l should show a slower variation with l for heavier projectiles.

All these experiments were performed using our local facilities, except for the system $^{28}\text{Si} + ^{154}\text{Sm}$, which was measured using the superconducting booster facility of SUNY at Stony Brook. The data analysis for this experiment has not yet been completed.

The first moment of the spin distribution, the average angular momentum $\langle L \rangle$, is deduced from M_γ as discussed in Ref. 2. Since our experimental technique only allows us to measure the reaction cross section of (HI, xn) for a single residue channel xn, we have used the relative yield predicted for these reactions by the statistical decay code CASCADE³ to estimate the total fusion cross section. This procedure was tested for the case of $^{16}\text{O} + ^{154}\text{Sm}$, where the yields are known experimentally⁴ and these results are nicely reproduced within a few percent.

In order to be able to compare the results of the different systems studied on the same footing, we found it useful to introduce the concept of

$\#_{\text{crit}}$ defined as

$$\sigma_{\text{fus}} = \frac{\pi}{k^2} \#_{\text{crit}} (\#_{\text{crit}} + 1).$$

In the extreme sharp cut-off model, $\#_{\text{crit}}$ would be the number of partial waves that are required to be removed from the elastic channel in order to obtain the experimental reaction cross section. Within this model one would also have $\#_{\text{crit}} = 1.5 \langle L \rangle$, corresponding to a triangular distribution.

In Fig. 4.3-1 we present our experimental results for the cases of α , ^{12}C and ^{16}O , together with the fits obtained using a one dimensional parabolic barrier penetration model, including deformation as discussed by Wong.⁵ The error bars in $\langle L \rangle$ include both the uncertainties in the measured multiplicities as well as the uncertainties in converting them to angular momentum as described in Ref. 2.

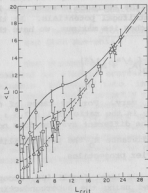


Fig. 4.3-1 $\langle L \rangle$ vs. $\#_{\text{crit}}$. Experimental results of $\langle L \rangle$ and $\#_{\text{crit}}$ obtained from M_{f} and σ_{fus} respectively, as described in the text. Full dots correspond to ^{16}O , squares to ^{12}C , and triangles to α . The calculations were all done using a one-dimensional parabolic barrier penetration model including deformation. The full line corresponds to ^{16}O , dashed line to ^{12}C and, dotted line to α . For the sharp cut-off model one expects $\langle L \rangle = 1.5 \#_{\text{crit}}$.

Our results clearly reproduce the expected results, namely that the larger the mass of the projectile the larger the deviation from the extreme sharp cut-off model for a given value of $\#_{\text{crit}}$, and consequently the broader the spin distribution. Also we see that as the energy increases (and so does $\#_{\text{crit}}$), the relation between $\langle L \rangle$ and $\#_{\text{crit}}$ tends to approach that of the sharp cut-off model.

References:

- * Nuclear Structure Laboratory, SUNY Stony Brook, NY 11794.
- 1. Nuclear Physics Laboratory Annual Report, University of Washington (1983) p. 21.
- 2. R. Vandenbosch, B.B. Back, S. Gil, A. Lazzarini, and A. Ray, Phys. Rev. C 28, 1161 (1983).
- 3. F. Puhlhofer, Nucl. Phys. A 280, 267 (1977).
- 4. R.G. Stockstad, Y. Eisen, S. Kaplanis, D. Pelte, U. Smilansky, and I. Tserruya, Phys. Rev. C 21, 2427 (1980).
- 5. C.-Y. Wong, Phys. Rev. Lett. 31, 766 (1973).

4.4 Search for High Spin States in ^{32}S

K.J. Davis, S. Gil, M. Hindi, A. Lazzarini, K.T. Lesko, D.-K. Lock, T. Murakami, A. Ray, and R. Vandenbosch.

Continuing our effort to locate the higher members of the yrast line in ^{32}S , this year we have performed a series of experiments in order to locate the particle unbound members of the band by using a particle-particle coincidence method.

We have explored the possibility of using the following reactions for populating the unbound states in ^{32}S :

- a. $^{24}\text{Mg}(^{12}\text{C}, \alpha)^{32}\text{S}$
- b. $^{28}\text{Si}(^{16}\text{O}, ^{12}\text{C})^{32}\text{S}$

While the first of these reactions did not show the desired selectivity for populating discrete states in the excitation energy region of interest, $E_x \approx 10\text{--}20$ MeV, the second reaction did show a good selectivity, and therefore this reaction was chosen for our subsequent experiments.

By means of a preliminary run we found that the main decay mode of these unbound states in ^{32}S was through α emission. We also found that at least two states in ^{32}S , at $E_x = 11.0(\pm 0.4)$ MeV and $12.5(\pm 0.4)$ MeV, strongly decay to the ground state of ^{28}Si .

For the determination of the spins of these states we adopted an angular correlation method² which can yield a model-independent spin assignment for the intermediate state in the reaction $^{28}\text{Si}(^{16}\text{O}, ^{12}\text{C})^{32}\text{S}(\alpha)^{28}\text{Si}(\text{g.s.})$. If the ^{12}C is observed along the beam axis, then the angular correlation function between the ^{12}C and α is proportional to the square of a Legendre polynomial $P_l(\cos\theta)^2$, where l is the angular momentum carried out by the α particle, and is equal to the spin J of the excited state in ^{32}S .

In order to observe the ^{12}C at small angles we used our momentum filter³ (m.f.) and blocked the elastically scattered ^{16}O . For technical reason the m.f. was placed at $\Theta_{\text{m.f.}} = 4 \pm 1.5^\circ$ rather than at 0° . A Bragg curve spectrometer⁴ was placed at the end of the m.f. for detecting the ^{12}C and operated in coincidence with a position sensitive detector (p.s.d.) for detecting the α particle and its position. The p.s.d. covered an angular range between 95° and 140° ($\approx 40^\circ$ range in the c.m. system), with an angular resolution of $\approx 1^\circ$. This setup allowed us to detect states with spins $J \geq 5$. For lower spin states the period of the angular oscillations is larger than the angular range of the p.s.d.

The results of the α angular distribution for the states mentioned above did not show any appreciable angular structure. These results are consistent with the fact either that these states are not simple states, i.e., there may be two or more states unresolved at each of these energies, washing out the angular structure, or that these states have spin lower than ≈ 5 , in which case the period of the angular oscillations would be too large to be detected with our set-up. This last possibility would also be consistent with the observed result that for these states, the branching ratio for the decay to the g.s. of ^{28}Si was larger than the corresponding decay to the 2^+ ($E_x = 1.78$ MeV). According to estimates obtained using transmission coefficients from an optical model calculation, this is expected to be the case for low spin states.

Summarizing the results of our studies of ^{32}S , through a particle-gamma coincidence experiment reported previously² we have been able to detect the gamma-decay properties of four levels at $E_x = 6.763$, 7.46, 8.3 and 8.5 MeV. The $E_x = 6.763$ MeV level was assigned $J^\pi = 5^-$, $E_x = 7.46$ MeV $J^\pi = (1^-, 2^+)$, $E_x = 8.3$ MeV $J^\pi = (6^+)$ and $E_x = 8.508$ MeV $J^\pi = (3^-, 2^-)$. Two α -unbound levels at $E_x = 11.0(\pm 0.4)$ MeV and $12.5(\pm 0.4)$ MeV are strongly populated with the reaction $^{28}\text{Si}(^{16}\text{O}, ^{12}\text{C})^{32}\text{S}$ at $E_{\text{lab}} \approx 70$ MeV, with an appreciable branching ratio for decay to $^{28}\text{Si}(\text{g.s.})$. Our experiment did not yield a definite spin assignment for them, but suggests overlapping levels or low spin values ($J^\pi < 5$).

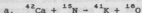
References:

- * University of Petroleum and Minerals, Dahrhan, Saudi Arabia.
1. Nuclear Physics Laboratory Annual Report, University of Washington (1983) p. 23.
2. J.G. Pronko and R.A. Lindgren, Nucl. Instrum. Meth. 98, 445 (1972).
3. Nuclear Physics Laboratory Annual Report, University of Washington (1983) p. 75.
4. Nuclear Physics Laboratory Annual Report, University of Washington (1983) p. 82.

4.5 A New Scheme for the Calibration of Sub-Coulomb Heavy Ion Proton Transfer Reactions

K.J. Davis, A. Lazzarini, and T. Murakami

A triad of proton transfer reactions can be used to isolate the product of a spectroscopic factor and the square of the radial wave function for the exchanged proton in the initial and final configurations. Such a set of reactions was described in last year's Annual Report.¹ Only one of those reactions proved to be feasible, so a new triad is being investigated and is shown below.



In each case we are planning to use the heavier nucleus as the projectile. We have performed beam development work with the sputter source and have achieved an 80 nA beam of $^{27}\text{Al}^{6+}$ after energy analysis and a 52 nA beam of $^{40}\text{Ca}^{8+}$. We expect similar results when isotopically enriched ^{42}Ca is used in the source.

The kinematics of these reactions is such that the sub-Coulomb transfer reactions, which are backward peaked in the center-of-mass reference frame, are forward peaked in the lab frame. We intend to use the momentum filter in the vicinity of 10 deg to remove the elastically scattered projectile particles. The Bragg curve spectrometer can be mounted at the final focus of the momentum filter and can be used for particle identification as well as energy determination. This technique has been used in preliminary experiments to investigate reaction c) near the Coulomb barrier. Our results indicate that the ^{15}N can be readily distinguished from other particles hitting the detector and that the peaks corresponding to the first and second excited states of ^{28}Si can be well resolved.

Reference:

1. Nuclear Physics Laboratory Annual Report, University of Washington (1983) p. 27.

4.6 Measurement of Total Reaction Cross Sections at 15 to 35 MeV/A

J.G. Cramer, A. Lazzarini, D.D. Leach, R.A. Loveman, W. Lynch,*
M.Y. Tsang[†] and J. Van der Plecht[‡]

We have measured the angular distribution for elastic scattering with the ^{12}C beam of the MSU Superconducting Cyclotron at 15, 25, and 35 MeV/A on

targets of ^{12}C , ^{28}Si , and ^{90}Zr . About twenty points were taken for each target energy in 0.25° to 0.5° steps starting at 1.5° . In addition, similar angular distributions were taken for gold, primarily to monitor the beam stability. From these measurements we will obtain total reaction cross sections and optical model potentials valid for this region.

At low energies the total reaction cross section σ_r for nucleus-nucleus scattering is determined primarily by average collective nuclear behavior, and σ_r is essentially geometrical. As the collision energy is increased the average nuclear behavior becomes less important and individual collisions of nucleons in the target with those in the projectile assume more importance. At the same time, the total cross section for nucleon-nucleon (n-n) scattering decreases dramatically. One can adopt the extreme view that the reaction cross section arises exclusively from scatterings involving individual nucleons in the target and projectile, and that for calculating σ_r the overall average effects can be neglected except as they modify the energies and trajectories of the nucleons in the interacting system.¹ This is essentially the optical limit of the Glauber model.²

The method which we have chosen to determine the total reaction cross section is an indirect one: to measure a forward angle portion of the angular distribution and to use these data to deduce σ_r and σ_t . The actual extraction of the cross section can be done in several ways: (1) by using a diffraction model generalization of the "quarter-point recipe"; (2) by employing a parameterized S-matrix analysis of the data and calculating σ_r directly from the resulting S-matrix; and (3) by fitting the data with the optical model and obtaining σ_r from the optical model S-matrix. Our estimates and those of other groups³ indicate that a combination of these methods should permit an absolute determination of σ_r to better than 2.5%. This error is due to model dependence, and actual errors due to experimental systematics should be less than 1%. Errors in the relative values of σ_r for different energies should also be less than 1%.

The precise angle of the beam relative to the spectrometer is of critical importance in these measurements. Absolute measurement of the scattering angle was obtained by rotating the spectrometer into the beam with a scintillator protecting the detectors at the end of the spectrometer. These measurements were corroborated by cross section measurements on both sides of the measured zero degree point. The error in the absolute angle of the beam was about 0.05° . We monitored the position stability of the beam with pairs of counters mounted symmetrically right-left and above-below with respect to the beam. The monitor counters were also used for beam integration in addition to the Faraday cup.

References:

- * Michigan State University, East Lansing, MI 48824.
1. R.M. DeVries and J.C. Peng, Phys. Rev. C 22, 1055 (1980);
N.J. DiGiacomo, R.M. DeVries, and J.C. Peng, Phys. Rev. Lett. 45, 527 (1980).
2. W. Czyz and L.C. Maximon, Ann. Phys. (NY) 52, 59 (1982).
3. A.J. Cole, W.D.M. Rae, M.E. Brandan, A. Dacal, B.G. Harvey, R. Legrain, M.J. Murphy, and R.G. Stokstad, Phys. Rev. Lett. 47, 1705 (1981).

4.7 Calculation of Critical Energies as a Function of Nuclear Size

J.G. Cramer and R.A. Loveman

We are beginning a study of critical energies of different systems. For this study we will be using folding model potentials calculated by the same method used by Satchler and Love.¹

There is a singularity in the classical deflection function of many potentials. In particular, the potentials used to characterize scattering of nuclei fall into this class. There is however a scattering energy above which this singularity in the deflection function disappears. This energy is the critical energy.² This energy divides elastic scattering into two regimes. Above the critical energy one might expect to see nuclear rainbows and negative angle scattering. Below it one would expect to see phenomena associated with nuclear orbiting.

We have started studying the critical energy as a function of the initial system. For the calculations of the critical energies we are using both real and complex potentials. For the real part of either potential we are using folding model potentials. For the imaginary part of the complex potential we are using Woods-Saxon potentials which have been used to fit data.

While the calculations are essentially classical there are quantum mechanical analogs to these quantities. The quantum mechanical deflection function is equal to twice the real part of the derivative with respect to k of the phase shifts from the s -matrix. If one uses the single-turning-point W.K.B. approximation to calculate the phase shifts, and then takes twice the derivative with respect to k , one derives the same function as the classical deflection function. There are several approximations used in going from quantum mechanics to classical mechanics, but they all seem to hold up well for heavy ion scattering.

References:

1. G.R. Satchler and W.G. Love, Phys. Rep. 55, 3, 183 (1979).
2. W.H. Miller, J. Chem. Phys. 51, 3631 (1969).

4.8 Projectile Breakup into Coincident Heavy Fragments

T. Aves,* S. Gil, M.N. Harakeh, M.J. Murphy, A. Ray, A.G. Seamster, and R. Vandenbosch

Projectile breakup is a type of reaction mechanism which becomes increasingly important as lab bombarding energies increase above the Coulomb barrier, and ultimately evolves into the high-multiplicity, dissociative reactions observed at relativistic energies. It is a peripheral (large impact parameter) reaction which occurs when the slight damping associated with quasielastic collisions dissipates enough energy in the projectile (or its residue) to cause it to dissociate. The dissociation can take one of several forms: the disintegration of the projectile at contact with the target, the ejection of an excited projectile remnant which decays by particle emission, or perhaps the fission of the projectile or remnant. Our recent investigations have discovered a new version of breakup in which heavy particles ($Z \geq 3$) are emitted by an excited projectile residue.

Our experiment was inspired by the question: does the breakup of a massive projectile ever produce multiple heavy fragments? By heavy we mean larger than the protons, deuterons, and alphas characteristically emitted by excited nuclei. To investigate, we designed a system of four solid-state detector telescopes which was sensitive to coincident heavy ions with energies in excess of several MeV/n. This system was used to observe projectile-like particles emitted in the reaction of $^{35}\text{Cl} + \text{Ta}$ at 18 MeV/n.

The measurement was made at the Holifield Facility at Oak Ridge National Lab, and succeeded in detecting projectile breakups into coincident heavy fragments. The results show a broad distribution of coincident events, representing all possible pairings of $Z = 3$ to $Z = 8$ projectile fragments. We obtained coincident energy spectra for all of these fragment pairs, and analyzed their features for information about the reaction mechanism. Most of the analysis employed Monte Carlo simulation of breakup scenarios as viewed by the detector system. We found that the simulation of a sequential breakup mechanism, in which the dissociation of the projectile remnant occurs far from the target, quantitatively reproduced all of the observed characteristics of the kinematic data. In contrast, prompt breakups simulated by introducing the Coulomb field of the target into the fragment final state, produced energy spectra distinctly different from the data, when the target was less than ≈ 40 fm from the fragments. We conclude that the heavy-particle coincidences are produced by the sequential breakup of excited projectile remnants. This can be viewed as either the fission of the remnant, or its decay through the emission of a heavy particle. The observation of such a phenomenon is

surprising - the prevailing wisdom has been that the heavy projectile-like products of sequential breakup are accompanied only by light particles and target products. Our analysis of this experiment is complete, and a letter reporting the result has been prepared and submitted for publication.

Reference:

* Oak Ridge National Laboratory, Oak Ridge, TN 37830

4.9 Reactions of ^{24}Mg With ^{16}O

S. Gil, M.A. Khandaker, D.D. Leach, D.-K. Lock, A. Ray, and R. Vandenbosch

We have recently performed an experiment to measure the angular distribution of the oxygen and carbon particles from the $^{16}\text{O}(^{24}\text{Mg}, ^{16}\text{O})^{24}\text{Mg}$ and $^{16}\text{O}(^{24}\text{Mg}, ^{12}\text{C})^{28}\text{Si}$ reactions at $E_{\text{lab}} = 79.5$ Mev at back angles. The motivation¹ for this measurement is to find out whether the large inelastic cross sections observed at backward angles in the carbon and oxygen channels in the $^{28}\text{Si} + ^{12}\text{C}$ reaction² are due to a compound nuclear process. We form a ^{40}Ca nucleus by the $^{24}\text{Mg} + ^{16}\text{O}$ reaction at the same excitation energy and approximately the same angular momentum (within 5%) as for the $^{28}\text{Si} + ^{12}\text{C}$ reaction and compare the relative intensities of the carbon and oxygen yields. If we see an entrance-channel effect, then the back-angle yields cannot be attributed to a compound nuclear process.

We used a 200 $\mu\text{g}/\text{cm}^2$ Al_2O_3 target and about 3 pna of ^{24}Mg beam. We used a gas- ΔE solid-state E telescope and measured the angular distribution of scattered carbon, nitrogen and oxygen particles from $\theta_{\text{lab}} = 5.6^\circ$ to 20° in steps of 3° . We placed a gas absorber cell in front of the telescope at $\theta_{\text{lab}} = 14^\circ$ for normalization and to monitor carbon build-up on the target. We also took measurements at all the angles using a 200 $\mu\text{g}/\text{cm}^2$ Al target and a 50 $\mu\text{g}/\text{cm}^2$ carbon target. We finally subtracted out aluminum and carbon backgrounds from the Al_2O_3 spectrum and also corrected for carbon build-up on the Al target and for a layer of 10 $\mu\text{g}/\text{cm}^2$ of oxygen on the blank aluminum target. We have estimated differential cross sections for scattered oxygen and carbon particles in the $(-8.5 \text{ MeV} \leq Q \leq 0.0 \text{ MeV})$ region. We could not get cross sections at 8° and 5.6° for more inelastically scattered oxygen particles because of absorption and multiple scattering of oxygen particles by the gas cell. The total subtraction due to aluminum and carbon background from the raw counts is not more than 45% in the worst case. We show in Fig. 4.9-1 our angular distribution for energy-integrated $(-8.5 \text{ MeV} \leq Q \leq 0.0 \text{ MeV})$ oxygen and carbon particles. The smooth curves show a $1/\sin\theta$ dependence. In the $^{28}\text{Si} + ^{12}\text{C}$ reaction,² the carbon cross-section is about four times the oxygen cross section. In the $^{24}\text{Mg} + ^{16}\text{O}$ reaction, we find that the oxygen cross section is about three to four times the carbon cross section in the $(-8.5 \text{ MeV} \leq Q \leq 0.0 \text{ MeV})$ region. Considering the entire spectra also, we find more oxygen particles than carbon particles. So our results clearly

demonstrate an entrance channel effect in the $^{28}\text{Si} + ^{12}\text{C}$ reaction and these results are consistent with the qualitative picture of the formation of a long-lived orbiting complex in these reactions.

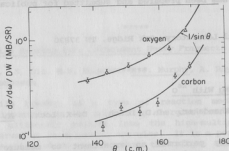


Fig. 4.9-1 Center of mass angular distribution for reaction yield at backward angles. Smooth curves show $1/\sin\theta$ dependence.

References:

1. Nuclear Physics Laboratory Annual Report, University of Washington (1983) p. 26.
2. D. Shapira et al., Phys. Lett. B **114**, 111 (1982).

4.10 How is the Excitation Energy Divided in Partially Damped Collisions?

A. Lazzarini, D.D. Leach, D.-K. Lock, A. Ray, A.G. Seamster, and R. Vandenbosch

One of the principal remaining questions concerning quasi- and deeply-inelastic collisions is the division of the excitation energy between the two fragments. The nucleon exchange mechanism leads one to expect rather similar fluxes of exchanged particles in each direction and thus similar excitation energies for each fragment. This should be particularly true for the partially damped events. For more fully damped events the contact time may be sufficiently long that thermal equilibrium can be attained, in which case the excitation energy is expected to divide according to the mass ratio.

These two limiting possibilities lead to a distinguishable difference only when there is a significant mass asymmetry in the exit channel. There are not many experimental observations which bear on this issue, but those that exist tend to indicate that thermalization is reached more rapidly than might have been expected. We have developed a new method for determining the division of excitation energy and applied it to the very mass asymmetric entrance channel system $^{56}\text{Fe} + ^{238}\text{U}$. We determine the total excitation energy

from the kinetic energy of the projectile-like fragment and the excitation energy appearing in the heavy fragment from the fission mass asymmetry of the coincident sequential fission fragments from the target-like partner. The relative yields of symmetric and asymmetric fission fragments is a very sensitive function of energy for excitation energies below about 60 MeV.

The experiment was performed using a 480-MeV beam of ^{56}Fe produced by the Lawrence Berkeley Laboratory SuperHILAC. The beam was incident on a self-supporting 0.8 mg/cm^2 ^{238}U target, and the projectile-like fragments were detected in a ΔE -E detector telescope located at 45° where there is a good yield over a broad range of inelasticities. The mass distribution of the fission fragments was determined by their time of flight. The mass resolution was very good, with peak-to-valley ratios of over 20 observed at the smallest inelasticities. We have restricted our analysis to those events with $Z = 24$, 25, and 26, corresponding to Pu, Np, and U complementary fragments. These are fissioning systems for which we have good calibration data on the dependence of the mass asymmetry on excitation energy.¹

Our results for the ratio of the excitation energy in the heavy fragment divided by the excitation energy in the light fragment are plotted as a function of total kinetic energy loss in Fig. 4.10-1. The upper horizontal

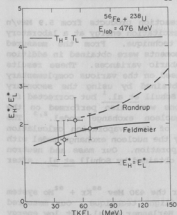


Fig. 4.10-1 Dependence of the ratio of the excitation energy of the heavy fragment to that of the light fragment as a function of the total excitation energy.

line is the expectation for equal temperatures (excitation energy partitioned according to mass ratio) and the lower horizontal line is the expectation for equal division of excitation energies. Our results are intermediate between these two expectations but closer to the latter. It is clear that the present results preclude a division based on thermal equilibrium. Our results are in fact in good agreement with dynamical transport model calculations of Randrup² and of Feldmeier.³ The driving term for equilibration in these calculations is the temperature imbalance resulting from the initial nearly equal division of excitation energy between the two fragments. It is seen that this driving

force is insufficient to equilibrate the temperatures unless the fragments are in intimate contact for an appreciable length of time.

References:

1. See e.g., D. Burnett, UCRL 11006 (unpublished); Z. Frankel et al., Phys. Rev. C 12, 1809 (1975); R.L. Ferguson et al., Phys. Rev. C 7, 2510 (1973); P. Plasil and H.W. Schmidt, Phys. Rev. C 5, 528 (1972).
2. J. Randrup, Nucl. Phys. A 383, 468 (1982).
3. H. Feldmeir, Proceedings of the Nuclear Dynamics Workshop III, Copper Mountain, CO, March 84, and private communication.

4.11 The Effect of Particle Evaporation in the $^{136}\text{Xe} + ^{86}\text{Fe}$ Reaction and a Reinvestigation of the $^{86}\text{Kr} + ^{92}\text{Mo}$ System

S. Gil, A. Lazzarini, D.D. Leach, K.T. Lesko, D.-K. Lock, R. Vandenbosch, and A.G. Seamster

The nuclide distributions of Fe-like reaction products from 5.9 MeV/n ^{136}Xe on ^{56}Fe were measured as a function of excitation energy at a laboratory angle of 55.5° using the time-of-flight technique. From the measured distribution of yields the first and second moments were obtained in addition to the correlation coefficients and the isobaric variances. These results were compared with evaporation calculation based on the various complementary primary distributions of light fragments obtained by using the secondary distributions of heavy fragments measured by Schull et al.¹ but corrected for neutron evaporation. Evaporation calculations were also performed on the primary distributions predicted by the nucleon exchange model.^{2,3} The comparison between our data and the results of the evaporation calculation shows that our data can be better described by the nucleon exchange model with the inclusion of the effect of particle evaporation. Our mass and neutron variances are consistently smaller than those obtained by Schull et al. after correction for particle evaporation.

The isobaric variances were measured for the 430 MeV $^{86}\text{Kr} + ^{92}\text{Mo}$ system at 39° in the laboratory using the time-of-flight technique. Our measured variances are smaller than those obtained by Berlinger et al.⁴ at low energy losses and are in agreement with the results from the nucleon exchange model. We reproduce the saturation of the isobaric variances observed by Berlinger et al. at large energy losses. We note however that this saturation only occurs at near and sub-barrier total kinetic energies in the exit channel and likely reflect fluctuations in the scission deformation rather than quantal effects.

References:

1. D. Schull, W.C. Shen, H. Freiesleben, R. Bock, P. Busch, D. Bangert, W. Pfeffer, and P. Puhlhofer, Phys. Lett. B 102, 116 (1981).
2. J. Randrup, Nucl. Phys. A 327, 490 (1979).
3. J. Randrup, Nucl. Phys. A 307, 319 (1978).
4. M. Berlander, A. Gobbi, P. Manappe, U. Lynen, C. Ngo, A. Olmi, H. Sann, H. Stelzer, H. Richel, and M.F. Rivet, Z. Phys. A 291, 133 (1979).

5. FUNDAMENTAL SYMMETRIES IN NUCLEI: $O^+ - O^-$ ISOSCALAR PARITY MIXING IN ^{14}N

5.1 Theory of the ^{14}N Parity Mixing Measurement

E.G. Adelberger, B.A. Brown,^{*} and P. Hoodbhoy,[†]

The general principles of our experiment to measure the $\Delta I = 0$ parity mixing between the $I = 1$ O^+ and O^- levels at $E_x = 8.618$ and 8.79 MeV in ^{14}N were given in last year's Annual Report.¹ A paper,² to appear in Phys. Rev. C, develops the formalism of longitudinal analyzing power (A_L) measurements over parity mixed resonances and applies this to the example of probing the parity mixing in ^{14}N by detecting A_L over the narrow O^+ resonance. The formalism utilizes the single-level approximation to Bloch's formulation of reaction theory³ in order to account for the strong (parity-conserving) reaction amplitudes and is restricted to parity nonconservation associated with the closeness of the two opposite parity resonances. An example of the parity conserving calculation is shown in Fig. 5.1-1 where we compare our calculation to existing⁴ unpolarized $^{13}\text{C}(p,p)$ data. In order to determine the widths and separation of the O^+ and O^- resonances we studied the $^{13}\text{C}(p,\gamma_0)$ reaction at $\Theta_{\text{lab}} = 90^\circ$. Results are shown in Fig. 5.1-2.

Because the PNC A_L is expected to change sign between forward and backward angles we have chosen to detect the observable $A_L(\text{back}) - A_L(\text{front})$, where $A_L(\text{back})$ is the longitudinal analyzing power averaged over the angles from $140^\circ - 170^\circ$ while $A_L(\text{front})$ is that averaged over the interval from $33^\circ - 37^\circ$. Because our observable is a difference of A_L 's, effects due to beam intensity modulation or of beam size modulation combined with target nonuniformities cancel to first order.

We estimate the PNC matrix element connecting the O^+ and O^- levels using the "best value" PNC NN interaction of Desplanques, Donoghue, and Holstein⁵ in a shell model calculation² in the ZBM space and obtain $H_{\text{PNC}} = -1.39$ eV. Haxton⁶ has done a complete $2h\omega$ calculation and obtains a very similar value $H_{\text{PNC}} = -1.04$ eV.

When the -1.39 eV matrix element is inserted into our A_L calculations, we discover that an A_L measurement has considerable statistical power (see Fig. 5.1-3). The predicted effect is $\sim 2 \times 10^{-5}$ and counting rates are high enough so that one can achieve a statistical error small enough to give a $\sim 5\sigma$ effect with an integrated beam charge of $1 \mu\text{A}\cdot\text{day}$. The statistical power of the experiment is due to an enhancement arising from the fact that $\Gamma(O^-) \gg \Gamma(O^+)$ and from the large size of low-energy elastic-scattering cross sections.

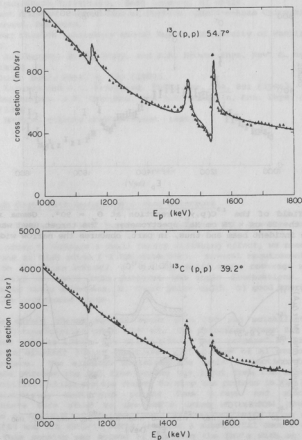


Fig. 5.1-1 Comparison of $^{13}\text{C}(p,p)$ data of Latorre and Armstrong⁴ with the parity conserving calculation. Resonance parameters have been taken from the latest compilation and no attempt was made to fit the data by adjusting any parameters.

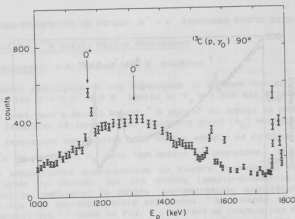


Fig. 5.1-2 Yield of the $^{13}\text{C}(p, \gamma_0)$ reaction at $\theta = 90^\circ$. Gamma rays were detected in the 25 cm \times 25 cm NaI spectrometer. The target used was ~ 20 kev thick to the incident beam and thus, in part, obscures the narrow width of the O^+ state.

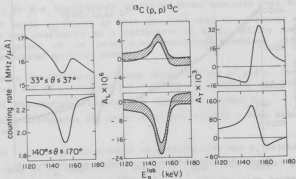


Fig. 5.1-3 Calculated counting rate, longitudinal and transverse analyzing powers over the O^+ resonance for a 10 kev thick ^{13}C target. We assumed full coverage of the solid angles between 33° and 37° (front counter) and 140° to 170° (back counter). The shaded band on the A_L plot corresponds to $\pm 1 \sigma$, where σ is the statistical error achieved after running with an integrated beam current of 1 μA -day under the above conditions.

References:

- * Michigan State University, East Lansing, MI 48824.
- † Present Address: Department of Physics, Quaid-e-Azam University, Islamabad, Pakistan.
- 1. Nuclear Physics Laboratory Annual Report, University of Washington (1983) p. 32.
- 2. E.G. Adelberger, P. Hoodbhoy, and B.A. Brown, Phys. Rev. C, to be published.
- 3. C. Bloch, Nucl. Phys. 4, 503 (1957).
- 4. V.A. Latorre and J.C. Armstrong, Phys. Rev. 144, 891 (1966)
- 5. B. Desplanques, J.F. Donoghue, and B.R. Holstein, Ann. Phys. (NY) 124, 449 (1980).
- 6. W.C. Haxton, private communication (1984).

5.2 High Count-Rate Low-Energy Proton Detectors

E.G. Adelberger, M.J. Murphy, J.L. Osborne, H.E. Swanson, and V.J. Zepa

In order to measure a small parity violating effect, we need to count ~ 1 MeV protons at high rates (~ 1 MHz/detector). Several requirements determined the proton detection scheme: a) a large solid angle coverage with relative insensitivity to small beam position and angle fluctuations, i.e., large detectors at large distances, b) short pulse width, c) good energy resolution and, d) low background noise.

The method chosen was to mount thin (50 μ m) scintillators on 5-cm diameter photomultiplier tubes (PMT's). The detectors cover 32% of the solid angle from 140° to 170° . The scintillators were prepared by Bicorn on 3-mm thick, 5-cm diameter lucite substrates with 0.4 μ m of Al evaporated on the front surface. The aluminum maximizes the light collection from a proton event, and shields the PMT from seeing the light from the other detectors. The scintillator thickness was chosen to stop the protons in the scintillator, while minimizing background pulses from γ rays and electrons. The scintillators were glued to the PMT's using an optical coupling cement developed by Nuclear Enterprises, Inc. Preliminary tests using some existing RCA 8575(6) and RCA 8850(1) PMT's revealed a substantial amount of low energy noise. This problem was solved by wrapping the PMT's with an Al shield at photocathode potential. Running the PMT's near optimum high voltage, we were able to attain proton pulses of ~ 0.8 V with 10-nsec pulse widths. The energy resolution varied from 18% to 30%, depending primarily on the photocathode uniformity. This, however, is not a critical factor, since we are interested only in counting the protons, and thus need only to be able to separate the proton peak from the low energy noise. To equalize the counting rate in the front and back counters, the front counters have been further collimated,

exposing only a 1.3-cm diameter hole. This reduces the effects of photocathode nonuniformity, improving the front counter resolution to ~13% (see Fig. 5.2-1). We decided to use the best 4 of 7 RCA PMT's, and to purchase 5 Hamamatsu R239-02 PMT's. The Hamamatsu tubes are equivalent to the RCA 8575's, with the added advantage of a built-in shield at photocathode potential as standard, a better tube wrapping and a much lower price. The PMT's were placed in specially designed holders which mount in the scattering chamber. In order to hold a vacuum, an O-ring seals against the 3-mm edge of the lucite substrate, with the aluminized surface of the scintillator exposed to the target, while the PMT remains outside the vacuum system.

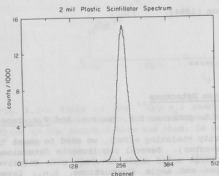


Fig. 5.2-1 Typical energy spectrum of 1.1 MeV protons on a ^{13}C target, as detected in a front counter. The energy resolution is 13%.

PMT bases were built following a standard design.¹ To achieve stability, a large divider chain current (2.2 mA at -2000 V) was employed and zener diodes were used to fix the photocathode to first dynode potential at 480 V.

Reference:

1. R.W. Engstrom, RCA Photomultiplier Handbook, (1980) p. 80.

5.3 ^{14}N Beam Position Stabilization System

E.G. Adelberger, N. Hill, J.L. Osborne, H.E. Swanson, and V.J. Zeps

The incoming proton beam is stabilized to remove position fluctuations. Using four independent control loops, the beam is dynamically steered to pass through the center of both the upstream slits and the Faraday cup. The major elements of the beam sensing and steering system are shown in Fig. 5.6-1 (see

Sec. 5.6). Beam current is measured by pairs of slits (horizontal and vertical) and a Faraday cup split into four quadrants. The physical positions of both slits and Faraday cup can be moved with micrometer adjusting screws. When in operation, these systems serve to maintain the position of the beam along the symmetry axis of the apparatus. Two parameters of the beam are controlled - position and angle at the target location. The upstream magnetic steerer near to the exit of the quadrupole is used to center the beam on the slits. These slits determine primarily the beam's position at the target but beam which was off the z-axis will have acquired an angle with respect to that axis. The steerer near the slit position is used to center the beam on the Faraday cup. This system assures the angle of the beam with respect to the z-axis is minimized.

In order to minimize the loop response times, wide bandwidth current preamps were designed and built. These operate in the range of 10 to 1000 nanoamperes with a bandwidth of DC to 40 kHz. Additional operational amplifier circuitry provides sum and difference signals for metering and control. These are displayed on meters to provide visual indication of the beam's intensity and position for tuning diagnostics. These signals are also sent to voltage to frequency converters (V/F's) which are scaled and routed identically to the pulses from the photomultipliers themselves. This allows us to correlate excursions in photomultiplier asymmetries with the beam's position, angle and intensity. Right-left and up-down difference signals are converted to the currents needed to drive the steerers using Kepco BOP operational amplifier power supplies in the case of the upstream steerers, and hybrid high current op-amps made by RCA in the case of the Faraday cup control loops.

The magnetic steerers were constructed by winding coils on each of the four legs of ferrite frames (rectangular toroids). These frames enclose a section of beam tube. Coils on opposite legs of the frames are connected to produce opposing B fields in the ferrite. This causes the field to leave the ferrite and fill the open area in the center of the frame with a very uniform B field. Ferrite has a high permeability and resistivity which allows modulation at rates comparable to the 40 kHz bandwidth of the current preamps.

Using a Hewlett Packard Spectrum analyzer, the power spectra of various difference signals were measured. These give an indication of the beam's fluctuations in different regions of frequency space. Over the frequency range of DC to 100 Hz, the stabilization system achieves a 30 dB overall reduction in the power spectrum when compared with an unstabilized beam.

5.4 ¹⁴N Data Collection Electronics

E.G. Adelberger, N. Hill, J.L. Osborne, H.E. Swanson, and V.J. Zepe

The data acquisition system uses a somewhat modified version of the Laboratory's singles data taking environment along with external electronics to route the Lecroy scalers. Due to the high data rates produced by the photomultiplier tubes, ADC's cannot be used. All events exceeding a lower level threshold are counted in the 100 MHz scalers, and these provide the peak sums used in the analysis. The Laboratory's polarized ion source controller generates the equal period routing sequence and provides the capability of synchronizing the starting and stopping of data acquisition with the transition to a new routing state. In addition, acquisition is inhibited for a preset time around the state transition to allow for transient effects to damp out.

A typical data acquisition sequence proceeds as follows: The computer, having initialized and cleared the CAMAC scalers, signals the external electronics that all is ready through an ADC test output jack. Data acquisition begins at the transition to the + route state. After a predetermined amount of charge has been collected, acquisition is stopped but only after equal time has been given to each route state. The PDP 11/60 computer is signaled through an ADC input, at which time the scalers are read, cleared, and displayed. This sequence proceeds until the desired number of readings has been acquired.

Presently two scaler banks are used, with the intent to expand to four. Routing is accomplished by sending beam (V/F) and photomultiplier pulses to both banks of scalers, but only gating one bank on at a time consistent with the present ion source state. The assignment of which bank corresponds to the + route state alternates with each sequential readout of the scalers. This was found necessary as the dead times of the individual scalers in each bank are all different. These differential dead times build in an asymmetry unless the individual scaler dead times are averaged over both route states. The analysis software then assumes sequential scaler readings have alternate route assignments and these are unfolded when computing the various asymmetries. The data acquisition system is thus very symmetric in its treatment of the two route states. In order to monitor proper operation of this alternation scheme, the symmetry is broken for one scaler in each bank. A constant frequency oscillator is gated into one physical bank when the assignments are normal and to the other bank when they are inverted. This has the effect of accumulating counts in only one route state. Any counts in the other state indicates a problem with the synchronization and the particular reading sequence could be removed from the totals accumulation.

5.5 Data Acquisition and Analysis Programs

E.G. Adelberger and R.S. Peabody*

The data acquisition program for the ^{14}N parity mixing experiment provides the master control for the data taking cycle, writes all results on tape and provides an on-line measure of the current and cumulative values of all the transverse and longitudinal asymmetries. A single data acquisition cycle consists of:

- a. Starting the polarized ion source spin flipper, the Lecroy and NPL scalars, and the ADC used for the 3×3 NaI.
- b. Stopping the counting after a predetermined beam charge has accumulated.
- c. Reading the Lecroy scalars, and clearing them and displaying the results.
- d. Starting a new "read cycle."
- e. After 40 read cycles the program writes the 40 sets of readings on magnetic tape, and computes the current and cumulative asymmetries. The counting rates and asymmetries are printed out and a new run is begun.

The program is based on the standard Laboratory singles package with the AUTO feature, but it required a number of new programs. The $4 \times 12 = 48$ Lecroy scaler values for each reading are stored as counts in a spectrum which can be displayed by the standard VT11 routines. Each scaler is labelled by a code denoting its function (i.e., left front counter in the + route). Thus all asymmetries can be based on the function code rather than the physical scaler number. The on-line output of the individual and cumulative counting rates and asymmetries provides an excellent diagnostic and will ultimately be used to control the polarized ion source spin precessor.

The data analysis program computes the various asymmetries and correlations and makes a statistical analysis of the individual values. By allowing us to compare the observed fluctuations of the individual data points with those expected from counting statistics we can determine whether our system is performing as expected.

Reference:

- * Present Address: Department of Chemistry, University of Washington.

5.6 Design and Construction of the ^{14}N Parity Experiment Beamline

E.G. Adelberger, C.A. Gossett, M.Z. Iqbal, J.L. Osborne, H.E. Swanson, and V.J. Zepp

As shown in the preceding sections of this report, the measurement of a small (2×10^{-5}) parity non-conserving effect in ^{14}N via the resonant elastic scattering of protons on ^{13}C requires novel designs in the apparatus. The proton counters must cover a large solid angle, yet produce pulses fast enough for the high counting rates. The beam transport system must provide fast automatic stabilization of beam position and angle. The beam line for this experiment must accommodate all of these design considerations while at the same time providing mechanical stability, to reduce asymmetries in the particle counting rates due to translation or vibration of the target chamber, and a clean high vacuum, to reduce carbon buildup on the target.

The final design for the beam line assembly is shown in Fig. 5.6-1. The position of the slits and the target were chosen to provide the optimum focus at the target position. The extent of the apparatus, more than 4 m from the cave quadrupole to the split Faraday cup, precluded its construction on any of the existing beam lines except for the L-30° leg, which is normally used only by the University of Washington Nuclear Medicine Group for the production of short-lived radionuclides (see Sec. 9.3). One prime consideration in the design of the beam line was that it not interfere with this pre-existing usage, therefore removable 30-cm stainless steel bellows and 15-cm section of tube were placed between the quadrupole and the isolation valve to allow their chamber to be re-attached in its usual position.

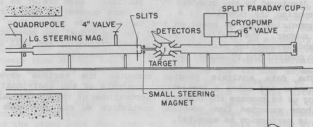


Fig. 5.6-1 A elevation view of the L-30° beamline. There are also an identical pairs of slits, forward-angle counters, back-angle counters and Faraday-cup segments in the horizontal dimension.

The construction of this beam line has now been completed. As shown in Fig. 5.6-1, the beamline components are attached to a $1/2$ " steel plate supported by two $8" \times 2"$ steel channels. These channels are attached at one end to the quadrupole support and at the other end to a 12" diameter steel pipe which extends through the cave floor to the floor of the basement. The

pumping system chosen for this experiment is a CTI Cryotorr 7 cryopump.

5.7 Studies of System Performances Using an Unpolarized Beam

E.G. Adelberger, C.A. Gossett, J.L. Osborne, H.E. Swanson, and V.J. Zepe

The slit and Faraday cup stabilizing feedback loops reduce the error signal by 30 dB and 10 dB, respectively, at low frequencies, while providing feedback control up to several kHz. A removable quartz viewer has been installed at the target position. This has proved to be both an excellent diagnostic tool and a sensitive way for determining the best beam focus. The best beam spots thus far have been $\approx 0.5 \text{ mm} \times 0.5 \text{ mm}$. Collimators have been put on the front counters in order to equalize the rate in the front and back counters. This has allowed us to raise the beam current, increasing the rate in the back counters, while maintaining a tolerable rate in the front counters. Because the collimators expose only the central portion of the scintillators to the scattered protons, the resolution in the front counters has improved from $\approx 25\%$ to $\approx 13\%$. At present the back counters can see protons scattered from further down the beamline, creating a continuum of noise that accounts for $\approx 10\%$ of the total back detector counts. Plans for a cold shroud which should eliminate this problem, are in the shop.

Before we attempt to make measurements using a polarized beam, we must understand possible systematic errors caused by imperfections in our data taking procedure and apparatus. Since the PNC effect is expected to be $\approx 2 \times 10^{-6}$, we would like to reduce systematic errors in A_z to a level of $\approx 2 \times 10^{-6}$. Many sources of systematic error can be probed with an unpolarized beam. Using the control circuit which normally flips the spin of the polarized beam to route the scaler banks, we collect unpolarized beam data exactly as we intend to when running with a polarized beam. Because there is no spin flipping, we expect all asymmetries to vanish. During our first runs, we noticed asymmetries up to 100 times larger than the statistical error. We discovered that the CAMAC scalers read differently, even when all scalers were fed by the same photomultiplier signal. To correct this, we electronically alternated the functions of the two scaler banks after each read, so that each spin state was averaged over the two banks, eliminating the correlation between "spin state" and scaler bank. This dramatically improved A_z (back-front), bringing it to within statistical error. We still found there to be a large analyzing power in the individual A_z (back) and A_z (front) measurements. This was strongly correlated with the asymmetry in the total beam current in each route. We discovered that the computer software would consistently cut short the positive route at the beginning of each sequence of reads. This caused a fairly consistent negative A_z (back) and A_z (front). After we corrected these known problems in the program and electronics, we observed, in a run with a total charge of $0.25 \mu\text{A-days}$, that all asymmetries were consistent with zero, A_z (front) = $(4.9 \pm 5.0) \times 10^{-6}$, and A_z (back) = $(5.7 \pm 6.0) \times$

10^{-6} , and $A_z(\text{back-front}) = (0.9 \pm 7.8) \times 10^{-6}$, with a total of $\approx 5 \times 10^6$ counts/detector. Thus, at the present level of accuracy, we are able to measure a null result with unpolarized beam. However more data must be taken to verify the result at the 2×10^{-6} level. All-in-all the system seems to be working extremely well, and we are ready to test our apparatus with polarized beam.

Below we discuss the systematic errors in our measurements. The first source of error is the uncertainty in the beam polarization. This is estimated to be $\pm 1\%$ from the results of the polarization transfer measurements. The second source of error is the uncertainty in the detector response. This is estimated to be $\pm 1\%$ from the results of the polarization transfer measurements. The third source of error is the uncertainty in the data reduction. This is estimated to be $\pm 1\%$ from the results of the polarization transfer measurements. The fourth source of error is the uncertainty in the theoretical predictions. This is estimated to be $\pm 1\%$ from the results of the polarization transfer measurements. The fifth source of error is the uncertainty in the statistical errors. This is estimated to be $\pm 1\%$ from the results of the polarization transfer measurements. The sixth source of error is the uncertainty in the systematic errors. This is estimated to be $\pm 1\%$ from the results of the polarization transfer measurements. The seventh source of error is the uncertainty in the total error. This is estimated to be $\pm 1\%$ from the results of the polarization transfer measurements. The eighth source of error is the uncertainty in the final result. This is estimated to be $\pm 1\%$ from the results of the polarization transfer measurements. The ninth source of error is the uncertainty in the overall error. This is estimated to be $\pm 1\%$ from the results of the polarization transfer measurements. The tenth source of error is the uncertainty in the final result. This is estimated to be $\pm 1\%$ from the results of the polarization transfer measurements.

Below we discuss the systematic errors in our measurements. The first source of error is the uncertainty in the beam polarization. This is estimated to be $\pm 1\%$ from the results of the polarization transfer measurements. The second source of error is the uncertainty in the detector response. This is estimated to be $\pm 1\%$ from the results of the polarization transfer measurements. The third source of error is the uncertainty in the data reduction. This is estimated to be $\pm 1\%$ from the results of the polarization transfer measurements. The fourth source of error is the uncertainty in the theoretical predictions. This is estimated to be $\pm 1\%$ from the results of the polarization transfer measurements. The fifth source of error is the uncertainty in the statistical errors. This is estimated to be $\pm 1\%$ from the results of the polarization transfer measurements. The sixth source of error is the uncertainty in the systematic errors. This is estimated to be $\pm 1\%$ from the results of the polarization transfer measurements. The seventh source of error is the uncertainty in the total error. This is estimated to be $\pm 1\%$ from the results of the polarization transfer measurements. The eighth source of error is the uncertainty in the final result. This is estimated to be $\pm 1\%$ from the results of the polarization transfer measurements. The ninth source of error is the uncertainty in the overall error. This is estimated to be $\pm 1\%$ from the results of the polarization transfer measurements. The tenth source of error is the uncertainty in the final result. This is estimated to be $\pm 1\%$ from the results of the polarization transfer measurements.

6. FUNDAMENTAL SYMMETRIES IN ATOMS: PARITY MIXING IN HYDROGEN AND DEUTERIUM

6.1 Introduction

T.A. Trainor

The object of this experimental program is to measure the weak interaction coupling of $n=2$ s and p states in hydrogen and deuterium via resonant two-photon s-s transitions induced in a fast atomic beam at 570 G. The sensitivity of the experiment remains, as it was reported last year, at about 1000 times the Standard Model prediction. Our efforts in the intervening period have been directed toward three of the four limitations of the apparatus: magnetic field inhomogeneity, background pressure, and stray electric fields. The fourth problem, motional electric fields due to the fast atomic beam, is indirectly improved by better magnetic field homogeneity.

Although the electric fields which induce the s-s transition amplitudes are generated by highly coaxial precision electrode systems, they are projected on a quantization axis referred to the axial magnetic field of the experiment. This field presently wanders in direction by $\sim 1/10^4$ over the length of the apparatus. The resultant unwanted transverse electric field components complicate the transition amplitudes and mimic the PNC weak interaction. Relative field magnitude variations of the same order also serve to distort the s-s resonance shape. The result is that various techniques used to discriminate against false PNC effects which depend on geometric symmetries and line-shape properties lose their effectiveness below the sensitivity level reported above.

Stray electric fields from various sources other than poor magnetic field geometry also serve to generate spurious amplitudes which make analysis difficult.

Finally, the non-zero residual gas pressure in the system produces collisional $1s-2s$ transitions which serve to dilute the data acquisition with a non-resonant background yield and reduce the statistical accuracy/time.

A major program has therefore been carried out, consisting of preparation of a new tape-wound solenoid and control system for installation, gold plating all electric field electrodes, and reconditioning the cryopump system, in order to achieve a 100 times improvement in the sensitivity of the apparatus. Progress with the solenoid system and gold plating are reported below. The cryopump system now provides 3-4 times lower operating vacuum than was available during last year's data acquisition runs.

6.2 Cleaning and Plating of RF Cavities:

D.W. Holmgren

The sensitivity of the present H-PNC experiment is limited by the ambient electric field in the RF cavities.¹ As part of the effort to understand and eliminate the stray fields, we cleaned, polished and plated the RF cavities.

The copper cavity sections were cleaned and electropolished in a phosphoric acid solution.²

A commercial plater³ performed further processing, including cleaning in a caustic alkaline and an acidic bath. Cavity sections holding apertures required a sulfuric acid etch to activate the exposed lead-tin solder for plating.

To minimize cost, only those surfaces of the cavity "seen" by the beam were plated. These surfaces, including the coupling loops, received 0.3-0.4 μ electroless nickel, followed by 2.5 μ gold plate.⁴

On return from the plater, the pieces needed further finishing. Stains presumed to be plating salts were removed, and the rough edges of the plated regions were finished with silicon carbide.

The cavities were reassembled and installed in the apparatus. We have not yet determined whether the ambient electric field has been significantly altered.

References:

1. Nuclear Physics Laboratory Annual Report, University of Washington (1983) p. 42.
2. N.V. Cherepnin, Treatment of Materials for Use in High Vacuum Equipment, (Ordentlich, Holon, Israel) p. 182.
3. Criton Hytek Finishes Co., Kent, WA 98032
4. American Chemical Refining solution 258.

6.3 Alignment and Field Scans of the New Solenoid

T.A. Trainor and P. Wong

Several years ago we manufactured an aluminum solenoid consisting of 20 tape-wound pancakes¹ when it was realized that our wire-wound copper solenoid did not produce a magnetic field of sufficient uniformity to permit an experimental sensitivity to the parameter c_{2p} of order unity, our original design goal. In principle it is possible more easily to produce a precision

solenoid with tape-wound pancakes, since jigs can be used to precisely locate the tape on cylindrical forms during the winding process, whereas the wire-wound solenoid is subject to various winding errors as each new layer is wound on the one below. However, in the course of routinely checking the new aluminum pancakes for major faults last year, preparatory to installation, we observed that a number of construction defects were present which would make the new solenoid not significantly better than the old. So we undertook a careful measurement program which determined the mechanical, electrical and magnetic properties of each pancake.

Mechanically, we found that the anodized aluminum cylinders used as forms for the pancakes had become warped, either during the winding process, or later when strains in the pancakes relaxed. The various tape layers also were not perfectly lined up at the outer faces. Shifts of 10-20 mils were observed. Each pancake consists of two layers, one wound inward and one wound outward with an annulus of mylar between, both layers wound from one continuous strip of anodized aluminum tape folded at the center. These halves were observed to have different diameters, as a rule, due to variations in tape thickness, as noted below.

In order to insure an important property of the pancakes, that the windings be lined up and the two outer faces parallel, all the pancakes were pressed between dies with a ten ton press. This had the desired effect on the pancakes, but the forms remained warped. It was decided therefore not to use the forms for axial location of the pancakes as intended but to use insulating spacers which reference to the faces of the pancakes.

Electrically, we found that there were shorts in several of the pancakes and that the aluminum tape varied in thickness in a step-like manner at various points within the windings. These measurements were made with a constant-current source and a 6-1/2 digit DVM to determine the IR drop as a function of position along the tape. Changes in tape thickness, as noted, mean that the effective radii of various pancake halves are different even if the measured outside diameters are the same. Each pancake was therefore surveyed for shorts and mean radii of both halves, as well as total resistance.

Magnetic measurements were made with a Bell 3-axis Hall probe in which the three Hall plates were mutually perpendicular to better than $1/2^\circ$. The probe was carried on a precision track referenced to the main coil support jig. Measurements of transverse field components for each pancake were correlated with various physical measurements. Variation in axial magnetic field strength per unit current were correlated with variations in mean radii and known shorts.

At the end of this measurement program the physical, electrical, and magnetic data for each pancake were self consistent at a level of a few parts in 10^5 . An assembly scheme was then devised which would produce the most homogeneous magnetic field with the available pancakes. For instance, the effect of two pancake halves having different mean radii is that the effective axial field maximum is displaced with respect to the physical pancake

position. If the pancake is placed in the solenoid at its normal axial position there will be a nonuniformity in the total field which cannot be removed by shunting neighbor pancake currents. Instead, the pancake must be shifted axially a small amount from its normal site by adjusting the axial spacers between pancakes in order to compensate for the radius variation.

The solenoid has been assembled according to the final scheme and awaits completion of the new current control system so that currents will be sufficiently stable to allow total field surveys at the $1/10^6$ level.

Reference:

1. Nuclear Physics Laboratory Annual Report, University of Washington (1981) p. 28.

6.4 Control System for a New Solenoid

P. Wong

Progress is being made on assembling and testing the new solenoid¹ for the H-atom project. The primary components of this solenoid system are 20 "pancakes" of wound aluminum tape, a 20 channel shunt board which determines the relative amount of current flowing in each pancake and a high performance dual current regulator.

One of the major advantages of the new solenoid is that the current through each pancake can be varied individually, allowing variations in B_z to be minimized. To accomplish this a large PVC board with 20 loops of Nichrome wire has been constructed. The resistance of each loop is varied by means of a copper slider. Each pancake field can be continuously varied over a range of ± 0.5 gauss and can be set to ± 1 milligauss. In addition to having very little noise, the shunts have excellent time and temperature stability. However, there are variations on the order of 20 milligauss/ 10° C if the temperature of the solenoid changes. If the pancakes are allowed to reach operating temperature before adjustments are made there should be no problem. The shunts will be trimmed using a Hall probe after the pancakes are installed within the flux return.

Because the all-aluminum solenoid has a higher resistance than its copper predecessor, a new power supply configuration capable of higher voltages is required. To reduce the magnetic field "droop" at the ends, the outer three pancakes will be run at a higher current than the remainder. These considerations dictate that a third separate power supply be used to operate the outer pancakes, and a new current controller capable of running all three supplies has been built. It is similar in design to its predecessor² and its performance should be the same.

The solenoid should be installed and tested in the next six months.

References:

1. Nuclear Physics Laboratory Annual Report, University of Washington (1980) p. 31.
2. Nuclear Physics Laboratory Annual Report, University of Washington (1983) p. 38.

7. MEDIUM ENERGY PHYSICS

7.1 Inclusive Scattering of Pions from very Light Nuclei at 100 MeV

J.F. Amann,* W. Burger,† K.G.R. Doss,‡ D.H. Dowell, I. Halpern,
M.A. Khandaker, D.D. Leach, T. Murakami, D.W. Storm, and D.R. Tiegler

Recently we performed an experiment on the inclusive scattering of pions from very light nuclei at 100 MeV. The experiment was motivated by our earlier finding^{1,2} that although inclusive pion scattering from elements heavier than ^{12}C appears to be mostly due to quasi-elastic scattering from nucleons, there are some features that cannot be accounted for in this way. We decided to study these features in light elements to avoid multiple scattering effects.

The present measurements were carried out using the QGD spectrometer in the M11 channel at TRIUMF (Experiment 224). Data were collected for π^+ on ^1H , ^3He , and ^4He at several laboratory angles, ranging from 40° to 125° , and for π^- on ^3He , and ^4He at 60° , 100° , and 125° . For normalization and diagnostic purposes some data were also collected for ^1H , ^{14}N , ^{12}C , and ^{208}Pb .

The target was a thin-walled 2 liter gas cylinder. It was run at room temperature and typical pressures of 1500 psi. Data were collected in three momentum bites of the spectrometer in order to cover up to 60 MeV in excitation energy. We had a preliminary run last summer and a final one this February. We are currently in the process of analysing the data. A preliminary set of energy spectra, relatively normalized, for π^+ on ^1H , ^3He , and ^4He at 60° , is shown in Fig. 7.1-1. The curves here are composites of all three momentum bites.

The main qualitative features of these spectra are as expected: the deuterium spectrum shows a clear quasi-elastic peak in addition to the elastic peak; the ^3He and ^4He spectra show additional yields at large energy loss, and appropriate gaps next to the elastic line, reflecting the absence of excited states below the particle breakup energy.

It is interesting to compare the ^3He and ^4He spectra. Quasi-elastic scattering for π^- (from the two protons) is likely to be more suppressed in ^4He than in ^3He due to the role of the extra neutron in pion absorption. A preliminary examination of the π^+ data indicates that at forward angles (60° , 75°) the ^4He inelastic cross-section, integrated from 24 to 60 MeV excitation energy, is slightly higher than that of ^3He , whereas at backward angles (100° , 125°) the cross-section for ^4He is slightly lower. Corresponding data for π^- show $^4\text{He}/^3\text{He}$ ratios that are about twice as large. We hope to account quantitatively for our findings in terms of simple models for the absorption and scattering of pions.

The experiment was designed to allow us to compare ^2H , ^3He , and ^4He directly. This should make it possible for us to interpret the observed differences in yields and spectra in terms of the effects of number of nucleon types and mean nucleon separations on the interactions of pions in nuclear matter.

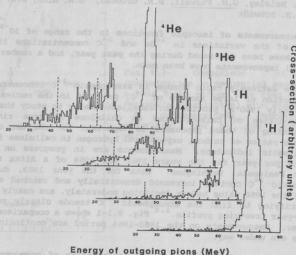


Fig. 7.1-1 Energy spectra for 100 MeV π^+ on ^1H , ^2H , ^3He , and ^4He at $\theta_{\text{lab}} = 60^\circ$.

- No efficiency correction has yet been applied to the spectra.
- The dashed lines show where the separate spectrometer momentum bites have been joined.
- The dip in spectra in the range 60-67 MeV is possibly due to fall-off of efficiency at the edges of the spectrometer's acceptance.
- The small tail on the elastic spectrum has been subtracted using the ^1H spectrum.
- The arrow in the ^2H and ^3He spectra shows the location of the quasi-elastic peak.

References:

- * Los Alamos National Laboratory, Los Alamos, NM 87545.
- † Massachusetts Institute of Technology, Cambridge, MA 02139.
- + Lawrence Berkeley Laboratory, Berkeley, CA 94720.
- 1. Nuclear Physics Laboratory Annual Report, University of Washington (1982) p. 98.
- 2. Nuclear Physics Laboratory Annual Report, University of Washington (1983) p. 54.

8. ACCELERATOR MASS SPECTROMETRY (AMS)*

8.1 AMS with Carbon and Beryllium: C-14 and Be-10 Radiochronology

D. Balsley, G.W. Farwell, P.M. Grootes, [†] G.M. Hinn, D.D. Leach, and F.H. Schmidt

Measurements of isotopic fractions in the range of 10^{-11} to 10^{-14} for studies of the variations in ^{10}Be and ^{14}C concentrations in environmental samples have been continued during the past year, and a number of significant technical improvements have been made.

The extremely rapid change in atmospheric ^{14}C concentration caused by the injection of large amounts of ^{14}C , produced in the nuclear weapons tests of the early 1960's, provides an excellent tracer to study the photosynthesis and deposition of carbohydrates as cellulose in tree rings. A better understanding of these processes is important for the use of the isotopic abundance ratios of carbon, oxygen, and hydrogen in cellulose in tree rings as paleoclimatic indicators. Measurements are in progress on ten sequential segments per year for the years 1962 and 1964 of a Sitka spruce from the Olympic Peninsula, Washington. Data for the year 1963, during which the atmospheric ^{14}C content increased dramatically and reached a peak at about 200% of the 1950 value before declining moderately, are nearly complete and it is gratifying to find the atmospheric ^{14}C trends clearly reflected in the single-year tree-ring profile.^{1,2} Fig. 8.1-1 shows a comparison of the two ^{14}C profiles. Measurements on the 1962-1964 period are continuing and modelling studies are under way.

A better understanding of the geochemistry of cosmogenic beryllium is needed for its successful use in understanding environmental processes and their chronologies. A study of ^{10}Be concentrations in rain water samples from different northern latitudes in Washington and Alaska is in progress; these measurements will provide information on the latitudinal and temporal variations in natural ^{10}Be deposition rates. We have also begun a series of measurements of ^{10}Be in surface layers of snow from the South Pole.

References:

- [†] Quaternary Isotopes Laboratory, University of Washington.
1. G.W. Farwell, P.M. Grootes, D.D. Leach, and F.H. Schmidt, in Proceedings of the Third International Symposium on Accelerator Mass Spectrometry (Zürich, 1984), Nucl. Instrum. Meth. (to be published).
 2. R. Nydal, K. Lovseth, and F.H. Sköglseth, Radiocarbon 22, 626 (1980).

* Our work has been supported in part by the M.J. Murdock Charitable Trust and the National Science Foundation (Grant EAR-8115994, Environmental Geosciences Program).

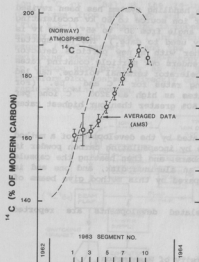


Fig. 8.1-1 Comparison of ^{14}C concentration in sequential segments of a 1963 Sitka spruce tree ring (Olympic Peninsula, Washington) with atmospheric ^{14}C concentrations (Norway and elsewhere, Ref. 2) for the same period.

8.2 AMS: Technical Improvements

D. Balsley, G.W. Farwell, H. Fauska, P.M. Grootes,* D.D. Leach, and F.H. Schmidt

Last year¹ we reported progress on two systems of normalization of the rare isotope beam (particle counting rate, ^{14}C or ^{10}Be) against the stable isotope beam or beams (^{12}C , ^{13}C or ^9Be ion current). In the concurrent monitoring method, the abundant isotope (e.g., ^{12}C) is monitored at the low-energy end of the accelerator while the rare isotope (e.g., ^{14}C) is monitored simultaneously following acceleration and high-energy ion analysis. In the sequential transmission method, the rare and abundant isotopic ion beams are alternated by adjustment of the entire set of accelerator parameters. The recent advent of a two-level, nuclear-magnetic-resonance-controlled isotope alternation system (see below, Sec. 8.3) has greatly enhanced the effectiveness of the sequential transmission method and we experienced little difficulty taking data on carbon from tree-ring segments with about $\pm 2\%$ accuracy for a single measurement. (Our measurements are made by comparison with working standard samples that have been accurately measured by β -counting

in the Quaternary Isotope Laboratory.)

Our low-energy (pre-accelerator) beam handling system has been revised to accommodate the elevation of the sputter ion source to 60 kv accelerating potential and a shift of the ion injection angle from 30° to 45°. (30 kv is the highest accelerating potential actually used to date.) The new sputter ion source-low energy beam system, together with a new particle detector telescope that has a larger aperture and renders our particle counting rates less sensitive to small fluctuations in accelerator terminal voltage, has led to increased stability and higher counting rates for ^{14}C and ^{10}Be . (For example, we recently observed counting rates as high as 3200 ^{14}C ions per minute from a 1964 carbon sample; this is 50% greater than our highest rates observed heretofore.)

The ^{14}C work has been greatly facilitated by the development of a method of direct conversion of carbon to graphite by encapsulating carbon powder in Ta tubing, compressing it to about 14 kilobars, and then heating the capsule to 2,500°C. The capsule is pressed into an aluminum disk, and one end is machined off in a lathe. The samples prepared by this method give beams of the same magnitude as commercial graphite.

Further details of these and related developments are reported elsewhere.^{2,3,4}

References:

- * Quaternary Research Laboratory, University of Washington.
1. Nuclear Physics Laboratory Annual Report, University of Washington, (1983) p. 122.
 2. G.W. Farwell, P.M. Grootes, D.D. Leach, F.H. Schmidt, and M. Stuiver, Radiocarbon 25, 711 (1983).
 3. G.W. Farwell, P.M. Grootes, D.D. Leach, and F.H. Schmidt, Radiocarbon 25, 755 (1983).
 4. G.W. Farwell, P.M. Grootes, D.D. Leach, and F.H. Schmidt, in Proceedings of the Third International Symposium on Accelerator Mass Spectrometry (Zürich, 1984), Nucl. Instrum. Meth. (to be published).

8.3 Isotope Alternation System: Two-Level, NMR-Controlled Rapid Switching

G.W. Farwell, H. Pauska, D.D. Leach, and F.H. Schmidt

In the sequential transmission method of normalization in AMS (Sec. 8.2, above) the magnetic parameters of the accelerator must be alternated between their values for the lighter and the heavier isotopes with as little loss of time as possible. Rapid changing of these parameters has been effected through a combination of computer control and nuclear magnetic resonance (NMR) search and lock control.

In the current applications of the system to ^{14}C and ^{10}Be , the abundant ion (^{12}C or ^9Be) is monitored at the image Faraday cup ("flap") and the rare ion (^{14}C or ^{10}Be) at the 24-inch scattering chamber, which is located downstream from the flap and some distance beyond the switching magnet (Fig. 8.3-1). In changing isotopes, then, it is necessary to adjust the low-energy injection magnet ("inflection magnet"), the high-energy 90° analyzing magnet ("90° magnet"), and the high-energy quadrupole magnet, but not the switching magnet. The high-energy quadrupole magnet is computer-controlled⁴ to change appropriately as the 90° magnet changes, and it is necessary, therefore, to control directly only the inflection and 90° magnets with the rapid-switching system.

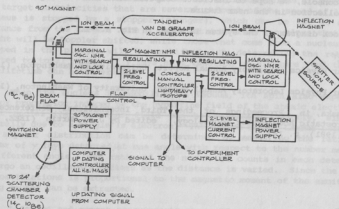


Fig. 8.3-1 Block diagram of two-level NMR-controlled rapid magnet-switching system.

The basic NMR magnet regulator system was described earlier.^{2,3}

To assure fast response in the two-level rapid-switching application, we have constructed two NMR marginal oscillator controllers with search and lock features. The NMR regulator fine tuning makes use of Varicaps (voltage variable-capacity diodes); accordingly, the rapid switching circuit generates two voltage levels corresponding to the appropriate NMR frequencies for the lighter and heavier isotopes.

The rapid-switching circuit is interlocked with "in regulation" signals from both the inflection magnet and the 90° magnet; these signals, together with appropriate time delays, are used to protect the rare isotope particle detector from the abundant isotope ion beam and to optimize the actual particle counting intervals.

Because the available NMR-controlled magnetic flux correction is limited, a step current increase is given through the main power supply of each magnet when an isotope shift occurs. In the case of the 90° magnet this is accomplished through computer control, and a corresponding change is imposed on the high-energy quadrupole magnet current.

The total response time for switching between isotopes is typically seven to eight seconds.

While at present the isotope switching control is manual at the operating console, we hope to institute computer-controlled isotope switching and data collection in the near future.

A block diagram of the system is shown in Fig. 8.3-1.

References:

1. Nuclear Physics Laboratory Annual Report, University of Washington, (1981) p. 147.
2. Nuclear Physics Laboratory Annual Report, University of Washington, (1972) p. 16.
3. H. Fauska, in Proceedings of the Third International Conference on Electrostatic Accelerator Technology, edited by J.A. Martin (IEEE, New York, 1981), p. 147.

9. RESEARCH BY OUTSIDE USERS

9.1 Lifetime and Magnetic Moments of States of ^{16}N by the Recoil-into-Vacuum Method

S.S. Hanna, * B.T. Neyer, † and J.L. Thornton, *

The lifetimes and magnetic moments of some of the low lying states of ^{16}N have been measured by means of the recoil-into-vacuum technique.

In this technique the nuclear states under study are produced by a nuclear reaction. The reaction causes the excited nucleus to recoil out of the target at velocities that are several percent of the speed of light. The nucleus is stopped by a stopper (plunger), which can be set at a variable distance from the target. The γ rays that come from a nucleus that decays in flight will be Doppler shifted, while those that come from a nucleus that has stopped in the plunger will be unshifted. By determining the ratio of the shifted to total number of γ rays as a function of distance (and thus time), the lifetime can be determined.

When the nucleus is recoiling in vacuum, its spin also experiences a Larmor precession induced by the hyperfine field of the atomic electrons. For light nuclei the hyperfine field can be calculated exactly, since it is generally due to a single electron. The effect of the Larmor precession on the angular distribution can be determined by measuring the ratio of the number of γ rays detected at one angle with respect to the number measured at a different angle. The ratio of the number of counts in each detector will undergo an oscillatory pattern as the distance is varied. Since the period of the oscillations is proportional to the magnetic moment of the excited state, the g factor can be extracted.

Lifetime and moment measurements were made on the 297 keV, 3^- state in ^{16}N and lifetime measurements were made on the 397 keV, 1^- state in ^{16}N , with the reaction $d(^{15}\text{N}, p)^{16}\text{N}$. Measurements detecting the outgoing coincidence proton were made at a beam energy of 34 MeV, while singles measurements were performed at 20 MeV. The preliminary results obtained are (see Fig. 9.1-1):

$$\tau(^{16}\text{N}, 297, 3^-) = 121.2 \pm 3.5 \text{ psec}$$

$$\tau(^{16}\text{N}, 397, 1^-) = 6.46 \pm 0.20 \text{ psec}$$

$$g(^{16}\text{N}, 297, 3^-) = 0.499 \pm 0.025$$

References:

- * Physics Department, Stanford University, Stanford, CA 94305.
- † Physics Department, Stanford University, Stanford, CA 94305 and Sandia National Labs, Div. 1234, Albuquerque, NM 87185.

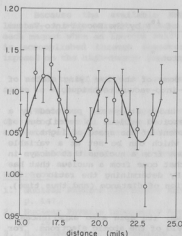


Fig. 9.1-1 Oscillation Curve of the 297 keV, 3^- state of ^{16}N . The ratio of total counts at 0° to total counts at 90° , I, as a function of stopper distance D is shown. The errors shown are statistical.

9.2 Simultaneous Measurement of Nuclear Magnetic Moments by the Transient Field Method

S.S. Hanna,* B.T. Neyer,[†] and J.L. Thornton,*

In the past year we have completed measurements of the magnetic moments of the first 2^+ states in all even Pd and Te isotopes except ^{150}Te , which was not measured because of its small counting rate. The primary goal of these experiments has been to determine deviations from the predictions of the collective model, $g = Z/A$. Of particular interest was the exact dependence of the magnetic moments on neutron number N and whether this dependence agreed with predictions of the Interacting Boson Approximation (IBA)¹ and with some previous data.^{2,3,4} In this regard special emphasis was placed on modifying the usual transient field method in order to obtain much reduced systematic errors. In this modified method several isotopes were measured at once, instead of the usual one per target and the resulting γ ray lines were separated with Ge(Li) detectors instead of being observed in NaI detectors. Due to the increased resolution of the Ge(Li) detectors this procedure results in a much cleaner extraction of the angular rotations from the data. In addition target dependent errors are virtually eliminated since now beam damage or target fabrication uncertainties will affect all the isotopes equally.

The results of this work are given in the table below where, following the work of Brennan et al.² and Dunham,⁴ we have taken $g(^{106}\text{Pd}) = 0.40 \pm 0.02$, $g(^{122}\text{Te}) = 0.36 \pm 0.02$, and $g(^{124}\text{Te}) = 0.28 \pm 0.03$ as our calibration points.

These latter values represent averages over various Integral Perturbed Angular Correlation (IPAC) measurements for the relevant magnetic moments. The final g factors have then been determined by doing a least-squares fit to all of our data plus the calibration data for a given isotopic sequence, in which the scale factor relating observed angular rotations to g factors for each target was allowed to vary. These results along with the Z/A and IBA predictions are shown in Fig. 9.2-1.

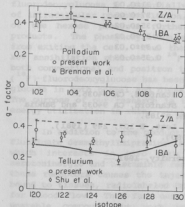


Fig. 9.2-1 Measurements of the 2^+ state g factor for palladium and tellurium isotopes. Dashed line gives Z/A ; solid line gives these predictions of the Interacting Boson Approximation.

The results for the Pd isotopes are seen to be reduced somewhat from Z/A and in good agreement with the IBA predictions. They are also in good agreement with the previous measurements of Brennan *et al.*² as might be expected since the Pd targets stand up very well in the beam and thus beam damage errors should be small. For the Te isotopes the measured magnetic moments, while also below Z/A , are seen to be consistently above the IBA predictions. In addition the dip at ^{126}Te predicted by the IBA and exhibited so dramatically in the data of Shu *et al.*³ is not observed either here or in the previous work of Dunham.⁴ The combined data for ^{126}Te is statistically inconsistent at better than the 99% confidence level and it seems likely that this discrepancy is due to target related error in the data of Shu *et al.* This is especially true since Te has a very high vapor pressure and we have observed visually dramatic changes in the Te targets even after short exposures to the beam. Thus while the traditional transient field method may be satisfactory in the case of targets that stand up well in the beam, in the case where they do not a simultaneous measurement would seem well warranted.

Table 9.2-1
G-Factors for Pd and Te Isotopes

Measured g-Factors for the First 2^+ States of even Pd and Te Isotopes.

Isotope	G-Factor
^{102}Pd	0.40 ± 0.05
^{104}Pd	0.38 ± 0.04
^{106}Pd	0.40 ± 0.02
^{108}Pd	0.33 ± 0.03
^{110}Pd	0.31 ± 0.03
^{120}Te	0.37 ± 0.06
^{122}Te	0.35 ± 0.02
^{124}Te	0.31 ± 0.02
^{126}Te	0.34 ± 0.03
^{128}Te	0.35 ± 0.03

References:

- * Physics Department, Stanford University, Stanford, CA 94035.
- † Physics Department, Stanford University, Stanford, CA 94035 and Sandia National Labs, Div. 1234, Albuquerque, NM 87185.
- 1. M. Sambataro and A.E.L. Dieperink, Phys. Lett. B 107, 249 (1981).
- 2. Brennan *et al.*, Phys. Rev. C 21, 574 (1980).
- 3. Shu *et al.*, Phys. Rev. C 24, 954 (1981).
- 4. J.S. Dunham, Ph.D. Thesis, Stanford University, 1981.

9.3 Short-Lived Radionuclides for Biomedical Research

P. Kremer, * K.A. Krohn, * and J. Link *

This past year we have continued to develop short-lived radioisotopes for biomedical research in the School of Medicine at the University of Washington. ^{18}F is being produced using the Tandem Van de Graaff accelerator by bombarding gaseous ^{20}Ne with 15 MeV deuterons. Added F_2 (1%) reacts with the nucleogenic ^{18}F to produce F^{18}_2 , a useful organic fluorinating agent. We are producing approximately 300 mCi of ^{18}F per 6 μA hours and can transfer 125 mCi from the target to a chemical reaction vessel in a hot cell. The target effluent contains no detectable ^{18}F .

Over the past year, most of the ^{18}F has been used to synthesize 2-fluorodeoxyglucose. The synthesis consists of introduction of the gaseous F^{18}_2 into a solution of ammonium acetate. The ^{18}F as F^- is ionically complexed with the acetate and ammonium ions. Triacetylglucal (TAG) is added to this mixture and the (^{18}F)-acetylhypofluorite reacts stereospecifically with the two position of TAG. The remaining acetic acid and ammonium fluoride can be conveniently evaporated from the solution. HCl is added and the mixture is heated for 12 minutes to effect hydrolysis of the protective acetyl

groups and yield (^{18}F)-2-fluorodeoxyglucose. The compound is purified by a combination of ion exchange and silica gel flash chromatography and taken to University Hospital for studies in animals. This past year, we have synthesized ^{18}F FDG nine times for use in animal studies by three different research groups. Synthesis yields are approximately 20% EOB of the fluorine removed from the target.

Fluorodeoxyglucose is of biomedical interest because it functions *in vivo* as an analog of glucose. The rate of cellular uptake of the fluorodeoxyglucose is essentially the same as that of glucose as is the rate of intracellular phosphorylation, but the fluorine atom on the second carbon of the hexose prevents further metabolism to fructose and smaller end products. The phosphorylation adds charge to the molecule and prevents it from exiting the cell. Thus the tracer is "metabolically trapped." The 511 keV annihilation photons of ^{18}F are convenient to detect quantitatively by both conventional and positron tomographic nuclear medicine imaging devices. (^{18}F)-fluorodeoxyglucose has been used to study *in vivo* kinetics and uptake of glucose in both normal and diseased animals by our biomedical collaborators. The purpose of our research is to use this tracer for measurements of tumor energy utilization in rats.

In addition to the production of (^{18}F)FDG, we have made two attempts to fluorinate desmethylinipramine (DMI) using ^{18}F . DMI is an antidepressant drug which interacts *in vivo* with muscarinic cholinergic, alpha adrenergic, serotonergic and histaminic receptors. Because interaction of the DMI with these receptors causes the injected DMI to be extracted from the blood and bound to tissues, radiolabeled DMI is potentially useful as an *in vivo* tracer for blood flow. Thus far, our attempts to label with ^{18}F have produced an unstable compound but work is continuing on this important class of molecules.

In addition to the work with ^{18}F , we are preparing to produce ^{11}C by the reaction of protons on ^{14}N . ^{11}C is of biomedical interest because carbon is a normal component of biochemicals; compounds which are both biologically active and easy to detect quantitatively can be synthesized using this isotope. Nucleogenic ^{11}C will be heated with a catalyst to produce (^{11}C)- CO_2 which will be reduced using LiAlH_4 to produce (^{11}C)- CH_2OH , and then refluxed with HI to yield (^{11}C)- CH_3I . Both of these compounds will be used as precursors for synthesis of other compounds of biomedical interest. In particular, the projects which are now in preparation will involve the synthesis of (^{11}C)-fatty acids for the study of cardiac function and (^{11}C)-deoxyuridine from (^{11}C)- CH_3I for the study of DNA synthesis in tumors and surrounding tissues as a function of cytotoxic therapy.

Reference:

- * Department of Radiology, University of Washington.

9.4 Irradiation of Optical Materials

K.L. Ballou,* C. Gulascik,* G.M. Hess,* and A.R. Tokuda,*

Samples of different optical glasses were irradiated with iodine ions for the Boeing Company. The resulting damage tracks were then etched to form a type of anti-reflecting surface. More work is planned to try to optimize the process.

Reference:

* Boeing Aerospace Company, Seattle, WA 98124.

9.5 Light Ion Irradiation Creep

E.R. Bradley,* C.H. Henager, Jr.,* E.P. Simonen,* and R.G. Stang†

The U.S. Department of Energy, Office of Basic Energy Sciences, supports a Radiation Effects on Metals and Ceramics program at Battelle, Pacific Northwest Laboratory (PNL). A light ion irradiation creep experiment, as part of the PNL research program, is being conducted at the Nuclear Physics Laboratory. Irradiation creep is defined as the time-dependent deformation of a material induced by stress during energetic particle irradiation in excess of that observed in the absence of irradiation. Pure nickel specimens were bombarded with deuterons, using the Van de Graaff accelerator, to further the understanding of low-dose irradiation creep mechanisms.^{1,2}

An irradiation creep model developed to explain irradiation creep of nickel³ has been able to rationalize all the irradiation creep data obtained during this experiment. Specimens of pure nickel with three different microstructures were irradiated at 473° K with 15 or 17 MeV deuterons.^{3,4} The effects of irradiation prior to the stress application and the effects of stress increases during irradiation were studied. There was a significant effect due to initial microstructure, predicted by the model, based on the relationship of the applied stress to the yield stress of the particular microstructures.⁵ Recently, the irradiation creep model has been used to rationalize low fluence creep data for 316 stainless steel irradiated with either charged particles or neutrons.⁶ The model successfully predicted low fluence creep rates and low fluence microstructural evolution in stainless steel. The experiments on pure nickel, therefore, produced results applicable to more complex metal.

References:

* Pacific Northwest Laboratory, Richland, WA 99352.

† Department of Materials Science and Engineering, University of Washington.

1. P.L. Bendrick, Nucl. Instrum. Meth. 161, 345 (1979).

2. C.H. Henager, Jr., J.L. Brimhall, and E.P. Simonen, *J. Nucl. Mater.* **90**, 290 (1980).
3. C.H. Henager, Jr., E.P. Simonen, E.R. Bradley, and R.G. Stang, *J. Nucl. Mater.* **117**, 250 (1983).
4. C.H. Henager, Jr., Ph.D. Dissertation, University of Washington (1983).
5. C.H. Henager, Jr., E.P. Simonen, E.R. Bradley, and R.G. Stang, presented at the 3rd Topical Meeting on Fusion Reactor Materials, Albuquerque, NM, 1983, and accepted for publication in *J. Nucl. Mater.*
6. C.H. Henager, Jr., and E.P. Simonen, accepted for publication in the Proceedings of the ASTM Twelfth International Symposium on the Effects of Radiation on Materials, Williamsburg, VA 1984.

9.6 Simulation of Cosmic-Ray Upset in Integrated Circuits

C.J. Malone,* L.S. Smith,* and J.A. Zoutendyk*

Cosmic rays are known to cause bit errors (cosmic-ray upset) in digital integrated circuit chips. Heavy ions in the cosmic-ray spectrum are the worst offenders due to their large stopping powers (dE/dX). Ionized charge (electron-hole pairs) created along an ion track in a silicon chip is collected at a junction within an integrated circuit in a manner very similar to what occurs in a solid-state nuclear detector. Traversal of a particle through a digital device can cause a bit error to occur provided the collected charge is greater than a critical value (or values) characteristic of that device.

The tandem Van de Graaff accelerator was used to determine experimentally the critical charge values characteristic of a bipolar random-access memory chip. Bromine ions with kinetic energies ranging from 20 MeV to 117 MeV (the latter energy was obtained with a charge state of 12 and a terminal voltage of 9 MV) were used to simulate cosmic-ray upset in the solid-state device. The data obtained for upset cross section as a function of Br-ion energy (collected charge) were in excellent agreement with theoretical modeling done earlier.¹ Structure in the data which was predicted by the theoretical model was observed by selecting twenty-two values of Br-ion energy within the 20-117 MeV range. This experiment is the first one in which the physics governing the interaction of an ion track within a complex integrated circuit has been examined in detail.

References:

- * Jet Propulsion Laboratory, California Institute of Technology, Pasadena, CA 91109.
1. J.A. Zoutendyk, *IEEE Trans. Nucl. Sci.* **NS-30**, 4540 (1983).

9.7 Fast Neutron Beam Radiotherapy: Medical Radiation Physics*

J. Eenmaa,[†] J. Kuan,[†] and P. Wiest[†]

The Medical Radiation Physics Division continued its routine support of the treatment of cancer patients and neutron beam radiobiology studies. The neutron beam facility has been described in detail in previous reports.¹ No significant developmental or research activity took place during the year.

The facility for treatment of cancer patients was deactivated at the end of February.

References:

- * Supported by NCI Grant No CA-12441
- † Division of Medical Radiation Physics, Department of Radiation Oncology, University of Washington.
- 1. Nuclear Physics Laboratory Annual Reports, University of Washington (1972-1981).

9.8 Fast Neutron Beam Radiotherapy: Clinical Program*

G.E. Laramore[†]

From 4/1/83 through 2/29/84, 26 patients have been placed on RTOG neutron protocols, 5 patients have been entered on an NCI-approved study (SWOG 83-67) to test the feasibility of combining chemotherapy with large dose per fraction neutron radiotherapy for non-small cell lung cancer, and an additional 12 patients have been treated on institutional pilot studies. Of the latter patients, 10 had sarcomas, 1 had a salivary gland tumor recurrent in a previously irradiated region (and, hence, was not protocol-eligible), and 1 had a malignant glioma which was treated with combined chemotherapy and neutron irradiation. The breakdown of the protocol patients is given in Table 9.8-1.

Table 9.8-1
Protocol Patient Distribution

Protocol	Patient Number
RTOG 76-08 (cervix)	1
RTOG 77-04 (prostate)	1
RTOG 79-07 (lung)	5
RTOG 79-21 (pancreas)	1
RTOG 80-01 (salivary gland)	3
RTOG 80-07 (glioma)	11
RTOG 81-10 (bladder)	2
RTOG 82-02 (head and neck)	2
SWOG 83-67 (lung)	5
TOTAL	31

Major New Findings

Lung: As of 6/1/83, protocol RTOG 79-07 had accrued a total of 110 patients. Patients are randomized to receive either conventional photon irradiation, fast neutron irradiation, or mixed beam (neutron/photon) irradiation. This study will likely be closed at the next high LET committee meeting to be held in June 1984. A preliminary analysis of the data seems to indicate a higher complete response rate for the neutron-treated patients but no improvement in median survival. The new SWOG pilot study utilized induction chemotherapy with two alternating cycles of vinblastine/mitomycin-C and vinblastine/cis-platinum prior to neutron irradiation in order to address this problem.

Prostate: Protocol RTOG 77-04 was closed to new patients entry in April 1983. A total of 95 patients were entered. This study compared conventional photon irradiation to mixed beam (neutron/photon) irradiation for patients with stage C adenocarcinoma of the prostate. A preliminary analysis indicated a statistically significant improvement in crude survival at three years in favor of the mixed beam group (82% vs. 49%) but no obvious correlation with clinically-assessed local control or time to the development of distant metastases. The significance of these findings is under study.

Sarcomas: A review of the world's literature on soft tissue sarcomas and bone sarcomas seems to indicate a much higher rate of local control with fast neutrons than would be expected for conventional photon irradiation. A total of 286 patients with large inoperable soft tissue sarcomas have been treated at the various neutron centers with an overall local control rate of 61%. Two review articles of this material are in preparation. We anticipate that sarcomas as well as salivary gland tumors are likely tumor systems to show improved local control with neutron irradiation in the next generation of studies to be carried out on the new clinical treatment facilities.

References:

* Supported by NCI Grant CA-12441.

† Department of Radiation Oncology, University of Washington.

9.9 Neutron Radiobiology in Support of Radiotherapy*

J.S. Rasey[†]

The Experimental Biology Division of The Department of Radiation Oncology continues to perform radiobiology experiments in support of the radiotherapy of human cancer with fast neutrons. Patient treatment with the 22 MeV d+Be neutron beam from the nuclear physics laboratory cyclotron ceased in February, 1984. Patient treatment will begin shortly with the 48 MeV p+Be neutron beam from the Clinical Neutron Therapy System (CNTS) at the University

Hospital. Our studies in the past year have been directed toward determining the relative biological effectiveness (RBE) of the 22 MeV beam relative to the 48 MeV beam. The RBE for the 22 MeV d+Be neutron beam relative to ^{137}Cs gamma rays has been determined using cell survival in V79 cells in vitro and two in vivo systems, acute response of mouse skin and survival of mouse intestinal crypt cells. The RBEs obtained with these three systems at various dose levels are summarized in Table 9.9-1. RBE is defined as dose of ^{137}Cs gamma rays required to produce a particular biological effect divided by the dose of neutrons required to produce the same effect. A late responding normal tissue, rat spinal cord, was added to the RBE comparison. It was deemed important to ultimately determine the RBE for 48 MeV p+Be neutrons relative to 22 MeV d+Be neutrons for this dose limiting tissue because neutron RBEs for central nervous system damage have proven to be high.

Table 9.9-1
RBEs for 22 MeV d+Be Neutrons Relative to ^{137}Cs Gamma Rays

System	Endpoint	^{137}Cs Gamma Ray Dose, rads	22 MeV d+Be Neutron Dose, rads	RBE
V-79 cells <u>in vitro</u>	0.5 surviving fraction	675	305	2.21
	0.1 surviving fraction	1240	590	2.10
Mouse intestinal crypt cells	50 surviving cells per circumference	1275	640	1.99
	10 surviving cells per circumference	1445	770	1.88
Mouse skin	0.75 average skin response (7-35 days post radiation)	2245	1140	1.97
	1.0 average skin response (7-35 days post irradiation)	3050	1390	2.19
	1.25 average skin response (7-35 days post irradiation)	3760	1600	2.34

The ideal way to determine RBEs between two neutron beams is to irradiate the test system with two radiation sources on the same day. However, the clinical neutron therapy system is not yet available for biological testing. Our approach therefore is to do a gamma ray experiment at the same time as each neutron irradiation, so that experiments with any neutron beam can be normalized to a common photon control. This will ultimately allow determination of relative biological effectiveness for the

new high energy CMTS neutron beam relative to the neutron beam from the Nuclear Physics Laboratory which had been used for patient treatment for over ten years. These studies will facilitate transition of patient treatment from the Nuclear Physics Laboratory cyclotron to the hospital based therapy unit.

References:

- * Supported by NIH Research Grant #1 R01 CA35478.
- † Department of Radiation Oncology, University of Washington.

9.10 Normal Tissue Neutron Radiobiology*

P.A. Mahler*

The University of Washington is one of three institutions being funded by the National Cancer Institute to examine the efficacy and feasibility of new hospital-based cyclotrons for cancer therapy with neutrons.

Past experience has indicated that central nervous system tissue is the most significant dose limiting normal tissue for neutron therapy.

We are currently conducting experiments to gain information about the new therapy beam by using damage to rat spinal cord as a measure of the beam's relative biological effectiveness (RBE). Using ^{137}Cs gamma rays, 22 MeV d+Be neutrons from the Nuclear Physics Laboratory and 48 MeV p+Be neutrons from the new hospital cyclotron we will determine the doses to produce equal levels of spinal cord damage. The ratios of the doses to produce equivalent effects

$$\frac{^{137}\text{Cs}}{\text{p+Be}} \quad \text{and} \quad \frac{\text{d+Be}}{\text{p+Be}}$$

will give measures of the RBE of the new beam compared to the two older beams. The two older beams have a base of human clinical data upon which to draw. Therefore it will be possible to estimate tolerance doses for the new neutron beam based on the experimental RBE's and the human data bases.

Reference:

- * Division of Medical Radiation Physics, Department of Radiation Oncology, University of Washington.

9.11 Effect of Antibiotic Decontamination of the GI Tract on Survival Time after Neutron and Gamma Irradiation*

J.P. Geraci,[†] K.L. Jackson,[†] and M.S. Mariano[†]

Antibiotic decontaminated and conventional rats were whole-body irradiated with 8 MeV neutrons (1.5 to 13 Gy) or ¹³⁷Cs gamma radiation (9 to 20 Gy). The animals were checked for survival at four hour intervals from the second to the seventh day postirradiation and at eight hour intervals on other days. After doses greater than 7.5 Gy of neutrons and 15 Gy of photons median survival time was relatively constant at 4.2 to 4.5 days, indicating death was primarily due to intestinal injury. After doses in the range of 5 to 7 Gy of neutrons and 10 to 14 Gy of photons median survival time was dose dependent and varied from 12 days to 4.5 days, suggesting a changing distribution of deaths due to intestinal injury as opposed to hematopoietic injury. Decontamination of the GI tract increased median survival time 1 to 5 days in this range of dose dependency, whereas the effect of decontamination was negligible for doses that produced mostly intestinal death. These results suggest that sepsis and endotoxin produced by bacteria from the intestinal tract play little role in acute intestinal radiation death.

References:

- * Research was conducted according to the principles enunciated in the "Guide for Laboratory Animal Facilities and Care," prepared by the National Academy of Sciences-National Research Council. Work supported by Defense Nuclear Agency contract #DNA001-83-C-0009.

[†] Radiological Sciences Division, Department of Environmental Health, University of Washington.

9.12 Measurement of Total Body Calcium by Neutron Activation

C.H. Chesnut,* B.L. Lewellen,* and R. Murano*

We have now completed 15 years using neutron activation to measure total body calcium in patients with bone wasting disease.¹ In the past year we performed 88 patient irradiations. Two therapeutic regimes were under test. Under the first regime, patients were treated with 1,25 dihydroxy calciferol (vitamin D).² Under the second regime, patients who had been treated with disodium chlodronate³ were followed after withdrawal of the drug. In both studies, an equal number of untreated control subjects were followed and many other tests were performed as well as neutron activation. Since June, 1982 we have also been measuring the bone mineral in the lumbar spine by the dual photon absorption technique developed by Mazess of the University of Wisconsin and applied extensively by Wahner and Riggs of the Mayo Clinic.

References:

- * Division of Nuclear Medicine, University of Washington.
1. Nuclear Physics Laboratory Annual Reports, University of Washington (1967-1982).
2. Hoffman-LaRoche Laboratories.
3. Proctor and Gamble.

10. ACCELERATORS AND ION SOURCES

10.1 Van de Graaff Accelerator Operations and Development

J.F. Amsbaugh, J.R. Cromie, H. Fauska, D.J. Hodgkins, D.D. Leach,
C.E. Linder, G.E. Saling, F.H. Schmidt, R.E. Stowell, T.A. Trainor,
T. Van Wechel, W.G. Weitkamp, and D.I. Will

Major development projects related to the tandem accelerator are described in Secs. 10.3, 10.4, and 10.5. Accelerator modifications required by the radiochronology group are described in Sec. 8.2. In addition to these projects, we have installed a new air cooled high energy cup.

Accelerator maintenance required during the past year has been quite routine. The charging belt presently in the machine seems to be the most long-lived we have had. As of April 15, 1984, this belt had run 10,300 hours.

One rather unexpected maintenance problem was pointed out by the radiochronology group. The calibration of the generating voltmeter on the tandem was found to be erratic. This was traced to deteriorating bearings on GVM motor, which had clogged up with belt dust after more than 100,000 hours of operation.

During the year from April 16, 1983 to April 15, 1984 the tandem operated 4842 hours. Other statistics of the accelerator operation are given in Table 10.1-1.

10.2 Cyclotron Operations and Development

J.R. Cromie, H. Fauska, B.L. Lewellen,* R. Murano,* G.J. Rohrbaugh,
R.E. Stowell, W.G. Weitkamp, and P. Wiest†

The 60 in. cyclotron is now in its 34rd year of continuous operation. Maintaining the cyclotron in operating condition required installation of a new oscillator tube, replacement of the variac coils on the main magnet power supply and overhaul of the main magnet oil circulating pump.

The new University Hospital clinical neutron therapy cyclotron is now operating so that cancer therapy operations at the 60 in. cyclotron stopped at the end of February, 1984. (See Sec. 9.7-9.11 for a description of those activities.) Calcium measurements, described in Sec. 9.12, will continue for the near future.

The machine ran 908 hours between April 16, 1983 and April 15, 1984. Other statistics of cyclotron operations are given in Table 10.2-1.

References:

* Nuclear Medicine, University of Washington.

† Medical Radiation Physics, University of Washington.

Table 10.1-1
Tandem Accelerator Operations
April 16, 1983 to April 15, 1984

Activity	Days Scheduled	Percent
A. Nuclear Physics Research		
Light Ions	96	26
Heavy Ions	76	21
Radiochronology	35	9
Total	207	56
B. Outside Users		
Battelle Northwest Laboratories	6	2
The Jet Propulsion Laboratory	6	2
The Boeing Company	4	1
Stanford University	27	7
University of Washington	4	1
Department of Radiology		
Total	47	13
C. Other Operations		
Accelerator Development	40	11
Accelerator Maintenance	37	10
Unscheduled Time	35	10
Total	112	31
Grand Total	366	100

Table 10.2-1
Statistics of Cyclotron Operations
April 16, 1983 to April 15, 1984

Activity	Days Scheduled	Percent
Department of Radiation Oncology		
Cancer Therapy	98	53
Experimental Oncology	5	3
Neutron Dosimetry	2	1
Division of Nuclear Medicine Total Body Calcium	50	27
Department of Radiological Sciences	4	2
Nuclear Physics Laboratory	2	1
Maintenance	24	13
Total	185	100

10.3 Predicting Tandem Parameters

W.G. Weitkamp

Most modern accelerators are built so that all the beam-optics parameters such as lens and steerer settings can be set automatically by a computer. Some parts of an older machine can be retrofit relatively easily to be automatically set by a computer. An example is the system used to set the high energy magnets on our machine.¹ However, retrofitting all the power supplies of an older tandem accelerator is probably not cost effective. Never-the-less, there are many cases in which an accelerator operator can use the guidance a computer can supply, especially when the operator is inexperienced.

We are developing a program to assist an operator in setting up our tandem accelerator. The program asks a number of questions to determine the ion species and the energy required and the configuration of the machine. It then calculates all beam-optics power supply settings and predicts the beam transmission, using simple algorithms or interpolating between sets of parameters known to give a good accelerator tune. The information is printed out in a form similar to an accelerator log sheet.

The program presently works well for beams from the direct extraction ion source and is soon to be completed for beams from the other ion sources.

Reference:

1. Nuclear Physics Laboratory Annual Report, University of Washington (1983) p. 147.

10.4 Crossed-Beams Polarized Ion Source

J.G. Douglas, C.A. Gossett, S.E. Kellogg, T.A. Trainor, D.I. Will, and V.J. Zeps

This ion source was to be produced by ANAC, Ltd. at Auckland, New Zealand. ANAC went into receivership in December, 1982, with work on the project only partially completed. Attempts early in 1983 to negotiate with the receiver a new contract for completion of the ion source ultimately bore no fruit, although all the interested parties were in agreement on the basic issues. This failure was due in large part to long delays in communication when various University departments acted as third parties in negotiations.

In August, 1983, negotiation turned to establishing terms whereby the the University could claim title to existing hardware. This process was completed in a period of days by telephone. The hardware was received by the University in Auckland and air freighted to Seattle in early October, 1983.

What we have received from ANAC is about 70% of the hardware required to complete the original design. This design calls for a cesium gun, a ground state atomic beam source, an ionizer region, a neutralizer/injector region and a spin precessor. In addition are required power supplies, racks, support stands, vacuum hardware, and control systems. Although only 30% of the hardware remained to be completed upon shipment, these items usually involved difficult design decisions which had not been made.

In the initial period after shipment these design questions were addressed, and negotiations were carried out with two sub-contractors, one to finish fabrication of some sub-assemblies and furnish specific designs, the other to provide software for the three control computers and to furnish the services of a controls technician to expedite wiring the source. These contracts were in place by the end of February, 1984.

To date, the ion source parts have been uncrated and assembled to the extent possible in an off-line area. Electrical power and cooling water have been delivered to the site. Cable ways have been designed and installed. Missing power supplies and vacuum hardware have been purchased and delivered. The control software has been completed and delivered. The power and control wiring is being installed.

Concurrently a major design effort is in progress. All detailed ANAC designs have been reviewed and significant changes or additions made based on operating experience at this and other laboratories with similar hardware. The goal, in addition simply to providing designs which did not exist, is to produce a device with good electrical and temperature stability and relatively easy maintenance at reasonable intervals. As an example, the cesium gun output beam can contain as much as 2 kW of power. This must be disposed of very carefully within the ion source under all operating conditions. Failure to do this properly will result in thermal instability, sputtering, melting, and outgassing.

In the immediate future, the atomic beam source assembly will be completed. This unit will then be powered up and its performance optimized. In about two months delivery of Cs gun parts should commence. In September, 1984 it should be possible to operate the Cs gun and atomic beam source together and optimize negative polarized beam output. Allowing about two months for this process and two months for installation of the accelerator system we foresee on-line use of the polarized source by end of 1984.

10.5 Sputter Source Elevation

P. James, T.A. Trainor, D.I. Will, and F. Willis

The elevation of our sputter source to improve beam transmission through our FN tandem, as mentioned in last year's annual report,¹ was largely completed and evaluated in the fall of 1983. The original 25 keV source, its frame and vacuum system, associated isolated power supplies, their rack, deionized cooling water lines, light pipe telemetry, the 100 keV Dowlish accelerating tube, and the 10 kVA isolation transformer have all been tested to 60 keV elevation (for a total injected beam energy of 85 keV.) In this test, no detectable corona or sparking was noted and the elevated source appears to be fully capable of operating at this injection energy. However, we have determined that our electrostatic quadrupole triplet injection-lens power supply is incapable of achieving the voltages required to focus and steer an 85 keV beam into our tandem. As a result, we are currently operating at 30 keV elevation for an injection energy of 55 keV, the highest energy beam our quadrupole triplet will focus adequately. Keeping the low energy beam current constant and raising the injection energy from 25 keV to 55 keV results in an increase in high energy beam current to 2.7 times that achievable at 25 keV. The slope of the measured curve of transmission as a function of injected beam energy suggests that operation at the full 85 keV injection energy design point might result in still better transmission. As a result we may upgrade the quadrupole triplet and its power supplies for operation at higher focusing voltages.

Reference:

1. Nuclear Physics Laboratory Annual Report, University of Washington (1983) p. 72.

11. NUCLEAR INSTRUMENTATION

11.1 Design and Construction of Electronic Equipment

H. Fauska, J. LaCroix, R.E. Stowell, T.D. Van Wechel, and M.R. Walker

The following major electronics projects were carried out and are described in detail in the indicated sections of this report.

- a. The hardware interface for the laboratory data collection system was rebuilt (see Sec. 12.3).
- b. A two-level NMR controlled rapid switching system was built for the radiochronology group (see Sec. 8.3).
- c. Design of the electronics for the pre-tandem buncher for the linac has been initiated (see Sec. 13.5).

Several additional electronic projects were undertaken:

- a. Two 5 MHz heads were constructed for the deposition monitor in the target laboratory.
- b. Four NIM bin power distribution modules were constructed.
- c. Two expanded computer terminal patch panels were constructed and installed for the DEC 11/60 and the VAX, featuring LED's to indicate which terminals are active.
- d. The number of computer terminal outlets in the laboratory has been expanded.
- e. Additional high quality 50 ohm cable systems have been installed between the counting rooms and cave areas.
- f. The second set of six beam scanners, partly constructed last year,¹ was completed and installed for cave and beam line areas.
- g. A double balanced mixer circuit with gain was constructed for testing the linac cavity.
- h. Extensive filtering of critical logic lines on the electronics associated with the momentum filter was installed to prevent spurious and random changes in current settings from occurring.
- i. As a result of source elevation (to 30 kV), two channels of lab built light pipe telemetry were added to the sputter ion source. This was accomplished using commercially available Hewlett-Packard light pipes and lab built voltage to frequency converters.
- j. The Van de Graaff GVM rotor and stator are being replaced with gold plated units to stabilize the dielectric properties of the surface materials and thus give a more correct voltage output. The plating has been completed but the unit has not been installed or tested yet.
- k. Several additional light safety flashers were built for use at various hazardous areas in the laboratory.

Reference:

1. Nuclear Physics Laboratory Annual Report, University of Washington (1983) p. 80.

11.2 Construction and Testing of a Breskin Counter

D.D. Leach

A Breskin type multiwire proportional chamber of 2×2 cm has been built and successfully tested. This counter uses two aluminized hostaphan foils operated at ground potential and separated by 6 mm. Midway between these two foils is a harp of 20 μ m gold-plated tungsten wires on 1 mm centers. These wires are all connected to a common bus.^{1,2} During operation 1-2 Torr of P-10 gas was circulated through the counter and +490 V was applied to the wire harp. The harp signal was amplified with a fast preamp and fed into a constant fraction discriminator. This signal was compared to a signal from a silicon surface barrier E detector. Time resolutions of 220 psec and 240 psec were recorded for 68 MeV ^{16}O and 94 MeV Br respectively.

References:

1. A. Breskin et al., Nucl. Instrum. Meth. 165, 125 (1979).
2. A. Breskin, Invited talk at the Hans Geiger Symposium on Detectors in Heavy Ion Reactions HMI-Berlin, October 1982, to be published in Lectures Notes in Physics, Springer-Verlag.

11.3 Use of the LED-PIN Diode Light Pulser for Gain Stabilization of the $10'' \times 10''$ NaI Spectrometer

D.H. Dowell, C.A. Gossett, and K.A. Snover

As interest in studies of the statistical decay of the giant dipole resonance increases (see also Sec. 3.1-3.9), the long term gain stability of the $10'' \times 10''$ NaI spectrometer has become particularly important. These studies involve the measurement of gamma-ray spectral shapes which vary by six orders of magnitude over a gamma-ray energy range of 20-30 MeV, but which have no prominent lines with which to monitor the NaI detector gain. In addition, (p, γ) studies of excited-state giant resonances (see Sec. 3.5), in which the gamma-ray spectra exhibit lines from many closely spaced states, also benefit from improved gain stability and from improved detector resolution resulting from a more stable gain.

We have recently begun routine use of an LED-PIN diode light pulser system for gain stabilization of the NaI spectrometer. The designs of the LED driver circuit and LED stabilization are described in an earlier annual report.¹ A special optical fanout bundle is used to couple a single LED to the seven photomultiplier tubes on the NaI detector. The tubes are "back-illuminated" by shining the LED light through the glass wall onto the rear of the photocathode,² and with proper matching of the optical couplings, the light is uniformly distributed among the phototubes. The couplings of the LED to the fiber bundle and to the PIN diode are balanced in such a way as to

allow for a good signal-to-noise ratio in the PIN signal, while operating the LED over a wide dynamic range up to effective gamma-ray energies well above 50 MeV.

Commercial gain stabilization units made by Williams and Harris are used for both the LED and NaI stabilization. The light output of the LED pulser is regulated with the signal from the PIN diode which is processed with a home-built preamp and a Tennelec TC203 BLR amplifier. The LED component of the NaI linear energy signal is used to control the detector high voltage power supply. The shape of the LED pulse¹ is designed to match the pulse shape of true gamma rays in the detector. Detector events from the LED are treated identically to gamma-ray events in the timing and linear signal processing electronics, so that the LED amplitude distribution in the NaI spectrum serves as a realistic indication of pileup.

Our experience with the gain stabilization system over the past few months indicates that the long term regulated stability of the NaI is better than 0.5%. In addition, no short term gain shifts are observed associated with varying detector rates in the range from 2 to 160 KHz, leading also to upper limits of 0.5%. An amazing aspect of our present operation is that the PIN stabilization circuit rarely provides a measurable correction, indicating that the intrinsic LED amplitude stability is very good. Currently we obtain a stabilized NaI detector resolution of 3.3% FWHM for 22.6 MeV gamma rays collimated to illuminate the full detector diameter at a depth of 8". When the collimation geometry is chosen to illuminate 90% of the rear face of the detector, the resolution is 2.6% for 22.6 MeV. While we are quite pleased with the improved detector performance, further improvements are desirable such as the elimination of a small dependence of the Williams and Harris units on LED rate, and also the incorporation of a zero-level stabilization system.

References:

1. Nuclear Physics Laboratory Annual Report, University of Washington (1982) p. 161.
2. Nuclear Physics Laboratory Annual Report, University of Washington (1983) p. 84.

11.4 Improvement and Testing of the Momentum Filter

J.F. Amsbaugh, K.J. Davis, T. Murakami, and D.W. Storm

During the past year we have made a number of modifications which permit easier and more reliable operation of the momentum filter. Leaks in two welded bellows in the quadrupole vacuum ducts were discovered. In order to replace these it was necessary to dismantle the quadrupole magnets and completely remove the vacuum ducts so that new bellows could be welded in place. Indium wire seals which had been used in the scattering chamber also

were found to develop leaks after cycling the vacuum. These were replaced by aluminum wire seals except for the 0 degree face of the scattering chamber which now has a rubber O-ring seal to permit easy exchange of the Faraday cup and 0 degree port. We also had to replace the cryopump on the scattering chamber. In addition we devised a technique for mounting the Bragg Curve Spectrometer (BCS) at the final focus without significantly affecting the vacuum throughout the rest of the system. This involves the introduction of a second Mylar window in front of the detector entrance window and using a roughing pump to evacuate the region between the two windows. With the scattering chamber open to the beamline and the BCS mounted and operating we were able to maintain a vacuum of 1×10^{-6} Torr in the scattering chamber, 1×10^{-7} Torr at the dispersed focus and 8×10^{-7} Torr at the final focus.

It was discovered that when the power supply was operated at its maximum current of 400 A, the circuit breaker would trip and fuses in both the primary and secondary circuits would burn out. This problem was corrected by improving the electrical joints by using copper rather than aluminum lugs, using joint compound and by periodically checking the tightness of the connections. We were able to substantially reduce the number of errors in the magnet control by putting filters on the clock lines to the DAC's in the shunt control circuitry. More careful magnetic field measurements were made which allow the fields to be set to an accuracy of a few parts in 10^4 . This requires that the magnet currents be set to 400 A and then slowly stepped down to the desired current setting. This procedure is automatically carried out by a new PORTMAN program with which the experimenter interacts. This program allows the option of setting the fields by requesting a particular momentum to change ratio value for the central ray.

By running a particle beam directly into the momentum filter we were able to determine ray trajectories at the dispersed focus by measuring currents on moveable pins and at the final focus by measuring beam positions on a plastic scintillator. These measurements confirm our previous findings that the foci are down-stream of their predicted positions. This situation can be corrected somewhat by reducing the quadrupole currents by between 10 and 15%. A few attempts were made to use the momentum filter at 0 degrees. These proved to be unsuccessful because of an unacceptably large count rate at the final focus resulting from slit scattering from the collimators and charge exchange in the momentum filter. More recently a successful preliminary measurement of the $^{16}\text{O}(^{27}\text{Al}, ^{28}\text{Si})^{15}\text{N}$ reaction was made at 10 degrees (see also Sec. 4.5).

11.5 A Polarimeter for the Momentum Filter

C.R. Christensen, T. Murakami and W.G. Weitkamp

Testing the proton polarimeter for use with the momentum filter described in last year's Annual Report¹ has continued. The polarimeter uses elastic scattering from ⁴He with vanes to restrict scattering to angles centered around 60°. The detectors are 114 by 6.4 mm disks of NE 102 plastic scintillator viewed by photomultipliers.

We have found that the plastic scintillators are too sensitive to neutrons. A small proportional counter has been installed in front of the polarimeter so we can use coincidence between this counter and the scintillators to reduce neutron induced background. We have also tested other scintillator materials. CsI is about 100 times less sensitive to neutrons than either NE 102 or CaF. CsI scintillators may be installed in the polarimeter in the future.

The focal properties of the momentum filter appropriate to the polarimeter have also been measured. Use of the polarimeter on the momentum filter will require maximum solid angle, minimum spot width at the final focus and minimum deviation between the the average direction of the particles emerging from the final focus and the axis of the polarimeter. To measure these properties, we placed energy absorbers at the final focus in such a way that the particle energy detected in a downstream detector was related to the position at which the particle crossed the final focal plane. We found that both the maximum solid angle and the minimum spot size occur when the magnet is set for a central-ray momentum 9% higher than the actual particle momentum. We also found that the angle between average particle direction and the polarimeter axis is 0.5°, which is within acceptable limits.

Reference:

1. Nuclear Physics Laboratory Annual Report, University of Washington (1963) p. 77.

11.6 Target Preparation

G.M. Hinn

In Table 11.6-1 are listed a few of the more interesting of the 210 targets prepared in the Laboratory last year.

Table 11.6-1

Target	Starting Form	Final Form	Method of Preparation	Backing	mg/cm ² Thickness
^{9,10} BeO	Ice, Alaska South Pole and carrier ⁹ Be	^{9,10} Be	chelex ion exchange	none	1,5
Ti ¹⁵ N	Ti metal	Ti ¹⁵ N	¹⁵ N nitriding high temperature	S.S.	1
^{28,30} Si	oxide	elemental	reduction E-bombardment	S.S.	1,2,3
⁵² Cr	oxide	metal	H-reduction E-bombardment	S.S.	1.5
⁵¹ V	metal	metal	E-bombardment	S.S.	0.5
Al ₂ O ₃	metal	oxide	anodization	S.S.	0.2
⁸⁸ Sr	carbonate	oxide	reduction evaporation	100 μg/cm ² Au	0.05
³⁰ KI	salt	salt	evaporation	20 μg/cm ² C	0.1
²³⁶ U	salt	metal	anodization	102 μg/cm ² Ni	0.3
nat. Mn	metal	metal	E-bombardment	S.S.	1

a. Beryllium. We continue to use powdered silver mixed with ^{9,10}BeO to produce sources for accelerator radio dating of Alaskan and South Polar snow. Currently, we are trying to increase production by multiple sample processing.

b. Cracked ethylene stripper foils. We now routinely make 3 μg/cm² cracked slacked carbon stripper foils. Most heavy ion experimenters prefer thinner foils because of greater transmission. Experience with stripper foil below 3 μg/cm² in thickness has shown erratic and poor transmission.

c. Thick 1-2.3 mg/cm² ²⁸Si. Research has continued with some degree of success in making enriched ²⁸Si targets starting with the oxide. Further work is being done with electron beam annealing and thermal annealing to extend shelf life beyond 2-3 weeks.

12. COMPUTER SYSTEMS

12.1 Data Acquisition System Enhancements

E.G. Adelberger, R.S. Peabody,* and R.J. Seymour

Our principal data acquisition system consists of a DEC PDP 11/60 computer with two 5 megabyte RK-01 disks, a 1600 bpi 75 ips 9 track tape drive, a Printronix P-300 printer/plotter with a Trilog Tektronix hardcopy board, a DEC VT-11 graphics display, a Tektronix 4006 terminal and a Bira MBD-11 controlling a CAMAC crate to connect with twelve Tracor Northern TN-1213 ADCs. 15 NPL-built 75 MHz scalars are read via an IEEE-488 bus interface.

New Data Acquisition Hardware

New data acquisition hardware for the DEC 11/60 includes an HP 3582A Spectrum Analyzer and two more LeCroy 2251 CAMAC Scalars.

Additional user control of the SINGLES display was obtained by installing a 20-key keypad to facilitate and extend the control available with the VT-11's light pen. This allows control such as moving the "penned" point in steps smaller than the display's resolution.

New Data Acquisition Software

a. The MBD-11 was reprogrammed to allow snapshots of a LeCroy 2256a Waveform Digitizer into both SINGLES spectra for set-up and MULTI histograms and events for investigating subcoulomb heavy ion proton transfer reactions.

b. Another custom SINGLES MBD program was generated for repetitive reading of the LeCroy scalars for use in the ^{14}N parity experiments (see Sec. 5.4). The SINGLES data structure has been given an additional data type to contain the LeCroy scalar totals. A section of the VT-11 display program was created to display status information and the totalized results of the runs.

c. Another SINGLES MBD program provided selectable routing of one ADC's reading based upon a TAC's output. It made use of coincidence gating of the lab-built ADC interface while running in an overall SINGLES software environment. Although originally used for measurements of the statistical decay of giant dipole resonances, (see Secs. 3.2-3.6), this program has also been used by other experiments.

d. Another SINGLES MBD program provides for 50 microsecond delays and decisions based on multiple ADC "hits" and the resultant readings (see Sec. 1.6). The "decisions" produce "routing" biases placed on some of the ADCs' readings.

An Apparent MBD "Bug"

The heavier use of custom-generated MBD programs has occasionally uncovered hardware bugs in the MBD-11 itself. These involve the MBD-11 processor improperly reading or modifying a minus one (-1) in some locations of its memory. The short-order fix has been to pad programs with zeros to move the -1's to less sensitive areas. Attempts to isolate the problem have been unsuccessful so far.

Programming Considerations

We try to have our experiments run with lab-standard software to avoid "version drift" as features are added or bugs are fixed. The increased control required by newer experiments has forced us to bend this rule on occasion. Some programs, such as the VT-11 display driver, remain lab-standard with additional subroutines for the experiment-specific functions. Others, in particular the MBD-11 CAMAC controller, require completely custom programs, although they are usually developed from the lab-standard programs' skeletons.

As people began to use more customized SINGLES-like software groupings, procedures were created to allow relatively transparent switching from one environment to the next. This was done by providing experiment-specific accounts which established their own environment as a part of the log-in procedure. Thus the computer verb "END" can invoke different results for different experiments, but the people just know that "END" will stop their current data collection cycle.

More use is being made of the inter-computer parallel link. Two experiment groups use it for automatic during-run transfer of intermediate files to the VAX for further processing. This provides both relief from a permanent lack of disk space on the 11/60 and provides access to the advanced environment of the VAX. One of these experiments uses spectra collected by the HP 3582A spectrum analyzer, read over the IEEE bus to the 11/60 and sent to the VAX for analysis.

Control of the Momentum filter has been achieved, and is discussed in Sec. 11.4 of this report.

Reference:

- * Present Address: Department of Chemistry, University of Washington.

12.2 Data Analysis System Enhancements

E.G. Adelberger, E.F. Garman, M.N. Harakeh, A. Lazzarini,
M.J. Murphy, R.S. Peabody, D.A. Patterson, and R.J. Seymour

Our data analysis system consists of a DEC VAX 11/780 with dual RK-07 disks, a SI Eagle disk, three 9 track and one 7 track tape drives on Western Peripheral controllers, a Printronix P-300 printer/plotter and an AED-512 color graphics display.

Hardware Developments

The principal hardware change was the installation of a Systems Industries Fujitsu Eagle disk system directly attached to the VAX's SBI data path. This replaced the Unibus-attached Systems Industries CDC 9766 system. This raised our user disk space from 256 megabytes to 414. This expansion has allowed more software aids and system programs to be available at all times. It has also speeded up the system by utilizing a much faster datapath between the disk drive and the VAX's memory. It also avoids long searches across the disk for free space.

We had been borrowing a megabyte of VAX memory from the Chemistry Department. When they reclaimed it we lost 40% of our user space, with a consequential slowdown in system speed. We have recently purchased a megabyte of our own to bring us back to 3.25 megabytes. This is fairly closely balanced to our current load.

We have begun the change from VT-52 emulating terminals to VT-100 emulators, some with Tektronix 4010 graphics emulation. This allows more efficient editing and more distributed graphics displays. We had many demonstration units brought in. They all had some bugs somewhere and part of the evaluation procedure was the vendor/manufacturers' response to the problems we had. We bought three Graph-On 140 s and three Micro-Term 301 s.

We have developed informal resource sharing with the UW Physics Department VAX to make use of their 6250-bpi tape drives. This allows us to read tapes generated at the Brookhaven National Laboratory.

We have installed the AED-512's DMA board. We have solicited and received three software drivers from other sites (Jet Propulsion Laboratory, Michigan State University and Oxford University), but lack of programmer time has prevented us from testing or installing any of them.

We have replaced our 300 baud modem with a USR Password 300/1200 baud auto answer/autodial modem. This allows our VAX to call other computers for direct file transfers. We have installed the program HOST to control the modem from a local terminal. This has proved faster and more convenient than transferring tapes.

Software Developments

We have installed Mathematical Sciences Northwest's Superscript word processing package with its requisite Santeo Variflex printer. This program was made available to the University by the manufacturer.

We are doing some of the Laboratory's budgeting calculations with a spreadsheet program CCALC. This program was acquired in return for providing some media transfer services and beta-site testing to the authors, Digitec Software Design.

The supported analysis programs were expanded and modified through user request and direct user efforts. The SINGLES analysis program HP has been modified to provide more functions and to handle stripping the SINGLES spectra from MULTI tapes. The two-dimensional analysis program SPAN's display section now asks if the user is on the AED 512 color terminal. If so, the z-axis information is displayed as color instead of variable density pixel patterns used on the Tektronix.

The standard multiparameter sorting program MUSORT has been given more custom "front ends" to read other labs' data tapes. TRIUMF's sorting program MOLLI has begun to gain acceptance, particularly for its ability to selectively display sorted events on a display. MOLLI's display has been modified to use color to show the time sequencing of the displayed events. Also, MOLLI was given MUSORT's front end for reading Laboratory tapes.

To aid users who want to write their own spectrum analysis programs we provide READEM. This subroutine performs all of the esoteric dirtywork needed to untangle any of the known singles-type data structures and tape formats people commonly bring into the Laboratory. It presents the extracted data in a standard form as well as in raw form for quick incorporation of new types as they are generated. Another subroutine READALL can serve as an outer shell for READEM by performing all of the terminal question and answer protocols, calling READEM and finally splitting the results into specific COMMON areas for the user to access. READALL provides the simplest user programming interface for standard operations, while READEM provides the maximum flexibility, yet shields the users from having to understand and coherently handle the linked-list SINGLES data structure and its look-alikes.

Cascades simulates and analyzes compound nuclear decay. It had been brought to the Laboratory before, but last year saw a major revision imported from KVI and modified for running on our VAX.

A general purpose graphics program FIGURE was imported from Oxford and built into DRAW, a command-file driven program for transferring a list of numbers to a well-formed, well-labeled curve.

Another Oxford import AUTOFIT has received work to make it far friendlier and bug-free than it was in its original form. It performs curve fitting on singles spectra.

Reference:

- * Present Address: Department of Chemistry, University of Washington.

12.3 Hardware Enhancements to the Laboratory Data Collection System

R.J. Seymour, R.E. Stowell, and T.D. Van Wechel

The core of the laboratory data collection system consist of 12 commercial Tracor Northern 200 MHz ADC's interfaced to a DEC PDP 11/60 computer. The operation of this system has been described in detail in earlier annual reports,¹ but to summarize, the experimenter may select any or all of the 12 ADC's to perform the following:

MODE 0 : ungated singles spectra acquisition.

MODE 1 : gated singles spectra acquisition.

MODE 2 : gated multicoincidence spectra acquisition.

MODE 3 : gated singles spectra acquisition until a multicoincidence occurs whereupon the hardware aborts and clears any singles events that may be in progress, enabling selected ADC's to receive the multicoincidence event.

Mode 4 through 9 : currently ADC lockout. Allows for future expansion.

Mode 9

Modes 0 and 4 through 9 are new to this interface. Selected groups of ADC's may be run in any of the various modes simultaneously.

Enhancement of this data collection hardware consisted of redesigning and constructing a new chassis for the ADC computer interface. This was done to: (1) increase reliability of the system, (2) incorporate all the changes that have occurred over the past four years, (3) provide a system that would allow in-track diagnosis and board swap repairs, and (4) provide extra room and connector and mode switch capacity for future expansion. This interface also provides a number of monitoring jacks and diagnostic lights to allow quick identification of system malfunctions. Construction has been completed and was accomplished using commercial vector card cages and wire wrap p.c. boards, flat ribbon interconnecting cables and mass terminated connectors. The unit has been installed and tested and has been in operation for the past few weeks. Aside from some required minor modifications, the interface works well and has met its design criteria.

Reference:

1. Nuclear Physics Laboratory Annual Report, University of Washington (1982)
p. 178.

12.4 A Continuous- ℓ Optical Model Program

J.G Cramer

In the study of heavy ion scattering it is often of interest to examine in detail the optical model S-matrix and functions derivable from the S-matrix such as the quantal deflection function $\langle\theta\rangle_\ell$. A problem which immediately arises in investigations is that the independent variable of the S-matrix, the orbital angular momentum ℓ of the scattered system, is quantized in units of \hbar . For this reason, the S-matrix cannot be studied as a continuous function, and the deflection function $\langle\theta\rangle_\ell$ can be approximated only by rather crude numerical differentiation with respect to ℓ .

However, there is a way of dealing with this problem. The orbital angular momentum ℓ appears in three roles in the partial wave numerical solution of the Schroedinger equation: (1) in the Legendre polynomials $P_\ell(\cos\theta)$ which are the expansion basis of the angular dependence, (2) in the centrifugal potential $\ell(\ell+1)/Kr$, and (3) in the regular and irregular Coulomb wave functions $F_\ell(\eta,\rho)$ and $G_\ell(\eta,\rho)$ and the Coulomb phase shift σ_ℓ . For evaluation of the S-matrix, only (2) and (3) are relevant. In the centrifugal potential there is no problem with treating ℓ as a continuous variable. For the Coulomb functions there is also no problem in principle, but the usual way of evaluating these functions employs recursion relations which depend on the unit quantization of ℓ . However, an alternative way of evaluating Coulomb wave functions and phase shifts for arbitrary real or complex values of ℓ has been developed at this Laboratory in connection with the investigation of relativistic dynamic effects in heavy ion reactions.¹ We have employed these relativistic Coulomb routines to de-quantize the orbital angular momentum ℓ and treat it as a continuous variable.

We have developed the computer program DEFL which evaluates the optical model S-matrix and the quantal deflection function in arbitrarily small steps of ℓ . Fig. 12.4-1 shows an Argand diagram of the "continuous" S-matrix calculated for the $^{16}\text{O} + ^{16}\text{O}$ system at 40 MeV, using the well known Gobbi potential developed at Yale.² The kinks in the S-matrix reflect shape resonances generated by the potential.

References:

1. Nuclear Physics Laboratory Annual Report, University of Washington (1977) p. 180.
2. A. Gobbi, R. Wieland, L. Chua, D. Shapiro, and D. A. Bromley, Phys. Rev. C 7, 30 (1973).

13. BOOSTER LINAC PROJECT

13.1 Introduction;

D.W. Storm

During the past year the DOE awarded us a contract to build the superconducting booster proposed in 1982.¹ Although the majority of the funds (\$8M) for the project are construction funds included in the DOE contract, part of the project is to be done with state funds (\$1.03M) and part with operating funds (3 FTE personnel as well as costs of prototyping the resonators). Therefore it is appropriate to outline the progress in this report. The overall design was changed somewhat from that described in last year's Annual Report. Instead of 12 split ring resonators optimized for beta = 0.10 and 12 for beta = 0.16, we have chosen to use 16 quarter wave resonators optimized for beta = 0.09 and 16 for beta = 0.18. The quarter wave resonators, which have two accelerating gaps instead of the three of the split rings, have a wider transit time factor, which is favorable for accelerating a broader range of particle masses. The quarter wave resonators are to be built of lead plated copper, following the design of Ben-Zvi and Brennan.²

The main effort to date, besides planning and design, has been the construction and testing of a prototype low beta resonator and the preparation of and signing of a contract for the helium refrigerator. Following the overall planning and design of the entire project,³ completed specific planning and design work includes preparation of a design for a plating lab which is under construction, and preparation of specifications for magnets for the part of the beam transport system between the tandem and the LINAC. A mechanical design for a low energy buncher (following the Argonne National Laboratory design⁴) has been completed, and the electronic design is underway. Also, design work for equipping a facility for testing resonators has nearly been completed. In progress are designs which will lead to contracts for production of cryostats and a cryogen delivery system, as well as designs of the control system. The specifics of this work are presented below.

References:

1. Nuclear Physics Laboratory Annual Report, University of Washington (1982) p. 130.
2. I. Ben-Zvi and J.M. Brennan, Nucl. Instrum. Meth. 212, 73 (1983).
3. Conceptual Design Report Superconducting Booster, Nuclear Physics Laboratory, University of Washington (1983).
4. F.J. Lynch, R.N. Lewis, L.M. Bollinger, W. Henning, and O.D. Despe, Nucl. Instrum. Meth. 159, 245 (1979).

13.2 Design and Construction of Superconductor Resonators

I. Ben-Zvi,* T. Goliak, D.W. Holmgren, and D.W. Storm

A low beta resonator was fabricated at the Nuclear Physics Laboratory, then plated and successfully tested at Stony Brook. The basic design (see Fig. 13.2-1) is a quarter wave, cylindrical cavity excited by a magnetic coupling loop. Before the copper prototype was made the exact design parameters were measured by the construction and RF testing of a brass model.

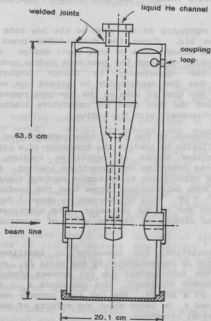


Fig. 13.2-1 Low beta resonator.

When the exact parameters of the design were finalized, the parts of the resonator were fabricated in the NPL shop with the first set of drift tubes made by the Weizmann Institute in Israel. An electron beam welding development program was completed with a contractor in California and the machined parts were then welded into the resonator. The drift tubes were brazed into place and the resonator was ready for polishing, plating, and rf testing at Stony Brook.

The design for the low beta resonator was taken from the Brennan and Ben-Zvi quarter wave resonator design,¹ with a change in the inner diameter of the outer conductor from 16 to 18 cm. The center conductor and drift tube geometry was identical to that used by Ben-Zvi. The extra 1 cm in radius was put into the gap between the center and side drift tubes. It was felt that this would decrease the surface fields on the center conductor. In retrospect, it appears that the gap is not the controlling element for the surface fields. To maintain the same average accelerating field with the larger diameter, the voltage on the center drift tube is increased proportionately. The surface field near the bottom of the drift tube is consequently higher than in Ben-Zvi's version, and that is where the maximum field is probably found.

Essentially, the high beta resonator is the same as the low beta one, except the diameter is twice as big. Since the drift tubes break the cylindrical symmetry, however, some thought must go into their design. Their length along the beam is about double, although the beam hole radius need not be changed. Thus one has the opportunity to change proportions substantially. Furthermore, one has the opportunity to extend the center drift tube somewhat more into the gap than it goes on the low-beta resonator. Finally, one must take into account the fact that the capacitive loading of the resonator will increase proportionately with the radius.

In order to guide the development of the drift tube geometry, we have performed a simple numerical calculation to predict the frequency of a tapered quarter wave resonator with various values of capacitive loading. By comparing with actual results we can determine the capacitive loading. Also, we have developed an electrostatic calculation to determine surface fields in an azimuthally symmetric model. Both calculations agree that the loading of the low beta resonator is 1.6 to 1.7 pF. This corresponds to about 7 degrees of phase angle at the high voltage end of the resonator. The electrostatic model gives guidance regarding the effects of various radii of curvature on the peak surface fields.

For the electrostatic calculation, the resonator is idealized as azimuthally symmetric. The geometry is characterized by the radii (r_i , r_o) of the inner and outer conductors, the longitudinal gap (g) between conductors and the end radius (r_e) of the center conductor. One can choose $r_e > r_i$ to represent the drift tube as part of a sphere. One can also compare results with various r_e smaller than a fixed r_i to learn about the effects of smaller curvatures on the end of a cylindrical structure.

The relaxation procedure solves the Poisson equation for Dirichlet boundary conditions. The volume of interest is bounded by the conductors and the plane at z_{max} , where the potential is set to the logarithmic radial dependence of infinite coaxial cylinders.

The results of the calculations suggest various center drift tube geometries which will provide lower ratios of peak surface field to average accelerating field, without excessive capacitive loading. These options will be tested with a model.

A full scale brass model has been completed for the development of a high beta resonator. As well as helping to optimize the drift tube shape, this model will be used to enable us to obtain parameters for a copper prototype resonator which will resonate at the same frequency as the low beta resonator. When this development effort is completed, the high beta resonator will also be polished, plated, and rf tested as was the low beta resonator.

References:

- * Weizmann Institute, Rehovot, Israel.
- 1. I. Ben-Zvi and J.M. Brennan, Nucl. Instrum. Meth. 212, (1983) 73; and I. Ben-Zvi, private communication.

13.3 Lead Plating of the Low Beta Resonator

J.M. Brennan,* D. Corcoran, R. Coughlin,* T. Goliak, D. Hodgkins,
P. James, A.G. Seamster, and J.H. Secora

Plating operations were performed at the lead plating facility at SUNY, Stony Brook. Initial procedures were based on the previous experience of prototype development by Ben-Zvi and Brennan.¹ Several attempts were made to produce satisfactory results, however the lead surfaces were consistently stained and lacked the bright metallic finish routinely achieved with the split loop resonator at SUNY. An unacceptable amount of particulate was also observed on the copper shorting plate, presumably originating at the surface of the lead anode. Two independent cold tests produced results which were below our requirements. The poor performances were attributed to the bulk lead surface as well as the appearance of a crack in the shorting plate.

The development of a new set of procedures was initiated, aided by reports of plating success from Ben-Zvi.² Controlled tests were conducted which suggested several changes in the plating parameters. Based on these results and suggestions from the staff at SUNY a new process was defined which was successful in producing the smooth reflective metallic surface known to be necessary for optimum resonator performance.

Following a successful repair of the shorting plate crack, the prototype was plated and chemically polished with the new techniques. The resultant surface was highly reflective and free of stains and particulates. The subsequent prototype cold test was successful.

The following alterations were made to the plating sequence:

- a. Increase the temperature of the lead bath to 30-32 °C.
- b. Filter the bath during plating through a 5 micron filter
- c. Reduce the current density from 10 to 5 mA/in².
- d. Punch several 0.20" diameter holes in the lead anode.
- e. Place the anode inside a polypropylene anode bag.

The following changes were made to chemical polishing sequence:

- a. Reduce the polish age time to 12 hours.
- b. Etch the lead layer in standing polish for 90 seconds.
- c. Fill the resonator rapidly with each processing solution and dump with a fast end-for-end rotation.

References:

- * State University of New York at Stony Brook 11794.
1. I. Ben-Zvi and J.M. Brennan, Nucl. Instrum. Meth. 212, 73 (1983).
2. I. Ben-Zvi, private communication.

13.4 Tests of the Low Beta Resonator

J.M. Brennan,* T. Goliak, and D.W. Storm

The low beta resonator was tested three times at Stony Brook between mid February and early April, 1984. The first two tests were unsuccessful in that fields only in the neighborhood of 1 MV/m were obtained with reasonable (less than 10 W) power in the resonator. In both cases the plating was poor. After techniques were developed to give good plating and after drilling out a crack in the bulk material of the resonator, the testing was successful. The techniques used for testing were the standard tests that have been used at Stony Brook for their resonators. The results of their tests typically agree with measurements using accelerated particles to better than 10%. We appreciate the help received and the opportunity to use the test equipment at Stony Brook.

The low beta resonator test consists of four parts. First, a bead test is done to establish the field profile and the ratio of the stored energy U to the square of the average accelerating field $\langle E_a \rangle^2$. For our resonator this ratio is $0.063 \text{ Joule}/(\text{MV/m})^2$. The uncertainty is estimated to be 0.003, based on estimates of the accuracy of frequency shifts in the bead tests and on repeatability.

Second, while superconducting, the voltage probe is calibrated. It delivers a signal whose amplitude V_p is measured with an oscilloscope. This voltage is proportional to the field in the resonator. The calibration is done by first measuring the Q of the resonator by measuring the decay time of the probe voltage when the power into the resonator is turned off. This decay time gives the loaded Q , Q_L , which includes the effects of the amplifier output resistance, and from Q_L the resonator Q , Q_0 , is obtained using measurements of reflected power. The variable coupler is either set to give no reflected power during steady state operation (critical coupling), or at the weakest setting if critical coupling is not attainable. The measurement is done at low power so the decay time is purely exponential. We found a value of 2.9×10^8 for Q_0 , with a 5% uncertainty.

Once the Q of the resonator is known, the stored energy can be determined by measuring the power P fed into the resonator from the amplifier, ($Q = \omega U/P$). The power supplied the resonator is obtained from the forward minus the reflected power, measured at the directional coupler. Again, the coupling is either set to be critical, or as weak as possible. The accuracy of the power measurement is estimated to be 7%. From the power absorbed and Q , we determine the stored energy and (using the bead results) the average accelerating field $\langle E \rangle$. The uncertainty in the field resulting from uncertainties in power, in Q , and in the bead test results is 5%. Simultaneous measurement of the voltage probe with the oscilloscope give V_p and permits calibration of the probe.

For the third part of the measurement, P_{abs} and V_p are measured at a number of power settings. (The results presented were obtained after "helium conditioning". In this process, helium is introduced into the vacuum of the cryostat and the resonator is pulsed to as high a field as possible. Presumably the discharges and ion bombardment of the high field points of the surface occurring during this process burn the points off and reduce field emission. After helium conditioning, substantially higher fields were achievable without the Q falling and without x-ray emission than before.) The value of $\langle E \rangle$ is obtained from V_p , and P_{abs} is obtained from the difference between forward and reflected power at the directional coupler. (If Q falls with power enough that we reach critical coupling, the coupler is adjusted to maintain critical coupling as Q falls further.) At the same time, a value of Q is obtained from the original one measured by decay times using the ratios of V_p and P_{abs} . A graph of those results is shown in Fig. 13.4-1. Those values for Q have been corrected for the contribution of the probe giving V_p . This probe produces an additional Q_{ext} of 1.3×10^6 . These corrections amount to a 20% increase at the high values of Q , and proportionately less at lower values.

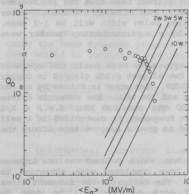


Fig. 13.4-1 Low beta resonator tests. Q of low beta resonator, measured after helium conditioning, plotted vs. $\langle E \rangle$, the average accelerating field. The lines show Q vs. E_a for fixed amounts of power absorbed by the resonator.

Finally, we phase lock the resonator and measure the power delivered by the amplifier to achieve lock. In an earlier test, this was done with one of the Stony Brook resonator controllers at a field of 1.1 MV/m. Lock required 4.4 W, 3.7 W of which was required before lock was established, i.e., 3.7 W was consumed in the resonator and 0.7 W reflected back into the amplifier. The coupler was set for critical coupling, and the Q value was fairly low. It was not possible to operate the resonator at 3 MV/m with that plating. However, one can conclude that if one wished to operate a successfully plated resonator with the same Q_L as was the case in the 1.1 MV/m test, then the power required to achieve lock at 3 MV/m would be $(3/1.1)^2$ times 4.4 W (33 W). The coupler would be adjusted to give a sufficiently large Q_{ex} to obtain this Q_L . The fact that lock was achieved without adding much power indicates that Q_L was larger than optimum. In the test with the successful plating, the controller was not operating, but we achieved lock using a voltage controlled oscillator and a phase detector. This lock was done at 50 W. Measurements of the frequency modulation of the resonator resulting from mechanical vibrations indicated maximum modulation of substantially less than 1 Hz.

Reference:

- * State University of New York at Stony Brook, NY 11794.

13.5 The Pretandem Buncher

J. Amsbaugh, L. Sima, D.W. Storm, R.E. Stowell, and T. Van Wechel

The LINAC booster will require beam from the tandem Van de Graff bunched to a time width around 100 psec. The direct current beam from the ion sources will be bunched with a single-gap gridded, four-harmonic buncher. After acceleration through the tandem the resulting pulse width will be 1-2 nsec. Beam pulses will then be further bunched by a superconducting quarter wave resonator to the required width.

Several pretandem bunchers of this type have been built and operated successfully.^{1,2,3} A 1 mm gap is formed by two aligned grids clamped to copper cones and held in place by a cylinder of MACOR. One cone is driven by an odd harmonic resonant line operating at 50 MHz and 150 MHz. The other is driven by an even harmonic resonant line at 100 MHz and 200 MHz, i.e., a N/2 resonator. The amplitude and phase of each frequency is controlled in a self excited loop. These parameters are adjusted to give a ramp voltage across the grids.

The mechanical design of the buncher box, which follows the new Argonne National Laboratory⁴ design closely, has been completed with attention to providing good rf current conduction paths. The design of the resonant lines is also complete. The construction of both designs will be done by September.

The control electronics have been designed copying the original ANL scheme. However the discrete component rf circuitry has been replaced by modern rf modules that are readily available. A 200 W rf amplifier and the associated electronics have been ordered, enabling a prototype of the control board to be built at the fundamental frequency of 50 MHz. The testing of this prototype should be finished by the end of July. This is consistent with our goal to begin beam test in December of 1984.

References:

1. F.J. Lynch, R.N. Lewis, L.M. Bollinger, W. Henning, and O.D. Despe, Nucl. Instrum. Meth. 159, 245 (1979).
2. A.D. Frawley and J.D. Fox, Nucl. Instrum. Meth. 204, 37 (1982).
3. E. Jaeschke, private communication and E. Jaeschke, R. Repnow, and S. Papureanu, Jahresbericht MPI für Kernphysik Heidelberg, 11 (1978).
4. R. Pardo, private communication.

13.6 Beam Dynamics for the UW Booster Project

J.G. Cramer and D.W. Storm

The beam transport line which injects the booster requires a "dogleg" isochronous transport system which displaces the tandem output beam from the beam axis of the tandem accelerator to a parallel axis 3.6 m to the south of the tandem axis. This transport must be independent (in first order at a given energy) of the path which a given particle takes through the beam transport system. This preserves the time structure quality of the bunched beam from the tandem. The system employs four 45° magnetic dipole bending elements and two pairs of magnetic quadrupole singlet focusing elements.

The characteristics of the dipoles and quadrupoles have been determined using the beam dynamics program TRANSPORT, and a request for information has been mailed to potential suppliers as a part of the UW procurement process. The TRANSPORT calculations have led to the following specifications:

Dipole 1: Deflection angle = 45°; Radius of curvature = 0.600 m; Magnetic rigidity = 1.04 T-m; Effective length = 0.471 m; Maximum $B = 1.73$ T; Entrance edge angle = +8.0°; Exit edge angle = -15.0°; Gap height in vacuum chamber = 3.8 cm.
(Dipoles 2-4 are either identical to or mirror images of Dipole 1)

Quadrupoles: Aperture diameter = 6.00 cm; Effective length = 0.24 m; Field gradient = 10.0 T/m; Gradient-length product = 2.40 T.

The six-dimensional Monte-Carlo beam dynamics program LYRA written by A. Schollendorf of Stony Brook has been modified so that it can be used to predict the performance of this booster. This has required expansion of the

program array space and modification of the part of the program which deals with resonator performance to describe the performance of quarter-wave resonators as well as split-loop resonators. Several minor bugs have also been corrected. The program is being used to determine the focusing requirements placed on the inter-cryostat quadrupole doublets by various beams so that the specifications for these elements can be determined and procurement initiated. The program is also being modified to make it more interactive and more realistic in its simulation of booster LINAC performance.

13.7 Phase Control System of the Tandem-LINAC System

T.A. Trainor

Successful operation of the tandem-LINAC accelerator combination relies, among other things, on proper control of the relative phases of the time-varying components of the system. In the absence of noise sources it should be possible to adjust each component phase with respect to a master clock according to established criteria. If, in addition, there are sources of phase noise in the system then one or more servo loops are required to reduce the noise to an acceptable level. The result is that correct phases are established and then maintained indefinitely.

Both elements of the phase control problem, establishment of quiescent phase values and dynamic control of relative phases, require some sort of beam phase detector. This detector can be active, as in a sweeper or a driver (accelerating) resonator, in which case subsequent analysis of the beam is required to determine relative phase, or passive, as in a secondary electron pickoff or an undriven (detecting) resonator. These devices vary considerably in sensitivity, range, physical size, band width, etc.

Establishment of quiescent values can be time-consuming. At existing installations manual set up typically requires twelve hours. This lengthy process is unacceptable as a design goal for a new LINAC. The setup procedure should be totally under computer control and take of order one hour to complete. Achievement of such a goal will require careful matching of phase detector properties to the computer control system.

Dynamic phase control is a totally separate problem requiring careful study of phase noise power spectra and response functions of various elements of the phase regulation loop, in order to secure maximum gain-bandwidth product and loop stability over the large range of beam currents anticipated. The transient response of the regulation loop is also critical. Phase transients derived from voltage breakdowns in the tandem or injector cause the regulation system to saturate because of its necessarily limited dynamic range. Recovery time from saturation must be minimized and "phase slip" avoided. That is, beam bunches must be registered in the proper rf cycle, not

prematurely locked into a nearby cycle during recovery from the transient.

To date these general design principles for the phase-control problem have been developed and a number of specific areas have been investigated. A typical phase-noise spectrum from the tandem injector combination has been inferred from voltage stabilities. Properties of various phase detectors have been reviewed. A study of longitudinal phase-space propagation through the dog leg just preceding the LINAC has been made. Some results of this study are for example that an additional transverse waist is desirable between dog-leg output and second stripper, and that both the high-field buncher and a large band-width phase detector should be located at this waist.

The next step is to examine the properties of several prototype phase detectors installed just after the tandem using the existing pre-tandem buncher, and to begin to sketch out a rapid algorithm for computer setup of LINAC phases.

13.8 Resonator Test Facility

R.E. Stowell, H.E. Swanson, and D.W. Storm

Progress on the test facility to date has largely been in the specification and procurement of rf components and test equipment needed for the lab. This facility is required to make measurements of quarter wave resonator (QWR) parameters such as Q and the resonant frequency. It will allow us to operate the QWR's both warm and at superconducting temperatures, at power levels simulating LINAC operating conditions. The first low beta prototype resonator was tested at Stony Brook and that experience was useful in writing specifications to obtain the appropriate capability.

This facility is to be housed here in laboratory space vacated by cyclotron user groups. It should be available for testing the prototype high beta resonator later this year. A list of the major items of equipment follows, with an asterisk showing that the item has been received.

- *Tektronics 485 oscilloscope
- *Tektronics 2213 oscilloscope
- *Hewlett Packard 432B power meter
- *Hewlett Packard 5382 frequency counter
- *Bird RF power meter (forward/reflected)
- *RF Power Labs 100 Watt broadband rf amplifier
- *RF Power Labs 200 Watt broadband rf amplifier
- *Narda directional couplers
- Wavetech 3006 rf signal generator
- Wavetech 148A function generator
- *Miscellaneous rf components
(Mixers, attenuators, phase shifters, splitters)

13.9 Resonator Control System

C. Stubbs and H.E. Swanson

The amplitude and phase of oscillation of each superconducting resonator in a linear accelerator determines the energy of a particle bunch as it traverses the accelerator. A master frequency synthesizer provides the reference phase for determining the initial bunching of the dc beam from the tandem. It also determines the phase of all subsequent resonators such that the particles appear in the accelerating gap at just the right moment to be accelerated. The amplitude of the oscillation determines the accelerating field seen in the gap.

Control of the resonators is to be achieved in a manner similar to that used on the Stony Brook LINAC. The resonant cavity is made to oscillate by making it part of a self-excited feedback loop. The loop consists of an rf amplifier and an electronic module whose phase shift and attenuation can be controlled. Oscillation occurs at the point where the total loop phase shift is a multiple of 360 degrees. If the phase shift external to the resonator differs from 360 degrees, then the resonator must oscillate off resonance to make up for this phase difference. In this manner control is achieved over the frequency of the resonator and it can be locked to the phase of the master oscillator.

Electronics to provide control of loop phase shift and attenuation has been designed by Ben-Zvi and Brennan at Stony Brook. Their circuit is built around an Olektron part, a complex phasor modulator, which is capable of independent modulation of the in-phase and out-of-phase components of the feedback signal. Using these two components, independent control of both amplitude and phase of the resonators oscillation is achieved. We have obtained schematics and a printed circuit board for this design from Stony Brook and have constructed one of the resonator control modules here. This unit is presently undergoing an evaluation of its operating characteristics.

The controller module requires analog input signals to set its operating parameters. A satellite control computer will provide digital-to-analog and analog-to-digital conversion as well as two way communication with a master control console. A Digital Equipment Corporation Falcon single board computer has been ordered and a prototype satellite controller system is being assembled. The Stony Brook control software has been brought up on the VAX computer and is being evaluated. A Whitesmith's C compiler has also been installed and work is ongoing to modify the software to work with the Falcon based satellite.

13.10 Booster Cryogenics

D.W. Storm, W.G. Weitkamp, and D.I. Will

During this past year we have ordered a helium refrigerator, developed cryostat specifications and come to understand better some of the potential problems to avoid in helium distribution systems. The helium refrigerator consists of a Koch Process Systems 2800HR with three type RS screw compressors. The 2800HR has two dry expansion engines, each with two 3" diameter pistons, and one wet expansion engine with a single 2" diameter piston. It has guaranteed capacities at 4.5°K of 440 W without liquid nitrogen precool and of 510 W with liquid nitrogen precool which compare favorably with our estimated need of 300 W.¹ We are pleased to report that this extra capacity was obtained under budget. At present we have nearly completed material, technique and performance specifications for our cryostats, pending a decision on bayonet design, and we are beginning preliminary specifications for our liquid helium distribution manifold and transfer siphons. We especially wish to thank John Hulbert of Chalk River Laboratory of Atomic Energy of Canada, Ltd., Jack Nixon of Argonne National Laboratory, and Tom Peterson of Fermilab for their assistance in matters cryogenic.

Reference:

1. Nuclear Physics Laboratory Annual Report, University of Washington (1983) p. 94.

13.11 The Plating Laboratory

A.G. Seamster and W.G. Weitkamp

The lead plating of the prototype resonator, described in Sec. 13.3, has been conducted entirely in the plating laboratory at SUNY Stony Brook. Because of the considerable cost and inconvenience in transporting personnel and materials to and from Stony Brook, it is clearly impractical to plate all the resonators there. Furthermore, the high-beta resonator cannot be accommodated at Stony Brook without modifying the set up there. Consequently we are constructing a plating lab in-house.

A suitable plating lab must have the following properties:

- a. It must contain a fume hood big enough to hold all the chemicals required for the plating process. Some of the chemicals such as acetone pose a fire hazard, and some such as the lead plating solution are slightly toxic.
- b. Safety equipment required in handling the chemicals must be near at hand.
- c. Equipment for maneuvering both the high and low-beta resonators as required during the plating process must be available.

d. The lab must be dust-free since dust adhering to the surfaces of the resonator either before or after plating can degrade the electrical properties of the resonator.

e. The lab must contain space and equipment for installing the resonators into the cryostat since it is preferable not to expose freshly plated resonators to the Laboratory environment any more than necessary.

No existing room in the Laboratory had all of the properties required. We found that we could construct such a room by expanding an old hot-chemistry lab adjacent to the high-bay student shop setup area (Room 165) as shown in Fig. 13.11-1. This room will enclose 580 ft² including a 90 ft² fume hood. A 2600 ft³/min fan will exhaust air from the hood. A 5 μ filter will remove dust from all incoming air.

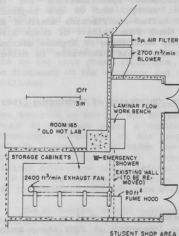


Fig. 13.11-1 The new plating laboratory.

The University Architect's Office has prepared final plans and arranged for a contractor. Work will begin in April; the lab is expected to be ready for occupancy by the end of August 1984.

14. APPENDIX

14.1 Nuclear Physics Laboratory Personnel

Faculty

Eric G. Adelberger, Professor
David Bodansky, Professor; Chairman, Department of Physics
John G. Cramer, Professor; Director, Nuclear Physics Laboratory
George W. Farwell, Professor
I. Halpern, Professor
Albert Lazzarini, Research Assistant Professor
Eric Norman, Research Affiliate Professor¹
Fred H. Schmidt, Professor
Kurt A. Snover, Research Professor
Thomas A. Trainor, Research Associate Professor
Robert Vandenbosch, Professor
William G. Weitkamp, Research Professor; Technical Director,
Nuclear Physics Laboratory

Research Staff

K.G. Radhamohan Doss, Research Associate²
David H. Dowell, Research Associate³
Elspeth F. Garman, Visiting Scientist⁴
Cynthia A. Gossett, Research Associate
Muhsin N. Harakeh, Visiting Scientist⁵
M. Zafar Iqbal, Research Associate⁶
Tetsuya Murakami, Research Associate
Martin J. Murphy, Research Associate
John L. Osborne, Research Associate
Daniel R. Tieger, Research Associate

Senior Professional Staff

Harold Pauska, Senior Research Scientist⁷
Derek W. Storm, Senior Research Scientist

Predoctoral Research Associates

John A. Behr
Keith J. Davis
Gerald Feldman
Salvador Gil
David W. Holmgren
Stephen Kellogg
Mahbubul A. Khandaker
Steve Lamoreaux⁸

Kevin T. Lesko⁹
Dat-Kwong Lock
Robert A. Loveman
Amlan Ray
Christopher Stubbs
Peter Wong
Valdis Zeps

Professional Staff

John F. Ambaugh, Research Scientist
Greg Douglas, Visiting Controls Engineer¹⁰
Thomas Goliak, Research Engineer
Gervas M. Hinn, Research Scientist/Target Maker
David J. Hodgkins, Research Engineer
Donald D. Leach, Research Scientist
H. Pamela McKenna, Computer System Engineer
R. Scott Peabody, Computer System Engineer¹¹
Alan G. Seamster, Research Scientist
Richard J. Seymour, Computer System Manager
Rod E. Stowell, Electronics Engineer/Electronic Shop Supervisor
H. Erik Swanson, Research Physicist
Timothy Van Wechel, Electronics Engineer
Douglas I. Will, Research Engineer

Technical Staff

Robert L. Cooper, Instrument Maker
James R. Cromie, Accelerator Technician
Ronald Floyd, Buyer
Louis Geissel, Instrument Maker, Student Shop Leadman
John M. LaCroix, Electronics Technician
Carl E. Linder, Engineering Technician
Georgia J. Rohrbaugh, Accelerator Technician⁶
George Saling, Accelerator Technician⁷
Lawrence Sima, Drafting Technician
Hendrik Simons, Instrument Maker, Shop Supervisor
Allen L. Willman, Instrument Maker⁷

Administrative Staff

William T. Dickie, Office Assistant⁵
Barbara J. Fulton, Administrative Secretary
Margaret M. Nims, Office Assistant
Victoria A. Palm, Accounting Assistant¹²
Maria G. Ramirez, Program Assistant

Part Time Staff

Frederick Bahr
David Balsley
Somjai Boonsripisal⁸
David Chan
Cindy Christensen
Ky Clifford
Dean Corcoran
Jim Davis
Mark DeFaccio
Jens Gundlach
Albert Herron

Norman Hill
Steven Holmes
Peter James
Donna Kubik⁹
Kevin McMurry
Margarethe Nelson⁸
David Patterson
Joel Schoen⁸
Michael Walker
Fawn Willis

1. Address: Department of Physics, Seattle University, Seattle, WA 98122.
2. Address: Lawrence Berkeley Laboratory, University of California, Berkeley, CA 94720.
3. Address: Brookhaven National Laboratory, Upton, NY 11973.
4. Address: Oxford University, Oxford, United Kingdom.
5. Address: Kernfysisch Versneller Instituut, Groningen, The Netherlands.
6. Address: Norman Bridge Laboratory of Physics, California Institute of Technology, Pasadena, CA 91125.
7. Retired - part time employee.
8. No longer associated with the Nuclear Physics Laboratory.
9. Completed Ph.D. degree. Present Address: Argonne National Laboratory, Argonne, IL 60439.
10. Group 3 Technology Ltd., Auckland, New Zealand.
11. Department of Chemistry, University of Washington.
12. Department of Computer Science, University of Washington.

14.2 Ph.D. Degrees Granted, Academic Year 1983-1984

Kevin T. Lesko - Fusion and Fission Properties of Rapidly Rotating Nuclei

Dat-Kwong Lock - The Effect of Particle Evaporation on the $^{56}\text{Fe} + ^{136}\text{Xe}$ Reaction and a Reinvestigation of the $^{86}\text{Kr} + ^{92}\text{Mo}$ Reaction

14.3 List of Publications

Published Papers

"The Arrow of Electromagnetic Time and the Generalized Absorber Theory," J.G. Cramer, Found. Phys. 13, 887 (1983).

"Cosmic Clocks," E.B. Norman, McDonald Observatory News, University of Texas, October, 1983, p. 4, (4th Prize Winner in the 1982 McDonald Observatory Science Writing Contest).

" ^{182}Hf Chronometer for the Early Solar System," E.B. Norman and D.N. Schramm, Nature 304, 515 (1983).

"On the Half-Life of ^{136}La ," E.B. Norman and M.A. Nelson, Nature 306, 503 (1983).

"On the Identification of γ -ray Lines Observed from SS433," E.B. Norman and D. Bođansky, Nature, 308, 212 (1984).

"The University of Washington Superconducting Booster Project," J.G. Cramer R. Vandenbosch, and D.W. Storm, Nucl. Instrum. Methods 220, 204 (1984).

"The g -factor and Lifetime of the $3^-(298\text{ keV})$ State in ^{16}N ," J. Billowes, E.G. Adelberger, O. Avila, N.A. Jelley, and W.R. Kolbl, Nucl. Phys. A, 413, 503 (1984).

"The t -forbidden Gamow-Teller Decay of ^{38}Ca ," E.G. Adelberger, J.L. Osborne, H.E. Swanson, and B.A. Brown, Nucl. Phys. A, 417, 269 (1984).

"Depolarization in Proton Inclusive Inelastic Scattering and in the (\bar{d}, p) Reaction on Medium Weight Nuclei," W.G. Weitkamp, I. Halpern, T.A. Trainor, S.K. Lamoreaux and Z.Y. Liu, Nucl. Phys. A 417, 405 (1984).

"Dynamics of Heavy-Ion Transfer Reactions," B.G. Harvey and M.J. Murphy, Phys. Lett. B 130, 373 (1983).

"Phase Space Constraints on the Momenta of Projectile Fragments," M.J. Murphy, Phys. Lett. B 135, 25 (1984).

" ^7Be Decay Scheme and the Solar Neutrino Problem," E.B. Norman, T.E. Chupp, K.T. Lesko, J.L. Osborne, P.J. Grant, and G.L. Woodruff, Phys. Rev. C 27, 1728 (1983); Erratum Phys. Rev. C 28, 1409 (1983).

"Proton Capture to Excited States of ^{16}O ; M1, E1 and Gamow-Teller Transitions and Shell Model Calculations," K.A. Snover, E.G. Adelberger, P.G. Ikossi, and B.A. Brown, Phys. Rev. C 27, 1837 (1983).

"The Beta Decays of ^{18}Ne and ^{19}Ne and their Relation to Parity Mixing in ^{18}F and ^{19}F ," E.G. Adelberger, M.M. Hindi, C.D. Hoyle, H.E. Swanson, R.D. Von Lintig, and W.C. Haxton, Phys. Rev. C 27, 2833 (1983).

"Properties of Fission Induced by Complete Capture of ^{40}Ar by ^{238}U at $E_{\text{C.M.}} = 291 \text{ MeV}$," K.T. Lesko, S. Gil, A. Lazzarini, V. Metag, A.G. Seamster, and R. Vandenbosch, Phys. Rev. C 27, 2999 (1983).

"Elastic and Inelastic Scattering of Polarized Protons from ^{206}Pb near Isobaric Analog Resonances," N.L. Back and J.G. Cramer, Phys. Rev. C 28, 1040 (1983).

"Penetration of the Centrifugal Barrier in the Fusion of ^{16}O with Heavy Targets," R. Vandenbosch, B.B. Back, S. Gil, A. Lazzarini, and A. Ray, Phys. Rev. C 28, 1161 (1983).

"The Giant Dipole Resonances in the Statistical Decay of ^{63}Cu , ^{78}Kr and ^{127}Cs Compound Nuclei," E. Garman, K.A. Snover, S.H. Chew, S.K.B. Hesmondhalgh, W.N. Catford, and P.M. Walker, Phys. Rev. C 28, 2554 (1983).

"Cross Sections Relevant to Gamma-Ray Astronomy: Alpha-Particle Induced Reactions," A.G. Seamster, E.B. Norman, D.D. Leach, P. Dyer, and D. Bodansky, Phys. Rev. C 29, 394 (1984).

"Current ^{14}C Measurements with the University of Washington FN Tandem Accelerator," G.W. Farwell, P.M. Grootes, D.D. Leach, F.H. Schmidt, and Minze Stuiver, Radiocarbon 25, 711 (1983).

"Technological Advances in the University of Washington Accelerator Mass Spectrometry System," G.W. Farwell, P.M. Grootes, D.D. Leach, and F.H. Schmidt, Radiocarbon 25, 755 (1983).

"Nuclear Probes of Fundamental Symmetries," E.G. Adelberger, Proceedings of the International Conference on Nuclear Physics, Florence, edited by P. Blass and R.A. Ricci, (Tipografia Compositori, Bologna, 1984), Vol. 2, p. 499, (invited paper)

"Breaking of Fundamental Symmetries in Nuclei," E.G. Adelberger, in Symmetries in Nuclear Structure, edited by K. Abrahams, K. Allaart, and A.E.L. Dieperink, (Plenum Press, New York, 1983), p. 55.

"Conclusion and Outlook," R. Vandenbosch, Nuclear Physics with Heavy Ions, edited by P. Braun-Munzinger, (Harwood Academic Publishers, New York, 1984) p. 447, (invited paper).

Papers Submitted or in Press

- "On the Half-Life of ^{180}Ta in Stellar Environments," E.B. Norman, S.E. Kellogg, T. Bertram, S. Gil, and P. Wong, *Astrophys. J.*, to be published.
- "Giant Dipole Resonances Built on Highly Excited States of Light Nuclei," K.A. Snover, *Comments on Nucl. Part. Phys.*, to be published.
- "Production of Thick Elemental Low-Oxygen Content nat_{28}Mg from $\text{nat}_{28}\text{MgO}$," G.M. Hinn, E.B. Norman, T.E. Chupp, and K.T. Lesko, *Nucl. Instrum. Methods*, to be published.
- "Parity Mixing of Elastic Scattering Resonances: General Theory and Application to ^{14}N ," E.G. Adelberger, P. Hoodbhoy, and B.A. Brown, *Phys. Rev. C*, to be published.
- "Determination of the Rate of Energy Partition in Deeply Inelastic Collisions," A. Lazzarini and R. Vandenbosch, submitted to *Phys. Rev. C*.
- "Non-Equilibrium Excitation Energy Division in Deeply-Inelastic Collisions," R. Vandenbosch, A. Lazzarini, D. Leach, D.-K. Lock, A. Ray, and A. Seamster, *Phys. Rev. Lett.*, to be published.
- "Comment on Fission Fragment Angular Distributions," R. Vandenbosch, *Phys. Rev. Lett.*, to be published.
- "Determination of a Time Scale for the Emission of Energetic Photons in Heavy Ion Fusion Reactions," A. Lazzarini, V. Metag, D. Habs, W. Hernerici, and J. Schmirmer, submitted to *Phys. Rev. Lett.*
- "Timescale for Projectile Breakup into Coincident Heavy Fragments," M.J. Murphy, T.C. Awes, G. Gil, M.N. Harekeh, A. Ray, A.G. Seamster, and R. Vandenbosch, submitted to *Phys. Rev. Lett.*
- "Some Methods and Problems Associated with Making Thick (1 Mg/cm^2) $^{28,29,30}\text{Si}$ Targets," G.M. Hinn, International Nuclear Target Development Society Workshop, Argonne National Laboratory, September, 1983, to be published, (invited paper).
- "The Conceptual Design of the University of Washington Superconducting Booster," W.G. Weitkamp, in *Proceedings of the Symposium of Northeastern Accelerator Personnel*, 1983, to be published.
- "Form Factors and Coupled Channel Analysis of Inelastic Excitations of Low-Lying Collective Bands in Rotational Nuclei," M.N. Harekeh, Kikuchi Summer School, 1983, Kyoto, Japan, to be published, (invited paper).
- "Excitation of Low-Lying Collective Bands in Inelastic Hadron Scattering," M.N. Harekeh, *Proceedings of RCNP Symposium on Light Ion Reaction Mechanism*, 1983, Osaka, Japan, to be published, (invited paper).

"A Review of the Fission Decay of the Giant Resonances in the Actinide Region," M.N. Harakeh, Proceedings of the International Symposium on Highly Excited States and Nuclear Structures, 1983, Orsay, France, Editions de Physique, to be published, (invited paper).

"Giant Resonances Built on Excited States," K.A. Snover, *ibid*, (invited paper).

"Giant Resonances Built on Highly Excited States," K.A. Snover, Proceedings of XV International Summer School in Nuclear Physics, 1983, Mikolajki, Poland, to be published, (invited paper)

Laboratory Reports

"Conceptual Design Report Superconducting Booster," R. Vandenbosch, D.W. Storm, J.F. Amisbaugh, A.G. Seamster, H.E. Swanson, T.A. Trainor, and W.G. Weitkamp.

"Program Management Plan Superconducting Booster," D.W. Storm.

Proceedings of the 11th World Conference of the International Nuclear Target Development Society, edited by G.M. Hinn, Nuclear Physics Laboratory, University of Washington, Seattle, Washington, 1983.

Abstracts

"The Role of Isospin in the Statistical Decay of the Giant Dipole Resonance Built on Excited States," M.N. Harakeh, D.H. Dowell, K.A. Snover, G. Feldman, E.F. Garman, J.L. Osborne, and R. Loveman, *Bull. Am. Phys. Soc.* 28, 965 (1983).

"Giant Dipole Resonances Built on Excited States," K.A. Snover, *Bull. Am. Phys. Soc.* 28, 972 (1983), (invited paper).

"Phase-Space Constraints on the Moments of Projectile Fragments," M.J. Murphy, *Bull. Am. Phys. Soc.* 28, 980 (1983).

"A Search for the β -decay of ^{160}Lu to $^{160}\text{Hf}^m$, S.E. Kellogg and E.B. Norman, *Bull. Am. Phys. Soc.* 28, 989 (1983).

"Forward-to-Backward Asymmetries in the (γ, n) Reactions around the E_2 Isovector Giant Resonance," T. Murakami, I. Halpern, D.W. Storm, P.T. Debevec, L. Morford, D.H. Dowell, and S.A. Wender, *Bull. Am. Phys. Soc.* 29, 707 (1984).

"The Accelerator Mass Spectrometry Program at the University of Washington," G.W. Farrell, D.D. Leach, P.M. Grootes, and F.H. Schmidt, *The Third International Symposium on Accelerator Mass Spectrometry*, Zurich, Switzerland, 1984.

" β -Decays of ^{180}Hf and ^{180}Lu and the Origin of ^{180}Ta , E.B. Norman and S.E. Kellogg, Proceedings of the 2nd Workshop on Nuclear Astrophysics, Tegernsee, West Germany, 1983, p. 92.

"Giant Dipole Resonances Built on Excited States of Light Nuclei," K.A. Snover, D.H. Dowell, G. Feldman, A.M. Sandorfi, M.T. Collins, and E.F. Garman, Proceedings of International Conference on Nuclear Physics, Florence, (Tipografia Compositori, Bologna, 1983), Vol. 1, p. 204.

"Searches for Double β^+ . $\beta^+\text{EC}$ and Double EC Decays, E.B. Norman and M.A. Nelson, *ibid*, p. 720.

"Possible Non-Quasi-Elastic Events in the Inclusive Inelastic Scattering of Pions from Nuclear," K.G.R. Doss, I. Halpern, M. Khandaker, and D. Storm, *ibid*, p. 368.

"Environmental Studies Using Accelerator Mass Spectrometry Measurements of ^{10}Be and ^{14}C ," G.W. Farwell, P.M. Grootes, F.H. Schmidt, M. Stuiver, M.A. DeFaccio, and D.D. Leach, *ibid*, p. 752.

" ^{182}Hf : A New Short-Lived r-Process Chronometer," E.B. Norman and D.N. Schramm, Meteoritics, 18, 365 (1983).

"The Role of the Giant Dipole Resonance in the Emission of High Energy Gamma Rays from $^{63}\text{Cu}^*$," E.F. Garman, K.A. Snover, J. Gundlach, D.H. Dowell, M.N. Harakeh, G. Feldman, and R. Loveman, The Spring Meeting of the British Institute of Physics Conference, 1984, Bradford, England.

Other Publications by Members of the Laboratory and Other Laboratory Research

"Calorimetric Beam-Current Integrator," J.L. Osborne and A.J. Howard, Nucl. Instrum. Meth., to be published.

"Determination of the α -induced K-shell Ionization Cross-Sections from the Measured Intensity Ratios of K X-Rays to (2^+-0^+) γ -rays in Even Deformed Nuclei," M.N. Harakeh, Z. Zujkowski, and D. Chmielewska, Nucl. Instrum. Methods, 219, 111 (1984).

"Low Energy Behavior of the ^3He + ^4He Cross Section," J.L. Osborne, C.A. Barnes, R.W. Kavanagh, R.M. Kremer, G.J. Mathews, J.L. Zyskind, P.D. Parker, and A.J. Howard, Nucl. Phys. A, 419, 115 (1984).

"Structure in the $^{12}\text{C} + ^{12}\text{C}$ and $^6\text{Be} + ^{16}\text{O}$ Fission Width Distribution of ^{124}Mg Observed via the Reaction $^{12}\text{C}(^{16}\text{O}, \alpha)^{24}\text{Mg} \rightarrow \text{X} + \text{Y}$," A.J. Lazzarini, S.G. Steadman, R.J. Ledoux, A. Sperduto, G.R. Young, K. Van Bibber and E.R. Cosman, Phys. Rev. C 27, 1550 (1983).

"Pionic Fission Cross-Sections on Lithium," P.D. Barnes, B. Bassaleck, R.A. Eisenstein, G. Franklin, R. Grace, C. Maher, P. Pile, R. Rieder, J. Szymanski, W.B. Wharton, J.R. Comfort, F. Takeuchi, J.F. Amann, S. Dytman, and K.G.R. Doss, submitted to Nucl. Phys.

" $^{12}\text{C}(^{16}\text{O},\alpha)^{24}\text{Mg}$ Reaction in the Energy Region $E_{\text{c.m.}} = 26.6$ to 42.9 MeV," M.J. Bechara, A.J. Lazzarini, R.J. Ledoux, and E.R. Cosman, Phys. Rev. C 27, 1540 (1983).

"Inelastic Proton Scattering at 30-40 MeV from ^{12}C ," M. Harakeh, R. De Leo, G. D Erasso, and A. Pantaleo, Phys. Rev. C 28, 1431 (1983).

"Origin of the Structures in the $^{12}\text{C}(^{16}\text{O},\alpha)$ Reaction: Dominance of the 2^0Ne^* and 1^0O^* Sequential α -decay Processes," T. Murakami, E. Ungricht, N. Takahashi, Y.-W. Lui, Y. Mihara, R.E. Neese, E. Takada, D.M. Tanner, R.E. Tribble, and K. Nagatani, Phys. Rev. C 29, 847 (1984).

"Inclusive Pion Single Charge Exchange Reactions," D. Ashery, D.F. Geesaman, R.J. Holt, H.E. Jackson, J.R. Specht, K.E. Stephenson, R.E. Segel and P. Zupranski, H.W. Baer, J.D. Bowman, M.D. Cooper, M. Leitch, A. Erel, J. Comuzzi, R.P. Redwine, and D.R. Tieger, submitted to Phys. Rev. C.



Front row: Behr, Adelberger, Ansbrough, Trainor, Cramer, Fauska, Cooper, Storm, Weiskamp, Fulton

Middle row: Snover, Khandaker, Chan, Kellogg, Gossett, Gil, Loveman, Murakami, Ray, Cromie, Will, Stowell, Ramirez, Holmgren, Swanson, Tieger, Grootes, McKenna, Leach, Schmidt

Back row: Feldman, Murano, Corcoran, Geissel, Lock, Zeps, Fernandez, Seymour, James, Simons, Floyd, Hodgkins, Osborne, Linder, LaCroix, Van Wechel, Davis, Murphy, Farwell